

A GENERAL FRAMEWORK FOR ADAPTIVE RADAR DETECTION BASED
ON FAST AND SLOW-TIME PREPROCESSING

A THESIS SUBMITTED TO
THE GRADUATE SCHOOL OF NATURAL AND APPLIED SCIENCES
OF
MIDDLE EAST TECHNICAL UNIVERSITY

BY

UĞUR BERKAY SARAÇ

IN PARTIAL FULFILLMENT OF THE REQUIREMENTS
FOR
THE DEGREE OF MASTER OF SCIENCE
IN
ELECTRICAL AND ELECTRONICS ENGINEERING

AUGUST 2019

Approval of the thesis:

**A GENERAL FRAMEWORK FOR ADAPTIVE RADAR DETECTION
BASED ON FAST AND SLOW-TIME PREPROCESSING**

submitted by **UĞUR BERKAY SARAÇ** in partial fulfillment of the requirements for
the degree of **Master of Science in Electrical and Electronics Engineering De-
partment, Middle East Technical University** by,

Prof. Dr. Halil Kalıpçılar
Dean, Graduate School of **Natural and Applied Sciences** _____

Prof. Dr. İlkey Ulusoy
Head of Department, **Electrical and Electronics Engineering** _____

Assist. Prof. Dr. Gökhan Muzaffer Güvensen
Supervisor, **Electrical and Electronics Engineering, METU** _____

Examining Committee Members:

Prof. Dr. Yalçın Tanık
Electrical and Electronics Engineering, METU _____

Assist. Prof. Dr. Gökhan Muzaffer Güvensen
Electrical and Electronics Engineering, METU _____

Prof. Dr. Seyit Sencer Koç
Electrical and Electronics Engineering, METU _____

Prof. Dr. Umut Orguner
Electrical and Electronics Engineering, METU _____

Prof. Dr. Orhan Arıkan
Electrical and Electronics Engineering, Bilkent University _____

Date:

I hereby declare that all information in this document has been obtained and presented in accordance with academic rules and ethical conduct. I also declare that, as required by these rules and conduct, I have fully cited and referenced all material and results that are not original to this work.

Name, Surname: Uğur Berkay Saraç

Signature :

ABSTRACT

A GENERAL FRAMEWORK FOR ADAPTIVE RADAR DETECTION BASED ON FAST AND SLOW-TIME PREPROCESSING

Saraç, Uğur Berkay

M.S., Department of Electrical and Electronics Engineering

Supervisor: Assist. Prof. Dr. Gökhan Muzzaffer Güvensen

August 2019, 104 pages

This thesis is about the design of an adaptive radar detector under heterogeneous clutter environment using a small number of secondary data, which is at the same time robust to Doppler mismatch. To this end, the observations taken from heterogeneous clutter environment are first processed with a specially designed fast-time preprocessing matrix, cleansing the target contamination in the secondary range cells. Using these clean secondary data, the covariance matrix of the clutter is estimated via the parametric spectral estimation method proposed by Burg. Using this clutter space and the target space in which the targets are assumed to be in Generalized Eigenspace operation, a reduced dimension space which includes the target space and escapes the clutter space is found. After the observations which are purified in the fast-time dimension are projected in this newfound space, the detection mechanism is activated using the reduced dimension Kelly detector. In this thesis, all steps described here are explained in detail and the performance of the proposed detector is evaluated and compared with the other detectors in the literature by using the MATLAB simulation results.

Keywords: Adaptive Radar Detectors, Kelly's Detector, Burg's Method, Dimension Reduction, Generalized Eigenvectors

ÖZ

HIZLI VE YAVAŞ ZAMANDA ÖN İŞLEMeye DAYANAN UYARLAMALI RADAR DETEKTÖRLERİ ÜZERİNE GENEL BİR ÇERÇEVE

Saraç, Uğur Berkay

Yüksek Lisans, Elektrik ve Elektronik Mühendisliği Bölümü

Tez Yöneticisi: Dr. Öğr. Üyesi. Gökhan Muzaffer Güvensen

Ağustos 2019 , 104 sayfa

Bu tez, heterojen kargaşa altında az sayıda ikincil menzil hücresi kullanarak çalışılan, aynı zamanda Doppler uyumsuzluklarına karşı gürbüz olan bir uyarlamalı radar detektörü tasarımıyla ilgilidir. Bu amaçla heterojen kargaşa altında alınan gözlemler önce özel tasarlanmış bir hızlı-zaman işleme matrisiyle işlenip, hedef yankısının ikincil menzil hücrelerindeki uzantıları temizlenmektedir. Sonrasında bu temizlenmiş verileri kullanarak, Burg tarafından önerilen parametrik spektrum kestirim metoduyla kargaşanın kovaryans matrisi kestirilmektedir. Kestirilen bu kargaşa uzayı ile hedefin içinde olduğu tahmin edilen hedef uzayı kullanılarak, Generalized Eigenspace operasyonu ile hedef uzayını içerip kargaşa uzayından kaçan, düşük boyutlu bir uzay bulunmaktadır. Hızlı-zaman ekseninde temizlenmiş gözlem verileri, bu yeni bulunan uzaya düşürüldükten sonra, düşük boyutta Kelly detektörü kullanılarak tespit mekanizması çalıştırılmaktadır. Bu tezde yukarıda anlatılan her adım detaylı olarak açıklanmış, Matlab ortamında yapılan gerçekleştirme sonuçlarıyla da önerilen detektörün başarımı değerlendirilmiş ve literatürdeki diğer detektörlerle kıyaslanmıştır.

Anahtar Kelimeler: Uyarlamalı Radar Detektörleri Kelly Detektörü, Burg Yöntemi,
Boyut Düşürme, Genellenmiş Özvektörler

To all my loved ones...

ACKNOWLEDGMENTS

I would like to thank to my student and thesis advisor Assist. Prof. Gökhan M. Güvensen for his priceless guidance. This thesis would not be completed without his never-ending helps and on target advices.

I would like to thank to Prof. Ali Özgür Yılmaz for his efforts to raise me as an engineer and keep me studying when I lose my motivation.

I would like to thank to my family for giving me what I need to be here and supporting me after all decisions I made.

Finally, my deepest gratitude is for my caring, loving, supportive fiancée Anış Büşra Baran, for being my source of dedication to hope for happiness when everything went really bad.

This work was supported by the Scientific and Technological Research Council of Turkey (TÜBİTAK) through the 2210-National Scholarship Programme for MSc Students 2016/1 with the application number 1649B021600085.

TABLE OF CONTENTS

ABSTRACT	v
ÖZ	vii
ACKNOWLEDGMENTS	x
TABLE OF CONTENTS	xi
LIST OF TABLES	xv
LIST OF FIGURES	xvi
LIST OF ABBREVIATIONS	xix
NOMENCLATURE	xx
CHAPTERS	
1 INTRODUCTION	1
1.1 Brief History of Radar	1
1.2 General Description of Radar Systems	2
1.3 Adaptive Radar Detectors	5
1.4 Notation	9
2 SYSTEM MODEL FOR HETEROGENEOUS ENVIRONMENTS	11
2.1 General System Description	11
2.2 Clutter Model	13

2.2.1	Statistical Model of the Clutter Process	13
2.2.2	Statistical Model of the Clutter Power in Heterogeneous Clutter Environments	17
2.2.3	Clutter Process in the System Model	19
2.3	Matrix Notation and Hypothesis Testing Problem	20
2.3.1	Hypothesis Testing	22
2.3.2	Statistics of the Interference Matrix	23
3	SLOW-TIME AND FAST-TIME PREPROCESSING METHODS FOR ADAPTIVE RADAR DETECTION	27
3.1	Fast-Time Preprocessing	28
3.1.1	Matched Filter	29
3.1.2	Unitary Transform	31
3.1.3	Effect of Fast-time Preprocessing on the Slow-time Characteristics of the Interference	33
3.2	Slow-Time Preprocessing	34
3.2.1	Optimal Right Subspace Construction for Parametric Clutter Models: Dimension Reduction with Generalized Eigenspace	35
3.2.2	Conventional Non-Adaptive Technique Based on DFT Subspace: Post-Doppler Processing	37
3.2.3	Adaptive Construction of Generalized Eigenspace with Parametric Spectral Estimation Methods	39
3.2.3.1	Estimation of Signal Subspace	40
3.2.3.2	Estimation of Interference Subspace	42
	Yule-Walker Equations	43
	Reverse Levinson-Durbin Recursion	44
	Extrapolating the Autocorrelation Sequence	44

Estimating the ICM	45
4 DETECTORS	49
4.1 Non-Adaptive Detectors	51
4.1.1 Genie-Aided Max-SINR Detector	51
4.1.2 Windowed DFT	53
4.2 Full-Dimension Adaptive Detectors	54
4.2.1 Full Dimension Adaptive Matched Filter Using Burg Method	55
4.2.2 Full Dimension Kelly-Like Detector Using Burg's Method	56
4.3 Subspace-Aware Adaptive Detectors	57
4.3.1 Subspace-Aware Kelly Detector Using GES with Burg's Method	58
4.3.2 Subspace-Aware Kelly Detector Using GES with Perfect Interference Knowledge	61
4.3.3 Subspace-Aware Kelly Detector Using Conventional DFT Subspace	62
5 NUMERICAL RESULTS	65
5.1 Scenario	65
5.2 Results	67
5.2.1 Homogeneous Clutter	68
5.2.2 Heterogeneous Clutter with Shape Parameter = 1	76
5.2.3 Heterogeneous Clutter with Shape Parameter = 0.25	82
5.2.4 Heterogeneous Clutter with Shape Parameter = 0.1	88
6 CONCLUSION	95
REFERENCES	99

APPENDICES

A BURG'S PARAMETRIC SPECTRAL ESTIMATION METHOD 103

LIST OF TABLES

TABLES

Table 5.1 Parameters used in the simulations	66
--	----

LIST OF FIGURES

FIGURES

Figure 1.1	Block diagram of a general radar system	2
Figure 1.2	The nominal radar frequency bands [1]	4
Figure 1.3	Block Diagram of the radar detector proposed in this thesis	8
Figure 2.1	The observation matrix for a single target without any interference or noise	13
Figure 2.2	The system model between transmitter and receiver	20
Figure 4.1	The tree of detectors described in this thesis	50
Figure 5.1	P_d vs Doppler Curves, SNR = 20 dB, $D = 3$, $L = 3$, Homogeneous Clutter	69
Figure 5.2	P_d vs SNR Curves, $f_d = 0.2$ PRF, $D = 3$, $L = 3$, Homogeneous Clutter	70
Figure 5.3	P_d vs SNR Curves, $f_d = 0.225$ PRF, $D = 3$, $L = 3$, Homogeneous Clutter	71
Figure 5.4	P_d vs SNR Curves, $f_d = 0.25$ PRF, $D = 3$, $L = 3$, Homogeneous Clutter	71
Figure 5.5	P_d vs SNR Curves, $f_d = 0.3$ PRF, $D = 3$, $L = 3$, Homogeneous Clutter	72

Figure 5.6	P_d vs L Curves, $f_d = 0.225$ PRF, SNR = 23 dB, $D = 3$, Homogeneous Clutter	73
Figure 5.7	P_d vs L Curves, $f_d = 0.25$ PRF, SNR = 23 dB, $D = 3$, Homogeneous Clutter	74
Figure 5.8	P_d vs D Curves, $f_d = 0.25$ PRF, SNR = 20 dB, $L = 3$, Homogeneous Clutter	74
Figure 5.9	P_d vs D Curves, $f_d = 0.25$ PRF, SNR = 20 dB, $L = 6$, Homogeneous Clutter	75
Figure 5.10	P_d vs D Curves, $f_d = 0.25$ PRF, SNR = 30 dB, $L = 3$, Homogeneous Clutter	75
Figure 5.11	P_d vs Doppler Curves, SNR = 20 dB, $D = 3$, $L = 3$, SP = 1	76
Figure 5.12	P_d vs SNR Curves, $f_d = 0.2$ PRF, $D = 3$, $L = 3$, SP = 1	77
Figure 5.13	P_d vs SNR Curves, $f_d = 0.225$ PRF, $D = 3$, $L = 3$, SP = 1	77
Figure 5.14	P_d vs SNR Curves, $f_d = 0.25$ PRF, $D = 3$, $L = 3$, SP = 1	78
Figure 5.15	P_d vs SNR Curves, $f_d = 0.3$ PRF, $D = 3$, $L = 3$, SP = 1	78
Figure 5.16	P_d vs L Curves, $f_d = 0.225$ PRF, SNR = 23 dB, $D = 3$, SP = 1	79
Figure 5.17	P_d vs L Curves, $f_d = 0.25$ PRF, SNR = 23 dB, $D = 3$, SP = 1	80
Figure 5.18	P_d vs D Curves, $f_d = 0.25$ PRF, SNR = 20 dB, $L = 3$, SP = 1	80
Figure 5.19	P_d vs D Curves, $f_d = 0.25$ PRF, SNR = 20 dB, $L = 6$, SP = 1	81
Figure 5.20	P_d vs D Curves, $f_d = 0.25$ PRF, SNR = 30 dB, $L = 3$, SP = 1	81
Figure 5.21	P_d vs Doppler Curves, SNR = 20 dB, $D = 3$, $L = 3$, SP = 0.25	82
Figure 5.22	P_d vs SNR Curves, $f_d = 0.2$ PRF, $D = 3$, $L = 3$, SP = 0.25	83
Figure 5.23	P_d vs SNR Curves, $f_d = 0.225$ PRF, $D = 3$, $L = 3$, SP = 0.25	83
Figure 5.24	P_d vs SNR Curves, $f_d = 0.25$ PRF, $D = 3$, $L = 3$, SP = 0.25	84

Figure 5.25	P_d vs SNR Curves, $f_d = 0.3$ PRF, $D = 3$, $L = 3$, $SP = 0.25$	84
Figure 5.26	P_d vs L Curves, $f_d = 0.225$ PRF, SNR = 23 dB, $D = 3$, $SP = 0.25$	85
Figure 5.27	P_d vs L Curves, $f_d = 0.25$ PRF, SNR = 23 dB, $D = 3$, $SP = 0.25$.	86
Figure 5.28	P_d vs D Curves, $f_d = 0.25$ PRF, SNR = 20 dB, $L = 3$, $SP = 0.25$.	86
Figure 5.29	P_d vs D Curves, $f_d = 0.25$ PRF, SNR = 20 dB, $L = 6$, $SP = 0.25$.	87
Figure 5.30	P_d vs D Curves, $f_d = 0.25$ PRF, SNR = 30 dB, $L = 3$, $SP = 0.25$.	87
Figure 5.31	P_d vs Doppler Curves, SNR = 20 dB, $D = 3$, $L = 3$, $SP = 0.1$. .	88
Figure 5.32	P_d vs SNR Curves, $f_d = 0.2$ PRF, $D = 3$, $L = 3$, $SP = 0.1$	89
Figure 5.33	P_d vs SNR Curves, $f_d = 0.225$ PRF, $D = 3$, $L = 3$, $SP = 0.1$. . .	90
Figure 5.34	P_d vs SNR Curves, $f_d = 0.25$ PRF, $D = 3$, $L = 3$, $SP = 0.1$	90
Figure 5.35	P_d vs SNR Curves, $f_d = 0.3$ PRF, $D = 3$, $L = 3$, $SP = 0.1$	91
Figure 5.36	P_d vs L Curves, $f_d = 0.225$ PRF, SNR = 23 dB, $D = 3$, $SP = 0.1$.	91
Figure 5.37	P_d vs L Curves, $f_d = 0.25$ PRF, SNR = 23 dB, $D = 3$, $SP = 0.1$.	92
Figure 5.38	P_d vs D Curves, $f_d = 0.25$ PRF, SNR = 20 dB, $L = 3$, $SP = 0.1$.	92
Figure 5.39	P_d vs D Curves, $f_d = 0.25$ PRF, SNR = 20 dB, $L = 6$, $SP = 0.1$.	93
Figure 5.40	P_d vs D Curves, $f_d = 0.25$ PRF, SNR = 30 dB, $L = 3$, $SP = 0.1$.	93

LIST OF ABBREVIATIONS

PRF	Pulse Repetition Frequency
PRI	Pulse Repetition Interval
ICM	Interference Covariance Matrix
SMI	Sample Matrix Inversion
CPI	Coherent Processing Interval
CUT	Cell Under Test
CW	Continuous Wave
GLRT	Generalized Likelihood Ratio Test
WSS	Wide Sense Stationary
PSD	Power Spectral Density
AWGN	Additive White Gaussian Noise
SNR	Signal-to-Noise Ratio
SINR	Signal-to-Interference-plus-Noise Ratio
GES	Generalized Eigenspace
DFT	Discrete Fourier Transform
MMSE	Minimum Mean-Square Error
CFAR	Constant False Alarm Rate
AR	Autoregressive
AMF	Adaptive Matched Filter
ACE	Adaptive Coherence Estimator

NOMENCLATURE

Scalars

α_k	Average power of the clutter at k^{th} range cell after convolving with pulse code
δ_{k-l}	Kronecker delta function at $k - l$
γ	Threshold in detectors
$\hat{r}_{\psi,m}^l$	Estimate of the m^{th} lag of r_{ψ} at the l^{th} secondary cell
λ	Wavelength of transmitted pulse
μ	Mean of the Gaussian PSD of any of the clutter processes
μ_{rain}	Mean of the Gaussian PSD of rain clutter process
μ_{sea}	Mean of the Gaussian PSD of sea clutter process
ϕ	Phase shift between two consecutive pulses
ρ	Target average signal to noise ratio
σ	Standard deviation of the Gaussian PSD of any of the clutter processes
σ^2	Variance of the Gaussian PSD of any of the clutter processes
σ_{rain}^2	Variance of the Gaussian PSD of rain clutter process
σ_{sea}^2	Variance of the Gaussian PSD of sea clutter process
σ_{rain}	Standard deviation of the Gaussian PSD of rain clutter process
σ_{sea}	Standard deviation of the Gaussian PSD of sea clutter process
τ_k	Average power of any of the clutter processes at k^{th} range cell
τ_k^{rain}	Average power of rain clutter process at k^{th} range cell
τ_k^{sea}	Average power of sea clutter process at k^{th} range cell
ζ	Window used in windowed DFT detector
a_k	k^{th} AR coefficient of a random process
b_k	k^{th} fast-time sample in the transmitted radar pulse

$c_{k,rain}^n$	Rain clutter signal from n^{th} pulse at k^{th} range cell
$c_{k,sea}^n$	Sea clutter signal from n^{th} pulse at k^{th} range cell
c_k^n	Any of the two clutter signals from n^{th} pulse at k^{th} range cell
$d_{\phi,n}$	Multiplicative phase term of n^{th} pulse w.r.t. first pulse
f_d	Doppler frequency of the target
F_i	The frequencies in which i^{th} filter in the filter bank gives the highest SNR
G	Diagonal loading factor
K	Length of the pulse code used
N	# of pulses in a CPI
N_0	Value of the white Gaussian noise PSD
n_k^n	White Gaussian noise signal in the n^{th} received pulse at k^{th} range cell
p	AR order of a random process
r_m	m^{th} lag of an autocorrelation sequence
$r_{c_{k,l}}$	Cross-correlation sequence between c_k and c_l
$r_{c_{rain}}$	Normalized autocorrelation sequence of rain clutter process
$r_{c_{sea}}$	Normalized autocorrelation sequence of sea clutter process
r_c	Normalized autocorrelation sequence of any of the clutter processes
s_k	k^{th} element of the impulse response of the target in fast-time
$S_c(f)$	Normalized PSD function of the clutter process
T	PRI
t	Hypothesis test for each detector
v_r	Radial velocity of the target
W	Weibull-distributed random variable from which w_k are drawn
w_k	Weibull-distributed texture parameter of clutter power at k^{th} range cell
y_k^n	The observed complex baseband signal taken from n^{th} pulse at k^{th} range cell
ψ_k^n	Observed interference signal in the n^{th} pulse at k^{th} range cell
\hat{a}_k^l	Estimate of the k^{th} AR coefficient of the l^{th} secondary cell

P_d Probability of detection
 P_{fa} Probability of false-alarm

Vectors

$\boldsymbol{\eta}$ Vectorized form of $\boldsymbol{\Psi}$
 $\boldsymbol{\psi}_k$ N -element vector whose n^{th} entry is ψ_k^n
 $\hat{\mathbf{r}}_{\psi}^l$ Vector whose m^{th} entry is $\hat{r}_{\psi,m}^l$
 \mathbf{b} Vector whose k^{th} element is b_k
 \mathbf{b}_k^\perp Vectors orthonormal to the complex conjugate of the pulse code
 \mathbf{c}^n K -element vector whose k^{th} entry is c_k^n
 \mathbf{c}_k N -element vector whose n^{th} entry is c_k^n
 \mathbf{d}_ϕ Steering vector for a target with phase shift ϕ
 \mathbf{d}_{f_d} Steering vector for a target with Doppler frequency f_d
 \mathbf{e}_n n^{th} generalized eigenvector of two matrices
 \mathbf{n}_k N -element vector whose n^{th} entry is n_k^n
 \mathbf{s} Target signal vector
 \mathbf{s}_0 Steering vector in the CUT
 \mathbf{w} Discrete-time filter applied in detectors
 \mathbf{y}_k N -element vector whose n^{th} entry is y_k^n
 \mathbf{z} Fast-and-slow-time preprocessed observation vector
 \mathbf{z}_l \mathbf{z} for the l^{th} secondary cell
 $\bar{\boldsymbol{\eta}}$ Vector form of fast-time preprocessed interference matrix
 $\bar{\mathbf{y}}_k$ Fast-time preprocessed \mathbf{y}_k
 $\tilde{\mathbf{d}}_\phi$ Reduced dimension \mathbf{d}_ϕ

Matrices

$\boldsymbol{\Psi}$ Interference matrix whose columns are $\boldsymbol{\psi}_k$
 $\mathbf{0}$ Zero matrix
 \mathbf{B} Convolution matrix for pulse code \mathbf{b}

C'	Matrix of normalized clutter returns
C	Matrix of clutter returns
I	Identity Matrix
N	Noise matrix whose columns are \mathbf{n}_k
Q	Fast-time preprocessing matrix
Q_m	Fast-time preprocessing matrix for matched filtering of pulse code \mathbf{b}
Q_u	Fast-time preprocessing matrix created with unitary transformation
\mathbf{R}_c	Normalized autocorrelation matrix of any of the clutter processes
\mathbf{R}_η	Autocorrelation matrix of η , whose k^{th} diagonal block is $\mathbf{R}_{\psi,k}$
$\mathbf{R}_{\psi,k}$	Autocorrelation matrix of the interference at k^{th} range cell (ICM)
$\mathbf{R}_{c_{rain}}$	Normalized autocorrelation matrix of rain clutter process
$\mathbf{R}_{c_{sea}}$	Normalized autocorrelation matrix of sea clutter process
S	SMI estimate of the autocorrelation matrix of \mathbf{z}_0
T	Diagonal matrix whose k^{th} diagonal entry is $\sqrt{T_k}$
U	Slow-time preprocessing matrix
U_{DFT}	DFT matrix
Y	Observation matrix whose columns are \mathbf{y}_k
Z	Fast-and-slow-time preprocessed observation matrix
$\bar{\Psi}$	Fast-time preprocessed interference matrix
\bar{Y}	Fast-time preprocessed observation matrix
$\hat{\mathbf{R}}_\psi$	Estimate of \mathbf{R}_ψ
$\hat{\mathbf{R}}_\psi^l$	Matrix whose $(i, j)^{th}$ entry is $\hat{r}_{\psi,(i-j)}^l$
$\hat{\mathbf{R}}_{s,i}$	Estimate of \mathbf{R}_s for the i^{th} filter
$\hat{\mathbf{R}}_s$	Estimate of \mathbf{R}_s

CHAPTER 1

INTRODUCTION

The term radar is an acronym which stands for RAdio Detection And Ranging. As it is obvious from the definition, general purpose of radar can be described as to detect objects using radio waves and to determine how distant they are to the radar. However, the radar is used to fulfill lots of different goals today, including measuring the speed of vehicles, predicting the meteorological events, mapping the surface of the earth, etc. This wide range of applications may be the underlying reason that scientific studies regarding understanding the nature of radar systems and improving their capabilities have never ended and still keep being published frequently.

This chapter starts with a brief history of radar technology and general information on radar systems. Then, adaptive radar detectors are introduced and the existing studies in the literature related to this thesis are summarized. The significance of the work proposed by this thesis is also going to be provided. Finally, the notation of symbols used throughout this thesis is going to be explained for convenience.

1.1 Brief History of Radar

The history of radar can be considered to start with the exploration of reflection of electromagnetic waves. Scottish scientist James Clerk Maxwell had formulated his famous equations describing the fundamental properties of electromagnetic waves when German scientist Heinrich Hertz showed experimentally in 1886 that metallic objects reflect electromagnetic waves [2]. This phenomenon made Serbian-American engineer Nikola Tesla propose electromagnetic detection and velocity measurement in 1900, followed by the ship detection experiments of German engineer Christian

Hülsmeier in 1904 [3].

The world wars played an important role in the development of radar systems as different countries worked on this technology in order to be able to use it in military applications. The use of radar for military purposes is still of great importance today.

1.2 General Description of Radar Systems

Due to the wide range of services in which radar systems are used, there is not a unique design for radar systems. However, it is convenient to define a general radar system as having a transmitter, a receiver, and a processor. The similarity of this system model to a general communications system model should be noted. In fact, when the connection between the transmitter and the receiver, namely the channel, is added to the model, the radar system model looks exactly the same as a general communications system. However, the elements of the two systems work quite differently, the biggest difference being in the processing part. A block diagram of a more detailed radar system is given in Fig. 1.1.

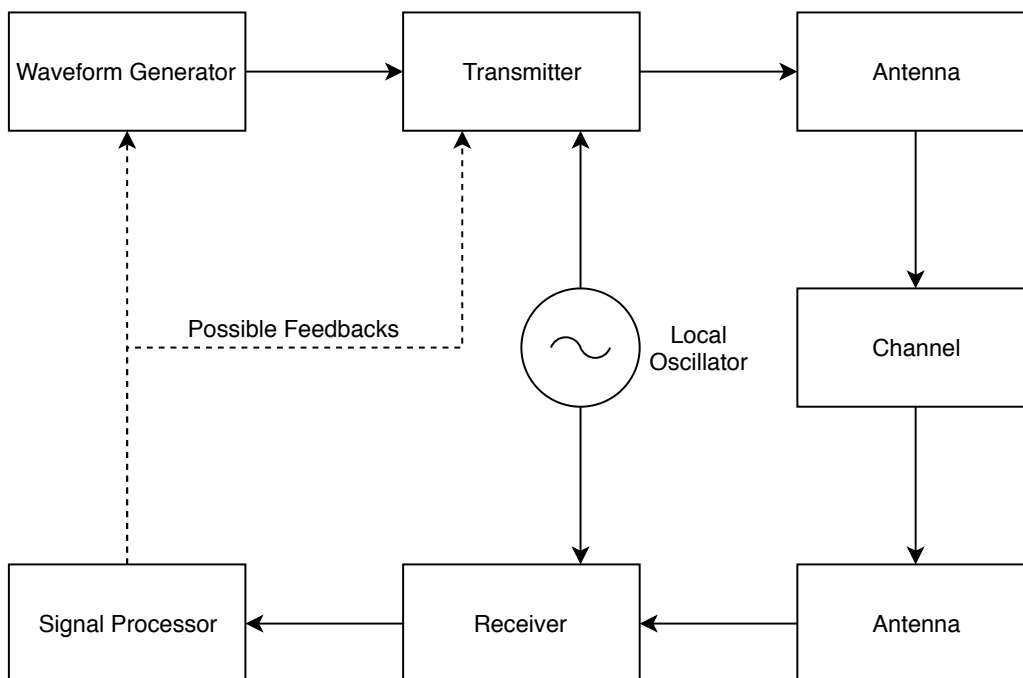


Figure 1.1: Block diagram of a general radar system

The transmitting and receiving antennas are responsible for generating and collecting the electromagnetic waves. If the two antennas are separated in their locations significantly, the radar system is called *bistatic* and if they are located near to each other, the radar system is called monostatic. The *monostatic* radars usually use the same antenna for both transmission and reception of the electromagnetic waves. The geometric properties of the antennas such as their width, height, shape, curvature, etc. determine the shape of the electromagnetic waves transmitted from them or their responses to the waves impinging on them. The radar antennas are usually designed such that they emit the waves directionally, rather than being isotropic, meaning that the radiation intensity is high in some specific directions in space and low in another directions. This directional electromagnetic waves are usually called *beams* and the mapping from each specific direction to the radiation intensity at that direction is usually called the *beam pattern*. The radar antenna's beam pattern directly influences the transmitted and received powers at different directions and thus it is almost always designed with respect to the specific requirements of the radar system.

The transmitter and receiver blocks in Fig. 1.1 are responsible for up/down conversion, noise elimination and amplification of the useful signals. The radar transmitters may have peak powers varying from milliwatts to megawatts, depending on the application they are being used [3]. Again depending on the application, the frequency of radar waveforms vary from 3 MHz to 300 GHz. There are some frequency bands inside this range according to IEEE [4]. The nominal radar frequency bands are shown in Fig. 1.2. The attenuation of the radar waveforms in the air generally increases with the frequency, so lower frequencies are used for longer range applications. On the other hand, the increase in the frequency results in a smaller antenna size requirement and finer resolution, so higher frequencies are used for applications that need shorter range and better resolution. The receiver usually includes a low-noise RF amplifier at its first stage, and its structure can be different for different applications. The radar waveforms can be categorized as continuous waves and pulsed waves. A *continuous wave (CW) radar* emits a continuous, possibly and usually modulated electromagnetic wave and receives the echoes of this wave at the same time. On the other hand, a *pulsed radar* emits several short duration electromagnetic waves, called *electromagnetic pulses* or simply *pulses*, each separated in time. The waveform generator

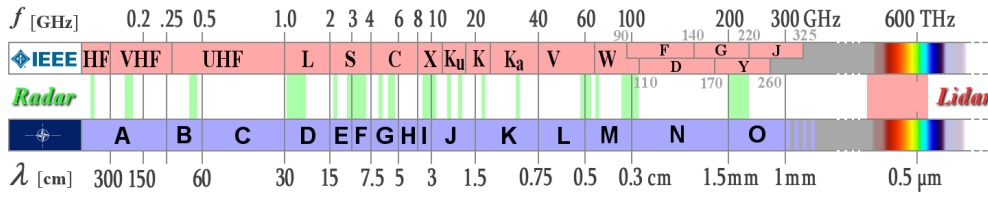


Figure 1.2: The nominal radar frequency bands [1]

block in Fig. 1.1 is responsible for determining the exact baseband waveform shape, including the adjustments on modulations used in the waves, the duration and time separation of pulses, etc.

In this chapter, a special kind of radar system, which is pulsed Doppler radar, and two interrelated signal models related to pulse Doppler radars will be introduced. A pulsed Doppler radar, as its name suggests, is a pulsed radar; that is, it transmits a number of short duration electromagnetic waves, pulses, and collect and process them together. The word Doppler states that this radar takes the famous Doppler effect into account while generating and processing the signals. Pulsed Doppler radars are especially useful for determining the range and the radial velocity of the targets. The way they fulfill this aim will be explained in the upcoming sections.

There are many parameters the pulse Doppler radars work with. *Pulse Repetition Interval (PRI)* is a characteristic parameter of this kind of radar systems; it is the time between the beginnings of two consecutive pulses that are transmitted. The reciprocal of PRI is the *Pulse Repetition Frequency (PRF)*. Although it is not obligatory for all cases, pulsed radar systems usually collect the echoes from a number of pulses and process them together. The duration of time in which the pulse echoes are collected and processed together is called *Coherent Processing Interval (CPI)*. The word CPI is also frequently used for the echoes themselves in the CPI. For the rest of this thesis, the pulse repetition intervals in a coherent processing interval are assumed to be the same. This constant PRI is denoted as T and the number of pulses in a CPI is denoted as N so that the duration of a CPI becomes NT , assuming that the time duration between the last pulse in the corresponding CPI and the end of that CPI is also equal to T . Obviously, the PRF is also constant in a CPI, and that constant frequency is denoted as "PRF" throughout this thesis.

Assuming that there is not any transmitters other than the radar transmitter in the scenario, the received signal at Δt amount of time after the transmission is the echo of the transmitted waveform from an object at distance $c\Delta t/2$. Here, c is the speed of light and it is taken as 3×10^8 m/s. This relation shows that there is a direct relationship between the time an echo is received and the distance at which the object causing that echo is located measured from the radar.

In practical radar systems, echoes are collected at discrete time instants. Following the discussion in the previous paragraph, the sampling in time corresponds to a sampling in distance. If two samples are taken $1 \mu s$ apart, they will correspond to objects located 150 m away from each other. In this case, if the duration of the pulse is less than $1 \mu s$, there will be some distances that the echoes coming from them are not sampled in the receiver, namely, lost in the environment. Therefore, in order not to lose the echoes from any distances, the *pulse duration* must not be smaller than the time between two consecutive samples taken at the receiver. This also means that the sampling rate must be higher than inverse of the pulse duration. The inverse pulse duration is approximately the bandwidth of a rectangular pulse. Therefore, the required sampling rate at the receiver can actually be generalized such that it must be higher than the Nyquist rate, which is the bandwidth of the transmitted signal [3].

1.3 Adaptive Radar Detectors

As a brief definition, adaptive radar detectors' parameters are adjusted according to the observed signals. In other words, the adaptive radar detectors observe the interference and try to estimate its characteristics in order to apply some kind of filtering and eliminate it.

The adaptive detectors were first studied by Kelly [5] in 1986. In this paper, the secondary data is added to the hypothesis test with Sample Matrix Inversion (SMI) and the GLRT expression for this hypothesis test is provided for the first time. The analytical false alarm and detection probabilities were also provided in this work.

After this study, many other detector schemes, similar to Kelly's one, have been proposed. One of them is the Adaptive Matched Filter (AMF) [6], which suggests that

the interference covariance matrix (ICM) of the cell under test (CUT) be estimated by using the secondary cells and this estimation be used in the hypothesis test as if it is perfect. AMF also uses SMI to estimate the ICM. This method also assumes that the interference in the CUT is Gaussian distributed. This method is shown to be sensitive to the ICM estimation errors, and it is also shown by Reed-Mallet and Brennan [7] that the number of secondary cells must be as at least twice the number of dimensions of ICM in order for the SNR loss due to the errors in ICM estimation with SMI to be reduced to below 3 dB. This thesis is built on a scenario in which only a few secondary cells are available, and the performance loss of this AMF technique in such a scenario is also provided in this thesis.

In other adaptive radar detector schemes like adaptive coherence estimator (ACE) [8] and adaptive normalized matched filter (ANMF) [9], the clutter environment is assumed to be heterogeneous. In these detectors, the normalized ICM in CUT and the secondary cells are assumed to be the same but the average powers of these matrices are considered as unknown nonrandom variables. The GLRT detector for this scheme is also provided in these studies. These works are similar to the work in this thesis in the way the heterogeneity of the clutter environment is assumed. [10] and [11] are also studies concerning the detectors and their performances under heterogeneous clutter environments.

Dimension reduction is another important part of this thesis, and there are several studies on reduced-dimension adaptive radar detectors in the literature. In [12, 13], the dimension reduction operation is explained to be a beneficial solution to the problem of small number of secondary cells. The motivation of dimension reduction in this thesis is the same as these studies; however, this thesis is unique in the way that it conducts the dimension reduction and the detection operation it applies in the reduced dimension.

There are also experimental works about adaptive radar detectors in the literature [14, 15, 16]. In [15], the false alarm rate of the detectors using real data is shown to be higher than the expected false alarm rate provided analytically in the papers. A large difference of average powers in the secondary cells or the correlation between the secondary cells are considered to be the possible reasons for this performance

loss. In [16], a robust recursive ICM estimation method is proposed in order to avoid such problems and the proposed detector is tested with real sea clutter data. The false alarm rate in the results are again higher than expected, and this situation is explained with the non-stationarity of the clutter in both time and space dimensions.

Following these works, this thesis proposes an adaptive radar detector which works under heterogeneous clutter environment with only a few secondary cells. By decreasing the number of secondary cells required, the effects of non-stationary clutter can be minimized whilst a faster convergence rate in adaptation can be achieved. This detector is shown to be significantly more robust to clutter heterogeneity than the conventional adaptive detectors. To achieve this, a two-stage adaptation operation is proposed. At the first stage, the ICM is assumed to be an AR process and it is estimated with Burg's parametric spectral estimation method. Then, generalized eigenspace of this estimated interference space and an estimated signal space is found in order to achieve a reduced dimension subspace to make detection inside. The Kelly's adaptive GLRT detector is then used in this reduced dimension subspace as the second adaptation stage.

In the detector scheme proposed, the dimension reduction technique, a parametric spectral estimation method and Kelly's adaptive radar detector are combined. The adaptive radar detector is required to make the detection under unknown or fast-changing clutter environments, but it needs secondary cells to do its work. The dimension reduction is required to make adaptive radar detector adapt itself to the environment when only a few secondary cells are available. The parametric spectral estimation provides a good subspace for dimension reduction, which helps eliminating the interference. Other than these three methods, a fast-time preprocessing method is also provided in order to purify the secondary cells from the contamination of target due to the pulse code used. This purification also helps finding a good subspace by preventing the ICM estimators considering the target signal as an interference. All of these methods are brought together to have a fast-converging adaptive radar detector which is robust to clutter heterogeneity, target Doppler mismatch and restrictions on the number of secondary cells. The block diagram of this radar detector is provided in Fig. 1.3.

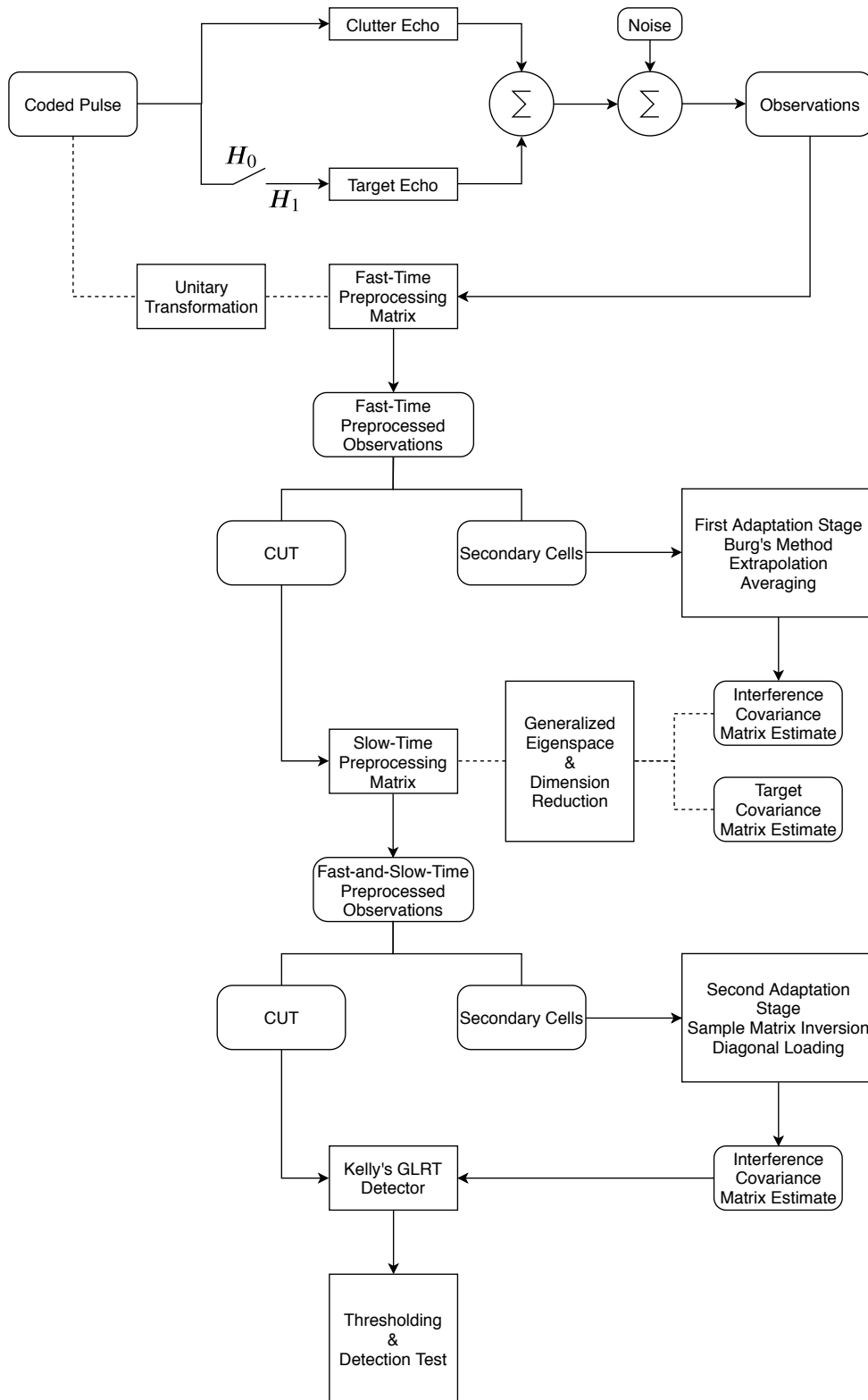


Figure 1.3: Block Diagram of the radar detector proposed in this thesis

1.4 Notation

In this section, the mathematical notation which will be used throughout this thesis will be described. Since this thesis is considered as a general framework, it includes lots of different variables and equations relating these variables. This section aims to help the readers follow the mathematics of this thesis by introducing general rules of notation used through all of this document.

In this thesis, scalar variables are noted as small italic letters like a whereas the vector variables are expressed with small and bold letters like \mathbf{b} . In this notation, whether the variable is random or deterministic is not important. In other words, no special notation is used for random variables. The variables in matrix form are denoted as capital bold letters like \mathbf{C} . The $(i, j)^{th}$ element of a matrix \mathbf{C} is denoted as $\mathbf{C}(i, j)$. Finally, the capital italic letters like T denotes the deterministic constants in this thesis. These notations do not change whether the variable is used as a subscript or superscript.

The capital subscripts of matrices depicts the dimensions of them. For example, \mathbf{I}_K is a $K \times K$ square matrix, and $\mathbf{Y}_{N \times K}$ is an $N \times K$ matrix. Small subscripts can be used to define the variables, there is not a general rule about them.

In this thesis, the estimation of a variable is denoted with a hat sign above the true variable. For example, if a is a scalar value, its estimation is denoted as \hat{a} and the estimation of a matrix \mathbf{C} is denoted as $\hat{\mathbf{C}}$.

Throughout this thesis, the autocorrelation vector of a scalar random variable a is denoted as \mathbf{r}_a . Similarly, autocorrelation matrix of a vector random variable \mathbf{b} is denoted as \mathbf{R}_b .

If a vector is written in a sequence form, its elements become scalars so that the sequence is denoted like $r_a[m]$. Here, $r_a[m]$ can denote both the whole sequence and the m^{th} element of this sequence. Which option is correct can be understood by the context in which this notation is used. The sequences can also be denoted like $\{a_k\}_{k=1}^p$. There is no difference between $\{a_k\}_{k=1}^p$ and $a[k]$ for $k = 1, 2, \dots, p$.

The explanations of each variable used in this thesis can be found in the section that it is first defined. However, the notation rules should make the readers understand the

meaning of the variable names easily.

CHAPTER 2

SYSTEM MODEL FOR HETEROGENEOUS ENVIRONMENTS

2.1 General System Description

In this section, the mathematical framework used throughout this thesis will be enlightened. The names of the vectors and matrices are introduced along with some basic equations about the scenario which is being investigated.

The problem is presented as a pulsed Doppler radar system, which uses N pulses in each coherent processing interval (CPI); but it is easy to convert the problem into other signal processing problems, such as a beamformer which has N sensors sampling the signals in space. Any consecutive two of these N samples are separated in time by T seconds. The received echoes of the pulses in the CPI are sampled in fast-time dimension such that there are K samples for each pulse. In other words, there are K fast-time samples for each N slow-time sample in the problem. The echoes received outside the CPI are ignored in this thesis.

Each fast-time sample of the transmitted radar pulse is denoted with b_k for $k = \{0, 1, \dots, K - 1\}$. b_k can also be depicted as the samples taken with a sampling rate of 1 samples per chip, from a pulse which is coded with a pulse code having K chips. We define this pulse code as:

$$\mathbf{b} \triangleq [b_0 \ b_1 \ \dots \ b_{K-1}]^T \quad (2.1)$$

and with no loss of generality, choose \mathbf{b} as a unit-norm vector.

If a target has a radial velocity with respect to the radar antenna, the echoes from different pulses will have their phases changed due to the Doppler shift. In order to make use of the phase difference of the consecutive pulses, the pulses must be

transmitted coherently. In fact, a CPI consists of only coherently transmitted pulses by its definition, which means that all pulses in a CPI must have a common fixed phase reference [3]. This way, the common initial phase of the pulses can be subtracted from the individual phases of each pulse in order to get the phase differences between them. After this phase correction operation, the firstly received pulse is considered to have zero phase, because its phase is exactly the same with the common phase reference.

In order to make Doppler shift operations easier, Stop-and-Hop approximation is also used in this thesis. The "Stop" part suggests that during the time in which a pulse is in the medium, all objects it reaches and echoes from and the radar system are motionless. The "Hop" part suggests that just before stopping for the transmission of a pulse, the radar system and all the objects in the scenario moves to their corresponding positions suddenly. This approximation is valid when the movements of objects during the duration of the CPI is not larger than the length of a pulse.

With the above assumptions, when the first pulse has zero phase, the next pulse will have a phase of $4\pi v_r T / \lambda$, where v_r is the radial velocity of the target, T is the pulse repetition interval (PRI) and λ is the wavelength of the transmitted electromagnetic wave [3]. Therefore, if all pulses in the CPI are normalized with the first pulse, the complex amplitudes of the pulses will construct the vector:

$$\mathbf{d}_\phi = \left[1 \quad e^{j\phi} \quad \dots \quad e^{j(N-1)\phi} \right]^T \quad (2.2)$$

while the phase term can be written as:

$$\phi = \frac{4\pi v_r T}{\lambda} = 2\pi \frac{f_d}{\text{PRF}} \quad (2.3)$$

where $f_d = 2v_r / \lambda$ is the Doppler frequency shift and PRF is the pulse repetition frequency. The elements of \mathbf{d}_ϕ are called $d_{\phi,n}$ for $n = \{1, \dots, N\}$. Then, $d_{\phi,n}$ is a multiplicative phase to all fast-time samples taken from the echo of the n^{th} pulse, when the target's radial velocity is $(\lambda / 4\pi T) \phi$. That is, when there is no interference and the power of the received signal is not considered, the received echo of the n^{th} pulse from a target at k^{th} range cell is $d_{\phi,n} b_k$. The observation matrix including the received and grouped echo signals from a single target when there is no interference or noise is given in Fig. 2.1. In the next section, the interference in the scenario of this thesis is going to be introduced and its statistical characteristics will be provided in detail.

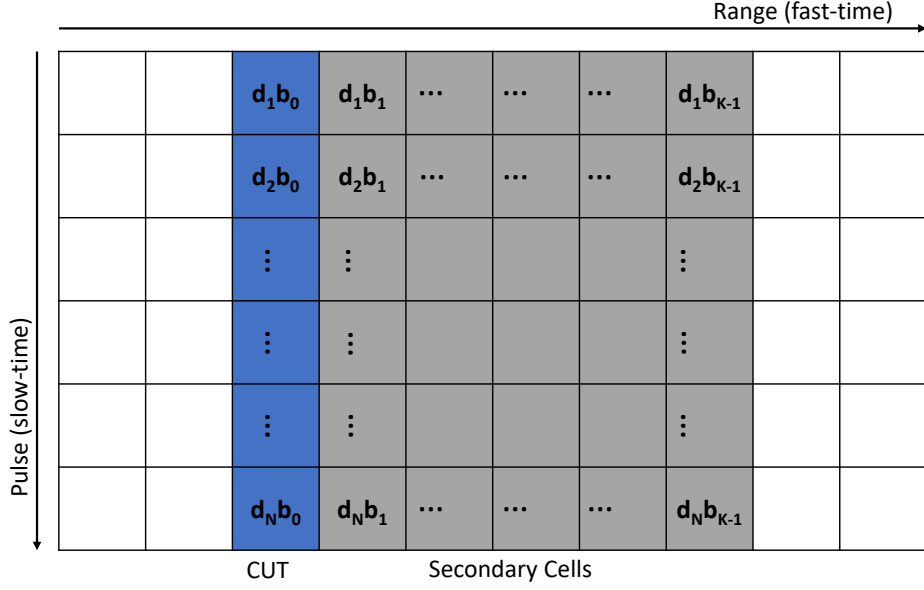


Figure 2.1: The observation matrix for a single target without any interference or noise

2.2 Clutter Model

In this thesis, the interference sources are considered to be the clutter signals and the noise. These two are common interference sources to nearly all radar systems; however, there might be some other interference sources like jammer signals or communication signals in some radar applications. In this section, the clutter model used throughout this thesis will be explained in detail. Describing the clutter model thoroughly is essential for this thesis because the research done here is about increasing the radar detection performance and the biggest challenge in this work is suppressing the received clutter returns. With this motivation, in this section, the statistical model of the clutter process and its power parameter are explained and they are followed by the role of this clutter process in the radar system.

2.2.1 Statistical Model of the Clutter Process

The scenario investigated in this thesis includes two separate, statistically independent clutter sources which are called as the sea clutter and the rain clutter. Say $c_{k,sea}^n$ is the sea clutter return from the n^{th} pulse at the k^{th} range cell and $c_{k,rain}^n$ is the

corresponding value for the rain clutter. For convenience, c_k^n will be used instead of any of these clutter returns. That is, c_k^n may represent any one of $c_{k,sea}^n$ and $c_{k,rain}^n$, the important point is that this term corresponds to a clutter echo received from the n^{th} pulse at the k^{th} range cell. If c_k^n is used to construct an $(N \times (2K - 1))$ matrix \mathbf{C} such that $(n, k)^{th}$ element of \mathbf{C} is c_k^n , then each column of this matrix is denoted as \mathbf{c}_k and each row of this matrix is denoted as $(\mathbf{c}^n)^T$. To be more clear, the \mathbf{C} matrix is defined as:

$$\mathbf{C}_{N \times (2K-1)} \triangleq \begin{bmatrix} (\mathbf{c}^0)^T \\ (\mathbf{c}^1)^T \\ \vdots \\ (\mathbf{c}^{(N-1)})^T \end{bmatrix} \triangleq \begin{bmatrix} \mathbf{c}_{-(K-1)} & \mathbf{c}_{-(K-2)} & \dots & \mathbf{c}_{K-2} & \mathbf{c}_{K-1} \end{bmatrix} \quad (2.4)$$

In this thesis, uncorrelated scattering assumption is used, i.e. \mathbf{c}_k are assumed to be uncorrelated from each other. This can be shown as:

$$r_{\mathbf{c}_k, l}[m] \triangleq \mathbb{E} \{ c_k^n (c_l^{n-m})^* \} = \mathbb{E} \{ c_k^n (c_k^{n-m})^* \} \delta_{k-l} \quad (2.5)$$

where δ is the Kronecker Delta function and $(*)$ is the complex conjugate operator. The second expectation in Eq. (2.5) can be defined as the autocorrelation function of the slow-time process \mathbf{c}_k , which is assumed to be a zero-mean circularly symmetric compound complex Gaussian process with a nonrandom texture parameter, uncorrelated among fast-time. This kind of clutter processes are examined in detail in [17].

Another assumption made in this thesis is that the clutter is wide sense stationary (WSS) in slow-time dimension. This assumption suggests that in addition to having a stationary mean, which is zero, the second order characteristics of the slow time clutter process \mathbf{c}_k is also stationary. In other words, the second expectation in Eq. (2.5), which is the autocorrelation of the slow-time sequence \mathbf{c}_k , depends only on m , which is the time difference between any two elements of this sequence. It can be noted that when the time difference m is zero, the autocorrelation function becomes equal to the average power of c_k^n and since it depends only on m and does not depend on n , it has the same value for all n pulses. Consequently, the WSS assumption also states that the average power of the slow-time process \mathbf{c}_k is also stationary.

Since the clutter process is zero-mean, its variance can also be depicted as its average

power. The variance can be defined as:

$$\tau_k \triangleq \mathbb{E} \{c_k^n (c_k^n)^*\} = \mathbb{E} \{|c_k^n|^2\} \quad (2.6)$$

and it is the average power of any sample in the slow-time sequence c_k . For clarity, it is repeated that the average powers of the samples in the slow-time sequence c_k are the same due to the slow-time WSS assumption. For a homogeneous clutter environment, τ_k will be equal for all k values, by definition, but in general the average power of clutter returns can change from a range cell to another. In such cases, the clutter environment is called to be heterogeneous. How the heterogeneous clutter environment is created in this thesis is explained in Section 2.2.2.

Even if the clutter environment is heterogeneous, c_k are still uncorrelated and have the same autocorrelation function shape for all k , only the average power of c_k changes with k . Then, the normalized autocorrelation function can be defined as:

$$r_c[m] \triangleq \frac{\mathbb{E} \{c_k^n (c_k^{n-m})^*\}}{\tau_k} \quad (2.7)$$

which is the same for all range cells. For clarity, the expectation in Eq. (2.7) is over the slow-time index n , which means that the defined normalized autocorrelation function is showing the correlations between each transmitted pulse in a CPI, no matter which range cell is being considered. On the other hand, $r_c[0] = 1$ by the definition of τ_k .

In this thesis, it is assumed that both rain and sea clutter processes have Gaussian shaped power spectral densities (PSD). For any clutter process, the PSD as a function of regular frequency is denoted as $S_c(f)$ and is given by the famous formula:

$$S_c(f) = \frac{1}{\sigma\sqrt{2\pi}} \exp\left(-\frac{(f-\mu)^2}{2\sigma^2}\right) \quad (2.8)$$

which forces the previously defined $r_c[m]$ to be in the form of:

$$r_c[m] = e^{j2\pi\mu(mT)} e^{-2\pi^2\sigma^2(mT)^2} \quad (2.9)$$

where T is the PRI of the radar system and μ and σ^2 are the mean and the variance of the Gaussian shaped PSD, $S_c(f)$, respectively. The autocorrelation function in Eq. (2.9) can be considered as the samples taken from the continuous time autocorrelation function at sampling period T . In general, the sea and the rain clutter have different mean and variance parameters, therefore $r_{c_{sea}}[m]$ and $r_{c_{rain}}[m]$ are two

different autocorrelation functions whose Fourier transforms are Gaussian functions with means μ_{sea} and μ_{rain} , and variances σ_{sea}^2 and σ_{rain}^2 , respectively.

The autocorrelation sequence defined in Eq. (2.9) for $m = 0, 1, \dots, (N-1)$ can easily be turned into an autocorrelation matrix using the fact that autocorrelation matrices have Toeplitz structure. The autocorrelation matrix \mathbf{R}_c and a new operator Toeplitz is defined as:

$$\mathbf{R}_c \triangleq \text{Toeplitz}(r_c[m]) \quad (2.10)$$

so that

$$\mathbf{R}_c(i, j) \triangleq r_c[i - j], \quad \text{for } i, j = 0, 1, \dots, (N - 1) \quad (2.11)$$

It should be noted that the diagonal elements of \mathbf{R}_c are equal to unity because of the normalization done in the definition of $r_c[m]$ in Eq. (2.7).

$\mathbf{R}_{c_{sea}}$ and $\mathbf{R}_{c_{rain}}$ are the slow-time autocorrelation matrices of the two clutter processes which are statistically independent. Let τ_k^{sea} denotes the average power of the sea clutter process at k^{th} range cell, and τ_k^{rain} be the same entity for the rain clutter. Then, the autocorrelation of the sum of these two clutter processes is equal to $\tau_k^{sea} \mathbf{R}_{c_{sea}} + \tau_k^{rain} \mathbf{R}_{c_{rain}}$. At the receiver, there is also a white noise process which is also independent from the other interference sources. The autocorrelation of this white noise process is \mathbf{I}_N , which is the $N \times N$ identity matrix, after the normalization with the white Gaussian noise PSD usually called as N_0 . However, the characteristics of the interference at the receiver cannot be found by simply adding the two matrices corresponding to the clutter echoes and the identity matrix corresponding to the white noise. This is because in contrast to additive white noise, the clutter echoes do depend on the pulse code used.

Throughout this thesis, it is assumed that the clutter does not fold over, or the clutter folding is eliminated properly. This means that the received signal from a range cell consists of only the echo of the last pulse transmitted, without any effect of the previously transmitted pulses.

In the next section, the statistical distribution used for τ_k in heterogeneous clutter case is explained in detail.

2.2.2 Statistical Model of the Clutter Power in Heterogeneous Clutter Environments

The proposed detector of this thesis is claimed to work well with little amount of secondary data, therefore it pays for its complexity mostly in heterogeneous clutter environments where large number of secondary cells cannot be used in the adaptation process. This is why examining the case where the clutter power is changing from one range cell to another is essential for featuring the significance of the work done. With this aim in this section, it is clarified that how the heterogeneity of the clutter environment is constructed in this thesis.

As specified in Section 2.2.1, the clutter process has a compound-Gaussian distribution with a nonrandom texture parameter, τ_k . A random process having compound-Gaussian distribution means that the random process is distributed with a Gaussian distribution with one or more parameters being also random. The clutter process is assumed to be uncorrelated in the fast-time domain, with the uncorrelated scattering assumption. Therefore, only the first order statistics of the fast-time clutter process is of importance. The clutter is also assumed to be zero-mean, so only the power (variance) of it is of importance.

As they are previously defined, the power of the fast-time samples of the clutter process is called as τ_k and τ_k^{sea} and τ_k^{rain} are the powers of sea and rain clutter samples, respectively. In this thesis, τ_k^{sea} and τ_k^{rain} are considered to be deterministic constants and they are called as the *scaling* parameters of the clutter power. However, another parameter called *texture* parameter defines how this power is distributed among fast-time. The texture parameter is called as w_k and w_k is assumed to be a realization of the random variable W for each range cell. In this thesis, W is chosen to be Weibull-distributed with probability distribution:

$$f_W(w; \lambda, m) = \begin{cases} \frac{m}{\lambda} \left(\frac{w}{\lambda}\right)^{m-1} e^{-(w/\lambda)^m} & , w \geq 0 \\ 0 & , w < 0 \end{cases} \quad (2.12)$$

where $m > 0$ is called as the *shape parameter* and $\lambda > 0$ is called as the *scale parameter* of the distribution. The shape parameter is also abbreviated as SP in some parts of this thesis for convenience. A special case of Weibull distribution is when the

shape parameter $m = 1$, reducing the pdf to an exponential pdf with rate parameter λ . The mean of the Weibull distribution is given as:

$$\mathbb{E}\{W; \lambda, m\} = \lambda\Gamma(1 + 1/m) \quad (2.13)$$

where $\Gamma(\cdot)$ is the famous gamma function which is given as:

$$\Gamma(z) = \int_0^{\infty} x^{z-1} e^{-x} dx \quad (2.14)$$

In order to make the mean of the Weibull distribution be equal to unity, a shape parameter is chosen and the corresponding scale parameter is calculated by using:

$$\lambda = \frac{1}{\Gamma(1 + 1/m)} \quad (2.15)$$

with the given shape parameter m . During the research, different m values are examined and it is seen that as m increases, the random variable W becomes nearer and nearer to a deterministic value of 1. On the other hand, as m decreases and becomes closer to zero, the number of "spikes" in the realizations increases and to compensate for this increase in the mean, other realizations decrease in the value. This creates the effect of heterogeneity; the clutter value can be small in one range cell but it can have a spiky value in the next range cell. As a result, it is observed that decreasing the shape parameter m increases the heterogeneity of the clutter texture.

As it is described in the previous paragraphs, the average power of the clutter processes are handled with τ_k parameters and how this power is distributed among fast-time is handled with w_k parameters. In order not to change the long-term average power of the clutter processes, w_k is chosen to have a unity mean. This way, the long term average power of the clutter processes are handled only with τ_k but in each realization (for each individual CPI) the power of the clutter process for each range cell depends on both τ_k and w_k .

It should be noted that w_k does not vary for sea and rain clutter, it multiplies both processes. This means that in a heterogeneous clutter environment, in each range cell, the power of the sea clutter is given as $w_k \tau_k^{sea}$ and the power of the rain clutter is given as $w_k \tau_k^{rain}$. This is an assumption made in this thesis and it may not be valid in real scenarios. On the other hand, assigning different power levels to sea and rain clutter means changing the slow-time autocorrelation structure of the clutter process in each fast-time cell, which is out of the scope of this thesis.

Another note should be that w_k are assumed to be uncorrelated among different range cells and CPIs. For the scenarios including land clutter, this assumption is not valid in most cases because the texture of the earth remains the same for very long times. However the texture of the sea surface is mostly determined by the sea waves, which are assumed to occur independently in different range cells and CPIs. Since the scenario of this thesis includes only sea and rain clutters, assuming that w_k are uncorrelated is considered to be convenient.

As the final discussion, all the explanations about w_k are useful only in heterogeneous clutter case. If the clutter environment is homogeneous, $w_k = 1$ for all K range cells and the average powers of the clutter returns are denoted as $\tau_k = \tau$ and it is a deterministic constant. However in heterogeneous clutter case, in order to keep the notation as simple as possible, the average powers of the clutter returns are again notated as τ_k with a difference that τ_k is now a Weibull-distributed random variable. It is needed that the reader distinguishes between the homogeneous and the heterogeneous cases and perceives the difference between the deterministic constant τ_k and the random variable τ_k .

Up to here in this chapter, both fast and slow-time characteristics of the clutter and noise processes are examined, and the target signal's slow-time behavior is described. To give a big picture of the radar system including the target signal, clutter and noise vectors, a general system model is provided in the next section.

2.2.3 Clutter Process in the System Model

In this section, the system model between the transmission of the radar pulse and the reception of it is given in a compact form for a clear understanding of how clutter process is being involved in the overall radar system.

In Fig. 2.2, the system model between the transmission and the reception of the n^{th} radar pulse is given. The scenario in this thesis assumes a co-located radar system but for clarity, transmitter and the receiver are separated in Fig. 2.2. The transmitter uses \mathbf{b} as the pulse code vector as previously described. If the time index of the discrete time processes is chosen as k keeping the convention, the discrete time sequence of

transmitted pulses can be written as $\{b_k\}$. Here, $\{b_k\}$ denotes the whole pulse code sequence, the k^{th} element of this code is, on the other and, denoted as b_k as the previous convention. Since the clutter signals are actually the echoes of the transmitted pulse, the clutter process can be considered as a channel between the transmitter and the receiver. This channel can be described by its impulse response, which is denoted as $\{c_k^n\}$. It should be noted that the time index of this sequence is k , n is a constant in this discussion and only represents which pulse is transmitted. If there is a target in the cell which is being tested, namely if the hypothesis 1 is true, then the transmitted pulse is also reflected back from that target. This is why the target is also considered as a channel between the transmitter and the receiver, the impulse response of which being denoted as $\{s_k\}$. After the pulse code is convolved with the channels, the discrete time white noise $\{n_k^n\}$ is added at the receiver side to form the discrete time observation $\{y_k^n\}$.

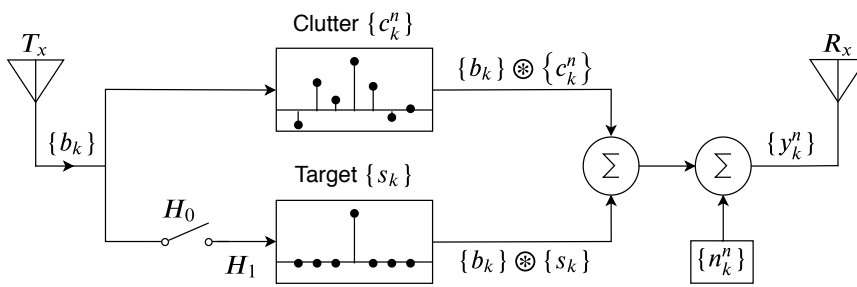


Figure 2.2: The system model between transmitter and receiver

In the next section, the slow-time index n is also going to be varied so that the slow-time vectors become matrices.

2.3 Matrix Notation and Hypothesis Testing Problem

In this section, the previously defined discrete time processes will be written compactly in a matrix form. This will simplify the calculations and enable the usage of some useful matrix identities. In addition to this, the hypothesis testing problem will be given in the matrix form, which will be the basis for the detectors to be described in Chapter 3.

Based on the previous definitions, the received clutter signal from k^{th} range cell due to n^{th} transmitted pulse is called as c_k^n . Following the same notation, the corresponding interference signal, which is called as ψ_k^n , can be defined as:

$$\psi_k^n \triangleq \{b_k\} \otimes \{c_k^n\} + n_k^n \quad (2.16)$$

where \otimes is the convolution operator, n_k^n is the additive white Gaussian noise (AWGN) included in ψ_k^n and the convolution is taken over fast-time dimension:

$$\{b_k\} \otimes \{c_k^n\} = \sum_{i=0}^{K-1} b_i c_{k-i}^n \quad (2.17)$$

for $k = 0, 1, \dots, (K-1)$. This operation can also be written in a vector and matrix multiplication form, using the previously defined $(\mathbf{c}^n)^T$, which is a row vector whose k^{th} entry is c_k^n , for $k = -(K-1), \dots, -1, 0, 1, \dots, (K-1)$. The convolution matrix of \mathbf{b} can be defined as:

$$\mathbf{B} \triangleq \begin{bmatrix} b_{K-1} & 0 & \dots & 0 \\ b_{K-2} & b_{K-1} & \dots & 0 \\ \vdots & \vdots & \vdots & \vdots \\ b_0 & b_1 & \dots & b_{K-1} \\ 0 & b_0 & \dots & b_{K-2} \\ \vdots & \vdots & \vdots & \vdots \\ 0 & 0 & \dots & b_0 \end{bmatrix}_{(2K-1) \times K} \quad (2.18)$$

Then, the result of the convolution operation in Eq. (2.17) is the k^{th} element of $(\mathbf{c}^n)^T \mathbf{B}$, which is a row vector containing K clutter returns received at the receiver.

The above operations can be done for all N pulses without any change. Then, combining the row vectors for different pulses together, the observed clutter matrix at the receiver side becomes:

$$\mathbf{\Psi} \triangleq \mathbf{CB} + \mathbf{N} = \begin{bmatrix} \psi_0 & \psi_1 & \dots & \psi_{K-1} \end{bmatrix} \quad (2.19)$$

where

$$\mathbf{N} \triangleq \begin{bmatrix} \mathbf{n}_0 & \mathbf{n}_1 & \dots & \mathbf{n}_{K-1} \end{bmatrix} \quad (2.20)$$

and the columns of the $N \times K$ matrix \mathbf{N} are the independent, identically distributed additive white Gaussian noise vectors \mathbf{n}_k . \mathbf{C} is the $N \times (2K-1)$ matrix of clutter

responses whose columns are independent, identically distributed random vectors \mathbf{c}_k , as previously defined. Then, the k^{th} column of Ψ , ψ_k , consists of a linear combination of the k^{th} column and the previous $K - 1$ columns of \mathbf{C} , the coefficients of these columns being the elements of the pulse code \mathbf{b} , and the white Gaussian noise added in the receiver side. To be more clear:

$$\psi_k \triangleq \sum_{i=0}^{K-1} b_i \mathbf{c}_{k-i} + \mathbf{n}_k \quad (2.21)$$

Thus, it can be noted that Eq. (2.19) is the matrix form of Eq. (2.16).

An important note should be that after being convolved with the pulse code \mathbf{b} , the clutter process loses its uncorrelatedness among fast-time. That is, even if the uncorrelated scattering assumption is made (\mathbf{c}_k are uncorrelated), ψ_k are correlated. This phenomenon is going to be explained in more detail in Section 2.3.2.

2.3.1 Hypothesis Testing

In this section, it will be explained that how the detection operation is conducted. The radar detection operation is a binary detection in which the two options from which the selection is done are the existence of a target at the investigated cell and the lack of one. Conventionally, the hypothesis which argues that there exists a target is called as H_1 and the opposing hypothesis is called H_0 .

Following the ongoing notation, the hypothesis testing for each range cell becomes:

$$\begin{aligned} H_0 : \mathbf{y}_k &= \psi_k, & k &= \{0, 1, \dots, K - 1\} \\ H_1 : \mathbf{y}_k &= \rho \mathbf{d}_\phi b_k + \psi_k, & k &= \{0, 1, \dots, K - 1\} \end{aligned} \quad (2.22)$$

where \mathbf{y}_k is the N -element observation vector taken at k^{th} range cell, ψ_k vectors are zero-mean circularly symmetric compound complex Gaussian vectors correlated among fast time with covariance matrix:

$$\mathbf{R}_{\psi_k} \triangleq \mathbb{E} \{ \psi_k \psi_k^H \} \quad (2.23)$$

and ρ corresponds to the unknown, non-random signal-to-noise-ratio (SNR). Since \mathbf{b} is a unit-norm vector, all SNR information is included in ρ parameter.

We can collect all K observation vectors into an observation matrix and redefine the hypothesis test in matrix form. Define $\mathbf{Y} \triangleq [\mathbf{y}_0 \ \mathbf{y}_1 \ \dots \ \mathbf{y}_{K-1}]$ and recall $\Psi = [\psi_0 \ \psi_1 \ \dots \ \psi_{K-1}]$. Then, the hypothesis test becomes:

$$\begin{aligned} H_0 : \mathbf{Y} &= \Psi \\ H_1 : \mathbf{Y} &= \rho \mathbf{d}_\phi \mathbf{b}^T + \Psi \end{aligned} \quad (2.24)$$

2.3.2 Statistics of the Interference Matrix

It can be shown that the convolution operation in fast-time does not affect the structure of the slow-time autocorrelation function of the received clutter signals. To explain this statement with an example, it is reminded that the (not-normalized) autocorrelation matrix of the clutter returns from k^{th} range cell was given as $\tau_k \mathbf{R}_c$ previously. The statement suggests that after convolving the clutter process with the pulse code, the autocorrelation of the k^{th} column of the matrix \mathbf{CB} will be $\alpha_k \mathbf{R}_c$ where α_k is the average power of the convolved clutter process at k^{th} range cell. It will also be shown that this new average power α_k will be a function of the pulse code \mathbf{b} and the average powers of the unprocessed clutter processes, τ_k , for $k = k - (K - 1), \dots, k$.

In order to examine the effects of the fast-time convolution operation on the statistical properties of the interference, the first step is to define the diagonal matrix \mathbf{T} and the operator diag so that:

$$\mathbf{T} \triangleq \text{diag}\{\sqrt{\tau_k}\}_{k=-(K-1)}^{K-1} \quad (2.25)$$

where k^{th} diagonal entry of \mathbf{T} is $\sqrt{\tau_k}$, for $k = -(K - 1), \dots, (K - 1)$. Note that this \mathbf{T} matrix is assumed to be invertible, meaning that the clutter echo coming from any range cell has nonzero power. Then, the normalized clutter return matrix \mathbf{C}' can be defined as:

$$\mathbf{C}' \triangleq \mathbf{CT}^{-1} \quad (2.26)$$

so that

$$\mathbf{C} = \mathbf{C}'\mathbf{T} \quad (2.27)$$

where the power of each column of \mathbf{C}' is 1. The next step is to rewrite the observation

matrix in Eq. (2.19) with this new notation and using vectorization:

$$\begin{aligned}
\boldsymbol{\eta} &\triangleq \text{vec}(\boldsymbol{\Psi}) = \text{vec}(\mathbf{C}'\mathbf{T}\mathbf{B} + \mathbf{N}) \\
&= \text{vec}(\mathbf{C}'\mathbf{T}\mathbf{B}) + \text{vec}(\mathbf{N}) \\
&= ((\mathbf{T}\mathbf{B})^T \otimes \mathbf{I}_N) \text{vec}(\mathbf{C}') + \text{vec}(\mathbf{N}) \tag{2.28}
\end{aligned}$$

where \mathbf{I}_N is the $N \times N$ identity matrix as defined before and \otimes is the Kronecker product operation. The last two equations in Eq. (2.28) are useful properties of vectorization operation and their proofs exist in the literature [18]. The $\boldsymbol{\eta}$ vector consists of each column of $\boldsymbol{\Psi}$ matrix concatenated vertically. Then, the autocorrelation matrices of the columns of $\boldsymbol{\Psi}$ matrix can be investigated by examining the autocorrelation matrix of the $\boldsymbol{\eta}$ vector. Writing the autocorrelation matrix of $\boldsymbol{\eta}$ yields:

$$\begin{aligned}
\mathbf{R}_\eta &= \mathbb{E} \{ \boldsymbol{\eta} \boldsymbol{\eta}^H \} \\
&= ((\mathbf{T}\mathbf{B})^T \otimes \mathbf{I}_N) \mathbb{E} \{ \text{vec}(\mathbf{C}') \text{vec}(\mathbf{C}')^H \} ((\mathbf{T}\mathbf{B})^T \otimes \mathbf{I}_N)^H + \mathbf{I}_{NK} \tag{2.29}
\end{aligned}$$

$$= ((\mathbf{T}\mathbf{B})^T \otimes \mathbf{I}_N) (\mathbf{I}_{2K-1} \otimes \mathbf{R}_c) ((\mathbf{T}\mathbf{B})^* \otimes \mathbf{I}_N) + \mathbf{I}_{NK} \tag{2.30}$$

$$= (\mathbf{B}^T \mathbf{T}^2 \mathbf{B}^* \otimes \mathbf{R}_c) + \mathbf{I}_{NK} \tag{2.31}$$

where a number of mathematical properties are used. In Eq. (2.29), the uncorrelatedness of the white noise processes for different range cells and uncorrelatedness of clutter and noise processes are used. In Eq. (2.30), the uncorrelatedness of the clutter processes for different range cells is used to form the block diagonal matrix. The fact that Hermitian of the Kronecker product of two matrices is the Kronecker product of the Hermitian of these matrices is also used in this equation. Finally in Eq. (2.31), the associativity property of the Kronecker product is used.

Returning to the investigation of the statistical properties of interference, the autocorrelations of the observation vectors $\boldsymbol{\psi}_k$ are the $N \times N$ block matrices on the diagonal of \mathbf{R}_η . It can be seen in Eq. (2.31) that each of these K blocks have the same structure, which is $\mathbf{R}_c + \mathbf{I}_N$, and different multipliers of \mathbf{R}_c which are the diagonal elements of $\mathbf{B}^T \mathbf{T}^2 \mathbf{B}^*$. Furthermore, the k^{th} diagonal element of $\mathbf{B}^T \mathbf{T}^2 \mathbf{B}^*$ can be written as the norm-square of the k^{th} column of $(\mathbf{T}\mathbf{B})^*$ or simply $\mathbf{T}\mathbf{B}$ because conjugation does not change the result of the norm-square. Left multiplying \mathbf{B} with the diagonal matrix \mathbf{T} multiplies its rows with the diagonal elements of \mathbf{T} , which are $\sqrt{\tau_k}$. In the other perspective, right multiplying \mathbf{T} with \mathbf{B} means convolving the columns of \mathbf{T} with the

pulse code \mathbf{b} . These perspectives help understanding the effect of the pulse code on the received clutter processes. Either one way or another, the resultant multiplier of the k^{th} diagonal block of \mathbf{R}_η is denoted as α_k and written as $\alpha_k = \sum_{m=0}^{K-1} |b_m|^2 \tau_{k-m}$, for $k = 0, 1, \dots, (K - 1)$. Consequently,

$$\mathbf{R}_{\psi_k} = \alpha_k \mathbf{R}_c + \mathbf{I}_N, \quad \text{for } k = 0, 1, \dots, (K - 1) \quad (2.32)$$

If the clutter environment is homogeneous, τ_k term will lose its dependence on k and $\alpha_k = \tau_k = \tau$ will be satisfied for all k because the pulse code is selected to be unit-norm. Then, \mathbf{R}_{ψ_k} will be the same for all range cells. It should be noted that these results are applicable to both the sea and the rain clutter. It is also important to notice that in heterogeneous environments, not only the pulse code used but also all other fast-time processing operations applied at the receiver affects the multiplier, or power in a sense, of the interference signals from different range cells. In fact, the same derivations will be used in Section 3.1 while fast-time preprocessing methods will be being explained.

As a final comment, it can be deduced from Eq. (2.31) that even if the uncorrelated scattering assumption is made, the cross-correlations of the observations from different range cells will not be zero but a scaled version of \mathbf{R}_c , due to the pulse code used. If it was possible to find a perfect pulse code such that $\mathbf{B}^T \mathbf{B} = \mathbf{I}_K$, then the observations from different range cells would be uncorrelated. Fortunately, the proposed detector in this thesis, which is a modified adaptive Kelly detector, uses only the slow-time correlation structure of the observations so that it is not affected by the fast-time correlation created by the pulse code.

CHAPTER 3

SLOW-TIME AND FAST-TIME PREPROCESSING METHODS FOR ADAPTIVE RADAR DETECTION

In this chapter, the signal processing stage between the reception of observations and the detection of possible targets is explained in detail. Although the contribution of this thesis seems to be a new fast and robust adaptive detector, the key differences that distinguishes this detector from already existing ones are the signal processing operations performed before the detection operation. This is why elucidating these pre-detection signal processing operations, namely the preprocessing operations, is necessary for enlightening the main focuses of this thesis, which are the improvements made on the existing detectors.

The predefined observation matrix \mathbf{Y} is preprocessed before entering the detection stage both in fast-time and slow-time dimensions in order to increase the performance of the detection. The term "fast-time preprocessing" implies that the operations will be implemented to the columns of \mathbf{Y} because each column represents the echoes from different range cells, which are sampled in fast-time. Since it is a column operation, fast-time preprocessing can be implemented with the right multiplication of \mathbf{Y} with a matrix which implements a fast-time filter, such as matched filter. Similarly, the term "slow-time preprocessing" means that the operations are conducted on the rows of \mathbf{Y} because each row represents the echoes of different pulses, which are sampled in slow-time. Because slow-time preprocessing is a row operation, it can be implemented via the left multiplication of \mathbf{Y} with a matrix which implements slow-time filtering, such as a Doppler filter bank.

The dimensions of the fast and slow-time preprocessing matrices are important in the context of this thesis. The number of columns of the fast-time preprocessing matrix

determines the number of range cells that the detector will use other than the cell under test, which are also called as secondary cells. The number of rows of the slow-time preprocessing matrix determines the dimension of these secondary cells. If there are enough number of useful secondary cells which the detector can use to estimate the interference characteristics, the detector performance will reach to its probabilistic limits. However, when the interference characteristics change rapidly in fast-time, the number of useful secondary data cannot be large enough to achieve those limits. It is known that especially when there is a small number of secondary cells available, reducing the dimension of the secondary data helps improving the detection performance [19]. Nonetheless, the dimension reduction operation is not optimized when the clutter is heterogeneous. Unlike the conventional reduced dimension techniques like Post-Doppler processing, the detector proposed in this thesis finds the dimension reducing matrix by a generalized eigenspace (GES) operation with the help of a parametric spectral estimation method. This detector pays for its complexity by increasing the detection performance, which will be shown in Chapter 5.

In the following sections, the fast and slow-time preprocessing methods will be explained separately.

3.1 Fast-Time Preprocessing

In radar signal processing, the fast-time processing, which is applied on the fast-time samples of the received echo signals, is usually used for integrating the energy of the meaningful waveform against the white noise and for determining the distance of the targets from the radar system. In the context of this thesis, the range detection is not important thus it will not be explained in detail, but the main focus is on the determination of the existence of targets. For this purpose, however, the energy integration plays an important role.

An example of a basic radar detection case will help explaining the more complex situations. If there is only a target but no clutter in front of the radar system, the radar pulse will be reflected back from the target and sampled at the receiver at some time which is not important. If the received signals are filtered with the matched

filter of the pulse, the autocorrelation sequence of the pulse code will be observed at the resultant signal. Considering the sampling at the receiver is done in correct time instants, the cell under test (CUT) will include the peak value of this autocorrelation sequence. In addition, this value will be equal to the total energy of the pulse code. This is the well-known matched filtering operation, and it is known for increasing the signal to noise ratio optimally, only when the sampling times are correct and the system is under white Gaussian noise.

Despite its optimality in increasing SNR at the CUT, matched filter also produces some unwanted distortions in the secondary cells. The autocorrelation sequence of the pulse code \mathbf{b} does not reduce to zero at the finite lags. This means that if there is a target at k^{th} range cell, after matched filtering, it will result in nonzero autocorrelation value at the cells between $k - (K - 1)$ and $k + (K - 1)$, K being the pulse length. This may create a problem if an adaptive detector would use those secondary cells to estimate the interference characteristics at the CUT because those cells contain information about not only the interference but also the target itself. This effect is called *target contamination* on the secondary cells, and it is a direct result of matched filtering with finite code lengths.

Target contamination on secondary cells is shown to be an important problem when the estimated Doppler frequency of the target is not correct, namely when there is a Doppler mismatch [20].

In the following two sections, the application of the matched filter and another fast-time preprocessing method using unitary transformation will be investigated. After these, the effect of fast-time preprocessing on the slow-time characteristics of the observations is going to be explained.

3.1.1 Matched Filter

The matched filtering is known as convolving a known signal with its time-reversed conjugate. This convolution operation can be implemented via using matrix notation, as described in Section 2.3. In that section, \mathbf{B} matrix is defined as the convolution matrix, which convolves the matrix it is multiplied from right with the pulse code

vector \mathbf{b} . Define a new matrix \mathbf{Q}_m , the subscript m denoting the matched filter:

$$\mathbf{Q}_m \triangleq \begin{bmatrix} b_0^* & 0 & \dots & 0 \\ b_1^* & b_0^* & \dots & 0 \\ \vdots & \vdots & \vdots & \vdots \\ b_{K-1}^* & b_{K-2}^* & \dots & b_0^* \\ 0 & b_{K-1}^* & \dots & b_1^* \\ \vdots & \vdots & \vdots & \vdots \\ 0 & 0 & \dots & b_{K-1}^* \end{bmatrix}_{(2K-1) \times K} \quad (3.1)$$

It can be seen that \mathbf{Q}_m has the same structure with \mathbf{B} and the only difference is that \mathbf{Q}_m is constructed with time reversed conjugate of \mathbf{b} instead of \mathbf{b} itself.

It should be noted that \mathbf{Q}_m cannot directly multiply the observation matrix \mathbf{Y} from right because \mathbf{Y} has only K columns. In order to make this multiplication possible, \mathbf{Y} matrix should be concatenated from right with $K - 1$ zero columns. If the observation matrix after fast-time filtering is denoted as $\bar{\mathbf{Y}}$ and fast-time preprocessed observation vectors are denoted as $\bar{\mathbf{y}}_k$, then:

$$\bar{\mathbf{Y}} \triangleq \begin{bmatrix} \bar{\mathbf{y}}_0 & \bar{\mathbf{y}}_1 & \dots & \bar{\mathbf{y}}_{K-1} \end{bmatrix} \triangleq \begin{bmatrix} \mathbf{Y} & \mathbf{0}_{N \times (K-1)} \end{bmatrix} \mathbf{Q}_m \quad (3.2)$$

for matched filtering. In order for compactness, the explicit notation of zero vectors will be omitted and matched filtering will be denoted as $\mathbf{Y}\mathbf{Q}_m$. Whenever the reader sees $\mathbf{Y}\mathbf{Q}_m$, s/he should understand that this is just a simple notation and the dimension mismatch between \mathbf{Y} and \mathbf{Q}_m is handled with zero-padding.

It is well known that in non-random parameter estimation under additive Gaussian noise, using matched filter (whitening matched filter for colored interference) yields the sufficient statistic, if the covariance matrix of the interference is exactly known. However in the scope of this thesis, the detectors do not know the covariance matrix of the interference, \mathbf{R}_ψ , rather they use an estimate of \mathbf{R}_ψ to realize the hypothesis test. In problems like this, matched filtering operation may not be the most suitable fast-time preprocessor. Indeed, it is shown that another fast-time preprocessing method based on a unitary transformation works better than the matched filter, especially increasing the robustness to the target Doppler mismatch [20]. In the next section, this new fast-time preprocessing method will be explained.

3.1.2 Unitary Transform

In the previous section, it is stated that the matched filter is optimal when there is no Doppler mismatch. However under Doppler mismatch, the target contaminates the secondary cells and decrease the performance of the radar system if matched filter is used. In order to eliminate the target contamination on secondary cells, another fast-time processing method is proposed in the literature [20]. This fast-time preprocessing matrix is unitary, meaning that the columns of this matrix are uncorrelated and each has unit power. Choosing a unitary matrix as the fast-time filter is completely optional but it simplifies the power calculations as all the information about power can be combined into one term. Since the proposed preprocessing matrix is a unitary one, it is denoted as \mathbf{Q}_u , and it is defined as:

$$\mathbf{Q}_u \triangleq \begin{bmatrix} \mathbf{b}^* & \mathbf{b}_1^\perp & \dots & \mathbf{b}_{K-1}^\perp \end{bmatrix}_{K \times K} \quad (3.3)$$

where \mathbf{b}_k^\perp for $k = 1, 2, \dots, (K - 1)$ are orthonormal to the \mathbf{b}^* vector, which is the complex conjugate of the pulse code. That \mathbf{Q}_u is unitary can be shown as:

$$\mathbf{Q}_u^H \mathbf{Q}_u = \mathbf{I}_K \quad (3.4)$$

because \mathbf{b} and all the other vectors orthonormal to it are unit-norm. Then, the fast-time preprocessed observation matrix and vector becomes:

$$\bar{\mathbf{Y}} \triangleq \begin{bmatrix} \bar{\mathbf{y}}_0 & \bar{\mathbf{y}}_1 & \dots & \bar{\mathbf{y}}_{K-1} \end{bmatrix} \triangleq \mathbf{Y} \mathbf{Q}_u \quad (3.5)$$

for filtering with this unitary transform. An important point which is needed to be noted here that this observation matrix \mathbf{Y} represents a bunch of observations collected through a range window used to preprocess the CUT. For example, if k^{th} range cell is the CUT, then the range cells from k to $k + K - 1$ are combined into the matrix \mathbf{Y} and multiplied with \mathbf{Q}_u from right. After the processing for k^{th} range cell is over, the CUT becomes $(k + 1)^{st}$ range cell and the unprocessed range cells from $k + 1$ to $k + K$ are combined into the matrix \mathbf{Y} and multiplied with \mathbf{Q}_u from right. Then, the reconstruction of \mathbf{Y} goes on in a similar fashion via the sliding window for other possible CUTs. The range cells outside this window are ignored in the processing of the CUT even if they may possibly carry some useful information.

It should be noted that \mathbf{Q}_u is not essentially a convolution matrix; therefore, this kind of fast-time preprocessing cannot be represented as a single filtering operation like in

the case of matched filtering. On the contrary, multiplying the observations with \mathbf{Q}_u can be considered as taking the inner product of each range cell under consideration with different K -length vectors. The inner product of a range cell with a K -length vector can also be considered as applying a K -length filter to that range cell and taking the K^{th} element of the result. In this point of view, the filter output at the CUT is the same as the matched filter output, and the other range cells are filtered with different filters, all being orthogonal to the matched filter.

It should also be noted that the first column of \mathbf{Q}_u is the same as the first column of the matched filter \mathbf{Q}_m , except for the zero terms in \mathbf{Q}_m needed for convolution operation. This is the optimality of matched filter, that is, if there is a target echo in the received signal, it will create the maximum amount of energy if it is filtered with its conjugate. However, the other columns of \mathbf{Q}_u are orthonormal to \mathbf{b} , so if there is a target echo in the secondary cells, it will give zero energy if it is filtered with vectors orthonormal to it. Using such a matrix as the fast-time preprocessor, the target signal contamination on the secondary cells are eliminated, increasing the detector robustness to the target Doppler mismatch. This kind of fast-time preprocessing also increases the slow-time preprocessing performance because the slow-time covariance matrix of the interference is better estimated using target contamination free secondary cells rather than contaminated ones.

In this kind of preprocessing, it is assumed that the echo signal from the target is the same as the pulse code used. In reality, the target echo has an extra phase term due to the radial velocity of the target, namely Doppler effect. However in this thesis, stop-and-hop assumption is used. This assumption states that the targets stop moving just after the pulse is transmitted and remain constant until the pulse reaches the receiver. This way, the Doppler shift of the pulse code is eliminated. It should be noted that this assumption is only valid when the pulse length is small enough, which is considered to be true in this thesis.

A final note on the fast-time preprocessing method should be that it does not consider the case in which there are targets in the secondary range cells. This method tries to purify the secondary cells only from the contamination of the possible target in the CUT. If there are targets in the secondary cells, the fast-time preprocessor does

nothing to eliminate them, and the overall processor treats those targets as interference sources. This scenario is not investigated in this thesis, relevant to the single target assumption.

As described in Section 2.3.2, multiplying the interference matrix with another matrix from right keeps the covariance structure of the interference the same but may change the power of the interference vectors from different range cells differently. Since the fast-time preprocessing is applied as a right-multiplication, it has the same effect on the observation matrix. In the next section this effect will be highlighted.

3.1.3 Effect of Fast-time Preprocessing on the Slow-time Characteristics of the Interference

The received interference signals are collected in the matrix Ψ and multiplied with the fast-time preprocessing matrix \mathbf{Q} from right in the receiver. $\bar{\Psi}$ is defined as the fast-time preprocessed interference matrix:

$$\bar{\Psi} \triangleq \Psi \mathbf{Q} \quad (3.6)$$

whose columns are fast-time preprocessed interference vectors:

$$\bar{\psi}_k \triangleq \Psi \mathbf{Q}(:, k) \quad (3.7)$$

where $\mathbf{Q}(:, k)$ represents the k^{th} column of \mathbf{Q} . Applying the same procedure used in Eq. (2.28), the vectorized form of $\bar{\Psi}$ can be written as:

$$\begin{aligned} \bar{\boldsymbol{\eta}} &\triangleq \text{vec}(\bar{\Psi}) = \text{vec}(\Psi \mathbf{Q}) \\ &= (\mathbf{Q}^T \otimes \mathbf{I}_N) \text{vec}(\Psi) = (\mathbf{Q}^T \otimes \mathbf{I}_N) \boldsymbol{\eta} \end{aligned} \quad (3.8)$$

Following the same steps in Eqs. (2.29) to (2.31):

$$\begin{aligned} \mathbf{R}_{\bar{\boldsymbol{\eta}}} &\triangleq \mathbb{E} \{ \bar{\boldsymbol{\eta}} \bar{\boldsymbol{\eta}}^H \} \\ &= (\mathbf{Q}^T \otimes \mathbf{I}_N) \mathbb{E} \{ \boldsymbol{\eta} \boldsymbol{\eta}^H \} (\mathbf{Q}^T \otimes \mathbf{I}_N)^H \\ &= (\mathbf{Q}^T \otimes \mathbf{I}_N) ((\mathbf{B}^T \mathbf{T}^2 \mathbf{B}^* \otimes \mathbf{R}_c) + \mathbf{I}_{NK}) (\mathbf{Q}^* \otimes \mathbf{I}_N) \\ &= (\mathbf{Q}^T \otimes \mathbf{I}_N) ((\mathbf{B}^T \mathbf{T}^2 \mathbf{B}^* \otimes \mathbf{R}_c) + (\mathbf{I}_K \otimes \mathbf{I}_N)) (\mathbf{Q}^* \otimes \mathbf{I}_N) \\ &= (\mathbf{Q}^T \mathbf{B}^T \mathbf{T}^2 \mathbf{B}^* \mathbf{Q}^*) \otimes \mathbf{R}_c + (\mathbf{Q}^T \mathbf{Q}^*) \otimes \mathbf{I}_N \end{aligned} \quad (3.9)$$

The first term in Eq. (3.9) is similar to the first term in Eq. (2.31), and it corresponds to the clutter part of the interference. It shows that each of the autocorrelation matrices of the fast-time preprocessed interference vectors $\bar{\psi}_k$, which are the $N \times N$ block diagonal matrices of the $\mathbf{R}_{\bar{\eta}}$, has the same structure \mathbf{R}_c for the clutter part. On the other hand, the power of the clutter process in the k^{th} range cell is the k^{th} diagonal element of the matrix $\mathbf{Q}^T \mathbf{B}^T \mathbf{T}^2 \mathbf{B}^* \mathbf{Q}^*$, which is equal to the norm square of the k^{th} column of the matrix $\mathbf{T} \mathbf{B} \mathbf{Q}$.

The second term in Eq. (3.9) is the noise part of the autocorrelation matrix of the fast-time preprocessed interference matrix. This term suggests that if \mathbf{Q} is a unitary matrix, which is the case in this thesis, $\mathbf{Q}^T \mathbf{Q}^* = \mathbf{I}_K$ and therefore the fast-time pre-processing operation affects neither the power nor the structure of the autocorrelation matrix of the noise process.

In the next section, the slow-time preprocessing method used in this thesis will be thoroughly described, along with some theoretical discussions and the comparison between the proposed method and the conventional counterpart of it.

3.2 Slow-Time Preprocessing

In order to increase the performance of the detector against the clutter, or more generally the interference, some slow-time operations can be applied to the raw observation data before it is fed to the detector. These operations are called as slow-time preprocessing, and they are implemented as a left multiplication in the notation of this thesis.

Throughout this thesis, the slow-time preprocessing matrix is denoted as \mathbf{U} , and this processing is applied to the observations via $\mathbf{U}^H \mathbf{Y}$. \mathbf{U} is, in general, an $N \times D$ matrix, so that after the slow-time preprocessing, the observations from each range cell becomes D -element vectors. This means that the slow-time preprocessing operation takes the observations from the N -dimensional observation space and map them to a D -dimensional subspace of it. D is called as the dimension of the subspace, and naturally, $D \leq N$.

The selection of a D -dimensional subspace inside an N -dimensional one is a problem

with various solutions. The main consideration in the solution of this problem should be increasing the detector performance. To this aim, it is clear that the selection must be in such a way that the echoes coming from the targets must be inside the selected subspace, as they are the signals which are to be detected. Besides this, if the detector will not use any other interference suppression techniques, the subspace should include as little interference signal as possible. On the other hand, if the detector will implement another interference suppression technique and it needs to estimate the interference characteristics, then an amount of interference must be included in the selected subspace in order for the detector to make the correct estimations. An example of such a detector is the adaptive Kelly detector which uses the data from secondary range cells for the estimation of interference statistics in CUT, to suppress the unwanted signals. If the subspace that adaptive Kelly detector works on includes only the useful target signals, then the detector will make a wrong interference estimation and suppress this useful signals.

The previous discussion showed that the slow-time preprocessing matrix depends on the type of the detector, the dimension of the subspace and how that subspace is selected. Fortunately, there are some optimal methods found in the literature which helps selecting the correct slow-time preprocessing matrix [20]. In the next section, an optimal subspace construction method, its optimality limitations and its role in the proposed detector in this thesis will be explained.

3.2.1 Optimal Right Subspace Construction for Parametric Clutter Models: Dimension Reduction with Generalized Eigenspace

Generalized eigenvalue problem of two matrices \mathbf{A} and \mathbf{B} tries to find the generalized eigenvectors \mathbf{e}_n and corresponding generalized eigenvalues λ_n which satisfy:

$$\mathbf{A}\mathbf{e}_n = \lambda_n\mathbf{B}\mathbf{e}_n \quad (3.10)$$

The generalized eigenvalue problem is, as its name suggests, a general problem and it can be reduced to simpler problems in some special cases. One such case, which is used in the scope of this thesis, is the one in which \mathbf{B} is invertible. In that case, the

generalized eigenvalue problem can be rewritten as:

$$\mathbf{B}^{-1}\mathbf{A}\mathbf{e}_n = \lambda_n\mathbf{e}_n \quad (3.11)$$

which is the standard eigenvalue problem for $\mathbf{B}^{-1}\mathbf{A}$. Intuitively, this eigenvalue problem finds the basis vectors of a space which is away from \mathbf{B} and near to \mathbf{A} . This operation is also mathematically proved to be the optimal dimension reduction technique with respect to several criteria when \mathbf{A} is selected to be the target signal's covariance matrix and \mathbf{B} is selected as the covariance matrix of the interference [20].

Since the resultant eigenvectors of generalized eigenvalue problem can be considered as the basis vectors of a vector space, the operation of finding the generalized eigenvectors of two matrices is also called as *Generalized Eigenspace (GES)* operation and this notation is used throughout this thesis.

In this thesis, the GES operation is used imperfectly in finding the optimum slow-time preprocessing matrix. In order to make use of the optimality of the GES operation, the detector must know the target signal and interference covariance matrices perfectly. However, both the exact velocity of the target and the interference characteristics are unknown at the receiver side, so the estimations of the covariances must be used in the detector.

Throughout this thesis, all estimations are denoted with a hat ($\hat{}$) symbol above the estimated variable's name. Following this notation, the estimation of the interference covariance matrix (ICM) is denoted as $\hat{\mathbf{R}}_{\nu}$ and the estimation of the target signal's covariance matrix is denoted as $\hat{\mathbf{R}}_s$. The estimation processes will be explained later in Section 3.2.3. The N generalized eigenvectors of $\hat{\mathbf{R}}_s$ and $\hat{\mathbf{R}}_{\nu}$ are found by solving for \mathbf{e}_n the generalized eigenvalue problem:

$$\hat{\mathbf{R}}_s\mathbf{e}_n = \lambda_n\hat{\mathbf{R}}_{\nu}\mathbf{e}_n \quad (3.12)$$

If the N eigenvalues are sorted in descending order such that $\lambda_1 > \lambda_2 > \dots > \lambda_N$, then, concatenating the eigenvectors corresponding to the largest D eigenvalues gives the dimension reducing matrix proposed to be used in slow-time preprocessing:

$$\mathbf{U} = [\mathbf{e}_1 \quad \mathbf{e}_2 \quad \dots \quad \mathbf{e}_D] \quad (3.13)$$

It should be noted that if $\hat{\mathbf{R}}_{\nu}$ is invertible, the generalized eigenvectors of $\hat{\mathbf{R}}_s$ and $\hat{\mathbf{R}}_{\nu}$ are also the eigenvectors of $(\hat{\mathbf{R}}_{\nu})^{-1}\hat{\mathbf{R}}_s$. Therefore intuitively, the \mathbf{U} matrix represents

a subspace which escapes the estimated interference space and includes the estimated target signal space. The optimality of this kind of slow-time preprocessing must be checked in future works.

In the next section, a simpler and widely used dimension reduction technique for slow-time preprocessing will be explained. This technique does not need an estimation of interference subspace by itself, so it is a non-adaptive technique and it works faster than the proposed adaptive technique. Comparing the detection performances of these two methods is thus essential for the sake of the significance of the proposed slow-time preprocessing technique in this thesis.

3.2.2 Conventional Non-Adaptive Technique Based on DFT Subspace: Post-Doppler Processing

Even if the slow-time characteristics of the interference are not known or estimated, the dimension reduction can be done by using simpler non-optimal dimension reduction matrices. One such matrix is the DFT matrix and the technique using DFT matrix to reduce the dimension of the observations is called as *Post-Doppler Processing*. Before getting in the details of this technique, the DFT matrix should be defined.

The \mathbf{d}_ϕ vector defined in Eq. (2.2) was written in terms of the phase difference of the two consecutive slow-time samples when the target is moving radially with respect to the radar system with a Doppler frequency f_d . The same vector is rewritten here with the name of \mathbf{d}_{f_d} in terms of the target Doppler frequency f_d in order to investigate the DFT matrix:

$$\mathbf{d}_{f_d} = \begin{bmatrix} e^{j2\pi f_d(0/\text{PRF})} \\ e^{j2\pi f_d(1/\text{PRF})} \\ \vdots \\ e^{j2\pi f_d((N-1)/\text{PRF})} \end{bmatrix} = \begin{bmatrix} 1 \\ e^{j2\pi f_d T} \\ \vdots \\ e^{j2\pi f_d (N-1)T} \end{bmatrix} \quad (3.14)$$

The structure of the \mathbf{d}_{f_d} vector can be used to construct a Vandermonde matrix:

$$\mathbf{U}_{DFT} = \begin{bmatrix} \mathbf{d}_0 & \mathbf{d}_{1/NT} & \mathbf{d}_{2/NT} & \dots & \mathbf{d}_{(N-1)/NT} \end{bmatrix} \quad (3.15)$$

$$= \begin{bmatrix} 1 & 1 & 1 & \dots & 1 \\ 1 & \omega^{1.1} & \omega^{1.2} & \dots & \omega^{1.(N-1)} \\ 1 & \omega^{2.1} & \omega^{2.2} & \dots & \omega^{2.(N-1)} \\ \vdots & \vdots & \vdots & \ddots & \vdots \\ 1 & \omega^{(N-1).1} & \omega^{(N-1).2} & \dots & \omega^{(N-1).(N-1)} \end{bmatrix} \quad (3.16)$$

where $\omega = e^{j2\pi/N}$. The \mathbf{U}_{DFT} matrix is called as the DFT matrix because for an N -element vector \mathbf{v} , $(\mathbf{U}_{DFT})^H \mathbf{v}$ operation gives the N -element Discrete Fourier Transform of \mathbf{v} . The columns of \mathbf{U}_{DFT} are called as the first DFT bin, the second DFT bin, etc.

In radar signal processing, each DFT bin is actually a steering vector of its corresponding frequency. That is, if the N slow-time samples are taken with a sampling period T , the n^{th} DFT bin is the steering vector of the Doppler frequency $f_d = ((n - 1)/NT)$ for $n = 1, 2, \dots, N$. On the other hand, the DFT bins can also be considered as the matched filters for the echo signals coming from the targets whose Doppler frequencies are exactly the multiples of $1/NT = \text{PRF}/N$.

In post-Doppler processing, the dimension reduction operation is conducted by using a matrix whose columns are some of the DFT bins. For example, if the target Doppler frequency is estimated to be $1/NT$ and the dimension in which the observations are to be reduced is 5, then, the dimension reducing matrix will be:

$$\mathbf{U} = \begin{bmatrix} \mathbf{d}_{(N-1)/NT} & \mathbf{d}_0 & \mathbf{d}_{1/NT} & \mathbf{d}_{2/NT} & \mathbf{d}_{3/NT} \end{bmatrix} \quad (3.17)$$

The periodicity of the DFT bins can be seen in Eq. (3.17), as the first Doppler bin is preceded by the last one in the increasing order of frequencies. This periodicity is caused by nothing but the periodicity of discrete-time complex exponentials with 2π .

The \mathbf{U} matrix, when applied to the fast-time preprocessed observation matrix $\bar{\mathbf{Y}}$, maps the observations taken in N -dimensional space to vectors in a D dimensional subspace. The new subspace is centered on the estimated target signal's steering vector, making sure that the target signal is included in the subspace. The other vectors in the subspace, whose amount is determined by the dimension of \mathbf{U} , are included

because the detector shall need them to estimate the interference characteristics later. It can be deduced that in this technique, first the dimension of the observations are reduced using the target's estimated Doppler frequency, and then another signal processing is done with the aim of estimating the interference characteristics and ultimately eliminating the interference. Since the interference elimination is conducted after applying a Doppler processing, the post-Doppler processing name is relevant.

Post-Doppler processing is significantly easy to implement, therefore it is a powerful alternative reduced dimension signal processing method to the one using GES operation. However, the drawback of post-Doppler processing is its performance. When the slow-time characteristic of the interference is not taken into consideration during the dimension reduction, a large amount of noise is allowed into the constructed subspace. As it will be seen in Chapter 5, this will greatly reduce the performance of the detectors using post-Doppler processing. Opposite to this, detectors using GES for dimension reduction eliminates most part of the interference already before conducting the detection operation. This is why the detectors using GES operation outperform the ones using post-Doppler processing as it will be seen in Chapter 5.

In the next section, it will be explained that how the GES operation is used adaptively in the proposed detector, or specifically, how $\hat{\mathbf{R}}_s$ and $\hat{\mathbf{R}}_\phi$ are constructed.

3.2.3 Adaptive Construction of Generalized Eigenspace with Parametric Spectral Estimation Methods

Adaptive construction of GES requires the estimations of the signal and interference covariance matrices, $\hat{\mathbf{R}}_s$ and $\hat{\mathbf{R}}_\psi$. $\hat{\mathbf{R}}_s$ requires predicting the target's Doppler frequency, which can be done via spectral estimation methods after a successful elimination of interference. However in general, the target is assumed to have one Doppler frequency among a number of predetermined Doppler frequencies. In other words, a number of filters adjusted for some Doppler frequencies are constructed and the received observations are filtered by all these filters at the same time. This kind of filtering is called as *Doppler filter bank*, and it helps bypassing the estimation of target's exact Doppler frequency while allowing an amount of mismatch between this real Doppler frequency and the ones for which the filters are adjusted. $\hat{\mathbf{R}}_\psi$, on the

other hand, requires a more complicated spectral estimation because the interference is not a target with a fixed Doppler frequency but instead is a cluster of different targets whose Doppler frequencies are spread all over the Doppler frequency band in use. Although there are lots of spectral estimation methods in the literature, the Burg's method [21] is the one being focused on in this thesis, due to some advantages which are going to be highlighted in Section 3.2.3.2.

In the next two sections, the estimation processes of $\widehat{\mathbf{R}}_s$ and $\widehat{\mathbf{R}}_p$ will be explained in detail.

3.2.3.1 Estimation of Signal Subspace

In Section 3.2.2, the steering vector for a target having Doppler frequency f_d was denoted as \mathbf{d}_{f_d} . The conventional post-Doppler processing used this \mathbf{d}_{f_d} vector for different predetermined f_d values. In reality, the possible values that a target's radial velocity can have are infinitely many. This is why the exact Doppler frequency of a target signal, the exact f_d , cannot be known at the receiver. Using Doppler filter banks enables the radar signal processors to estimate the target's Doppler frequency with an error which can be reduced as much as it is required. The error in the estimated target Doppler frequency is called as *Doppler mismatch*. It should be noted that an amount of Doppler mismatch is unpreventable in real detectors, therefore robustness to Doppler mismatch is an important property for the radar detectors.

In the problem of this thesis, N slow-time samples are taken from each range cell, meaning that in slow-time dimension, the observations are N -element vectors. Using a Doppler filter bank, on the other hand, is similar to taking the DFT of these observation vectors. It is known that the number of DFT points must be larger than or equal to N in order for the results not to be aliased [22]. Using larger number of DFT points gives more resolution in the frequency domain, decreasing the maximum possible Doppler mismatch, in exchange for the receiver complexity. The main goal of this thesis is proposing a radar detector which works with high-performance and high-speed at the same time, so the minimum number of Doppler filters are used in the scope of this thesis. In other words, there are N Doppler filters at the receiver side which are placed uniformly on the frequency axis in this thesis.

The first filter in the Doppler filter bank is assumed to be placed on zero frequency (DC filter). If the filter frequencies in the Doppler filter bank are denoted as f_i , then:

$$f_i = i/NT, \quad i = 0, 1, \dots, (N - 1) \quad (3.18)$$

The radar detector filters the incoming observation data from each range cell using all N Doppler filters separately and produces N decisions about a target's existence. If any of the decisions are "1", the detector claims "there is a target" in the corresponding range cell. The detector is not working as a target velocity estimator in the scope of this thesis, therefore it is not important in which filter frequency the detector finds a target. This detection rule can also be considered as the detector gives a "1" if the filter output with maximum SINR results in a "1", and "0" otherwise. This is because the higher the SINR in the filter output, the more possible the detector claims the existence of the target. If the highest-SINR filter results in a "no target" decision, other filters make the same decision for sure.

Each target steering vector \mathbf{d}_{f_d} has the highest correlation with the Doppler filter whose frequency f_i is the closest to f_d . That is, if a target has $f_d = 3.2/NT$ and f_i are selected as in Eq. (3.18), the filter with $f_i = 3/NT$ gives the highest correlation with f_d , and consequently this filter's decision will be dominant decision among all filters. If the target has $f_d = 3.6/NT$, then the decision of the target with $f_i = 4/NT$ would dominate. It is assumed that if the target has exactly $f_d = 3.5/NT$, whether the 4th or the 5th filter dominates is not important, those two would give the same results anyway.

From a different point of view, each filter in the Doppler filter bank is responsible for filtering the target signals whose Doppler frequencies are nearest. Then for each Doppler filter, the possible values of target signal's Doppler frequency are limited. Following this reasoning, the i^{th} filter in the filter bank is responsible for filtering the target signals whose Doppler frequencies are in the interval:

$$F_i \triangleq \left[\frac{f_{i-1} + f_i}{2}, \frac{f_i + f_{i+1}}{2} \right] \quad (3.19)$$

for $i = 0, 1, \dots, N - 1$. It should be noted that $f_N = f_0$ and $f_{-1} = f_{N-1}$ because of the periodicity of the DFT bins.

In this thesis, the estimation of target signal covariance matrix is the average of the

covariance matrices of the possible target steering vectors in the interval described in Eq. (3.19). The number of covariance matrices averaged is denoted as N_f . Then, the estimate of target signal covariance matrix for i^{th} filter is:

$$\widehat{\mathbf{R}}_{s,i} = \frac{1}{N_f} \sum_{f_d \in F_i} \mathbf{d}_{f_d} \mathbf{d}_{f_d}^H \quad (3.20)$$

where N_f can be indefinitely large. If $N_f = 1$, then $\widehat{\mathbf{R}}_{s,i} = \mathbf{d}_{f_i} \mathbf{d}_{f_i}^H$ would be satisfied. This estimate has a rank of only one, which is not wanted because the target signal subspace is needed to include the possible target steering vectors having Doppler mismatch. Increasing N_f clearly increases the rank of $\widehat{\mathbf{R}}_{s,i}$. However, since the steering vectors being averaged are centered on the i^{th} DFT bin, $\widehat{\mathbf{R}}_{s,i}$ has one prominent eigenvalue whose corresponding eigenvector is \mathbf{d}_{f_i} .

3.2.3.2 Estimation of Interference Subspace

In this thesis, the estimators of the interference subspace assume that the interference process is an auto-regressive process and try to find the underlying AR coefficients. An AR process is a random process whose elements can be expressed as a function of its p past elements and a noise term. If X is a zero-mean discrete-time AR random process and X_t is the random variable which is drawn from the ensemble of X at discrete-time t , then:

$$X_t = \sum_{k=1}^p -a_k X_{t-k} + n_t \quad (3.21)$$

where p is a positive integer and it is called as the order of the AR process, or simply AR order, $\{a_k\}_{k=1}^p$ are called as the AR coefficients of the process, $\sum_{k=1}^p -a_k X_{t-k}$ is a linear predictor of X_t and n_t is the prediction error at time t . The AR parameter estimators usually try to minimize this prediction error.

There are various methods to estimate the AR coefficients of a random process from the observations of that process [21, 23]. In this thesis, Burg's parametric spectral estimation method is used to achieve this goal. Burg's method is known as its ability to find good estimates for AR coefficients especially when there is a small amount of observation data, which is why it is suitable for being used in this thesis in which the observations are limited.

The details of Burg's parametric spectral estimation method is provided in Appendix A. In this section, how Burg's method is integrated into the estimation of ICM is explained in paragraphs for convenience.

Yule-Walker Equations

The AR coefficients and the autocorrelation sequence of a random process are related with each other through Yule-Walker (YW) equations [23]. If r_m denotes the autocorrelation of the random process at lag m , then the value of r_m can be found with the equation:

$$r_m = - \sum_{j=1}^p a_j r_{m-j} \quad (3.22)$$

If Eq. (3.22) is written for $m = \{1, 2, \dots, p\}$ in the rows of a matrix, the matrix form of YW equations are obtained:

$$\begin{bmatrix} r_1 \\ r_2 \\ \vdots \\ r_{p-1} \\ r_p \end{bmatrix} = - \begin{bmatrix} r_0 & r_{-1} & \dots & r_{2-p} & r_{1-p} \\ r_1 & r_0 & \dots & r_{3-p} & r_{2-p} \\ \vdots & \vdots & \ddots & \vdots & \vdots \\ r_{p-2} & r_{p-3} & \dots & r_0 & r_{-1} \\ r_{p-1} & r_{p-2} & \dots & r_1 & r_0 \end{bmatrix} \begin{bmatrix} a_1 \\ a_2 \\ \vdots \\ a_{p-1} \\ a_p \end{bmatrix} \quad (3.23)$$

where $r_{-m} = r_m^*$ can be used to determine the negative lags of the autocorrelation sequence.

It should be noted that in Eq. (3.23), the matrix is a valid autocorrelation matrix and it is invertible so that the equations are solvable for $\{a_k\}_{k=1}^p$. This means that if the autocorrelation sequence of a random process is exactly known up to lag p , then the AR coefficients of that random process up to order p can be found without any errors. However in real applications, the time during which the process is observed and stay wide-sense stationary is limited. This cause the autocorrelation sequence of the processes cannot be known exactly, neither can the AR coefficients. As a result, the estimation of AR coefficients gets harder as the time the process is observed gets smaller.

A significant characteristic of the proposed detector in this thesis is that it works with reduced dimension data in order to adapt itself to the changing environment faster.

The discussion in the above paragraph shows that this feature of the detector creates a challenge in estimating the ICM because working in reduced dimension means having a smaller number of slow-time samples of the interference process. In Chapter 4 of this thesis, the performance loss of the proposed detector compared to the same detector knowing the ICM perfectly is indicated explicitly. This shows that although performing better than all other detectors to compare in this thesis, the proposed detector can be improved by estimating the ICM better. In other words, better spectral estimation methods may increase the performance of the detector proposed in this thesis. Nevertheless in this thesis, Burg's method is selected to be used as the estimator of AR coefficients. In the next paragraph, a recursive algorithm which is used in Burg's method and also in the ICM estimating algorithm proposed in this thesis is going to be introduced.

Reverse Levinson-Durbin Recursion

The matrix equation given in Eq. (3.23) requires a matrix inversion. There are several algorithms with different complexities for applying the matrix inversion operation. One of these algorithms is Levinson-Durbin Recursion, which is a widely-used algorithm whose details are out of scope for this thesis [23]. On the other hand, this algorithm can be reversed so that given the AR coefficients, the matrix equation in Eq. (3.23) can be solved for the values of autocorrelation sequence [24]. This method first converts AR coefficients to so called *reflection coefficients* with an algorithm called Stepdown and then use Levinson-Durbin Recursion to swap from reflection coefficients to autocorrelation sequence. This process is called as Stepdown Levinson Recursion or Reverse Levinson-Durbin Recursion, and it is used in some of the detectors explained in Chapter 4 of this thesis. Burg's method also uses the reflection coefficients to find the AR coefficient estimates from the observations as explained in Appendix A.

In the next paragraph, how YW equations can be used to generate autocorrelation estimates up to infinite lag is going to be investigated.

Extrapolating the Autocorrelation Sequence

There exists an important and interesting issue about YW equations that they give

rise to the opportunity to estimate the autocorrelation sequence up to infinite lag. When equation Eq. (3.22) is examined, it can be seen that with the knowledge of p AR coefficients and p autocorrelation lags from $(m - p)$ to $(m - 1)$, the m^{th} autocorrelation lag can be calculated. With this new p -length autocorrelation sequence from $(m - p + 1)$ to (m) and p AR coefficients, $(m + 1)^{st}$ autocorrelation lag can be calculated by solving Eq. (3.23). Applying the same operations repeatedly, the autocorrelation sequence can be extrapolated infinitely. However in fact, also intuitively, this does not mean that the estimation errors can be reduced infinitely. In a hypothetical situation, an N -length observation vector may be present. With this vector, the N -length autocorrelation sequence can be estimated via different methods [23] and this estimation has an error by nature. Extrapolating this sequence to an M -length sequence ($M > N$) does not increase the accuracy of the estimation unlike having an M -length observation vector beforehand. This is because the real information is present only in the observations and applying some operations on these observations cannot increase the amount of information they carry, if not reducing it. Nevertheless in Chapter 4, the extrapolation operation is used in some detectors that find the $N \times N$ ICM estimate by using p^{th} order AR coefficients where $N > p$.

In the next paragraph, the ICM estimating algorithm of this thesis is going to be explained. This algorithm uses Burg's method, reverse Levinson-Durbin recursion, the extrapolation operation and averaging in order to estimate the ICM from the L observation vectors taken from the secondary cells which are fast-time preprocessed and cleansed from target contamination effects.

Estimating the ICM

The ICM estimating algorithm uses L secondary range cells in N dimension, and finds an $N \times N$ Toeplitz matrix as the ICM estimate. This algorithm takes advantage of Burg's parametric spectral estimation method, which is explained in Appendix A, in finding the p^{th} order AR coefficients from N -element observation vectors. The estimated p^{th} order AR coefficients for l^{th} secondary cell are denoted by $\{\hat{a}_k^l\}_{k=1}^p$. These AR coefficients can be turned into autocorrelation estimates $\hat{r}_{\psi_l}[m]$, $m = 0, 1, \dots, p - 1$ by using the reverse Levinson-Durbin recursion [24]. Then, these autocorrelation lags and the AR parameters are used to extrapolate the

autocorrelation sequence up to length N by simply using the Yule-Walker equations.

If the autocorrelation vector estimate of interference process ψ at the l^{th} secondary cell, ψ_l , is defined as:

$$\hat{\mathbf{r}}_{\psi_l} \triangleq [\hat{r}_{\psi_l}[0] \quad \hat{r}_{\psi_l}[1] \quad \dots \quad \hat{r}_{\psi_l}[N-1]]^T \quad (3.24)$$

then the covariance estimate of the interference is given as:

$$\hat{\mathbf{R}}_{\psi} = \frac{1}{L} \sum_{l=1}^L \text{Toeplitz}(\hat{\mathbf{r}}_{\psi_l}) = \frac{1}{L} \sum_{l=1}^L \hat{\mathbf{R}}_{\psi_l} \quad (3.25)$$

where

$$\hat{\mathbf{R}}_{\psi_l}(i, j) = \hat{r}_{\psi_l}[i - j], \quad i, j = 1, 2, \dots, N \quad (3.26)$$

The Toeplitz operation, as it is defined before, takes as input a vector or a sequence of scalars and creates the optionally complex Toeplitz matrix whose first column is the input vector or sequence of scalars. Thus, from Eq. (3.25) it can be seen that $\hat{\mathbf{R}}_{\psi}$ is the average of the Toeplitz covariance matrices found from each of the L secondary cells.

The process explained above is summarized in Algorithm 3.1.

Algorithm 3.1 Calculation of the ICM Estimate From AR Parameters

Initialize with the fast-time preprocessed observation matrix $\bar{\mathbf{Y}}$

for $l = 1$ to L **do**

Use Algorithm A.1 to find $\{\hat{a}_k^l\}_{k=1}^p$ and $\hat{\tau}$ from $\bar{\mathbf{y}}_l$

Use Reverse Levinson Recursion to find $\hat{r}_{\psi_l}[m]$, $m = 0, 1, \dots, p-1$, from $\{\hat{a}_k^l\}_{k=1}^p$ and $\hat{\tau}$

Extrapolation Algorithm:

for $m = p$ to $N-1$ **do**

Use YW equations to find $\hat{r}_{\psi_l}[m]$ from $\hat{r}_{\psi_l}[i]$, $i = m-p, \dots, m-1$, and $\{\hat{a}_k^l\}_{k=1}^p$

end for

$\hat{\mathbf{R}}_{\psi_l} = \text{Toeplitz}(\hat{r}_{\psi_l}[m], m = 0, 1, \dots, N-1) \quad (\hat{\mathbf{R}}_{\psi_l}(i, j) = \hat{r}_{\psi_l}(i - j))$

end for

Find the ICM Estimate: $\hat{\mathbf{R}}_{\psi} = \frac{1}{L} \sum_{l=1}^L \hat{\mathbf{R}}_{\psi_l}$

With the help of the parametric spectral estimation methods and GES operation, the slow-time preprocessing matrix is completed. Using the left and right preprocessing matrices, the dimension of the observation matrix \mathbf{Y} is reduced to $D \times L$ and the next step is the detection operation. Different detector schemes are explained in a comparative manner in Chapter 4.

CHAPTER 4

DETECTORS

In this chapter, the seven different detectors which are examined in this thesis are going to be described. These detectors are chosen to put emphasis on the significant properties of the proposed detector like two-stage adaptation, dimension reduction and fast conversion rate.

This chapter begins with a tree of detectors, given in Fig. 4.1, in which the seven detectors are classified and put under groups. This diagram helps understanding the differences and similarities between the detectors and summarizes the rest of the chapter. In the remaining sections of this chapter, the detectors and their hypothesis tests are explained in detail.

An important note for this chapter is that the threshold γ in each detection test is not determined by the detectors. The Monte-Carlo simulations are conducted and the threshold values are determined to get exactly $10^{-3} P_{fa}$. In real cases, the thresholds must be determined by the detectors; however, using training pulses and acquiring an empirical threshold is also a solution if the interference is stationary for a while.

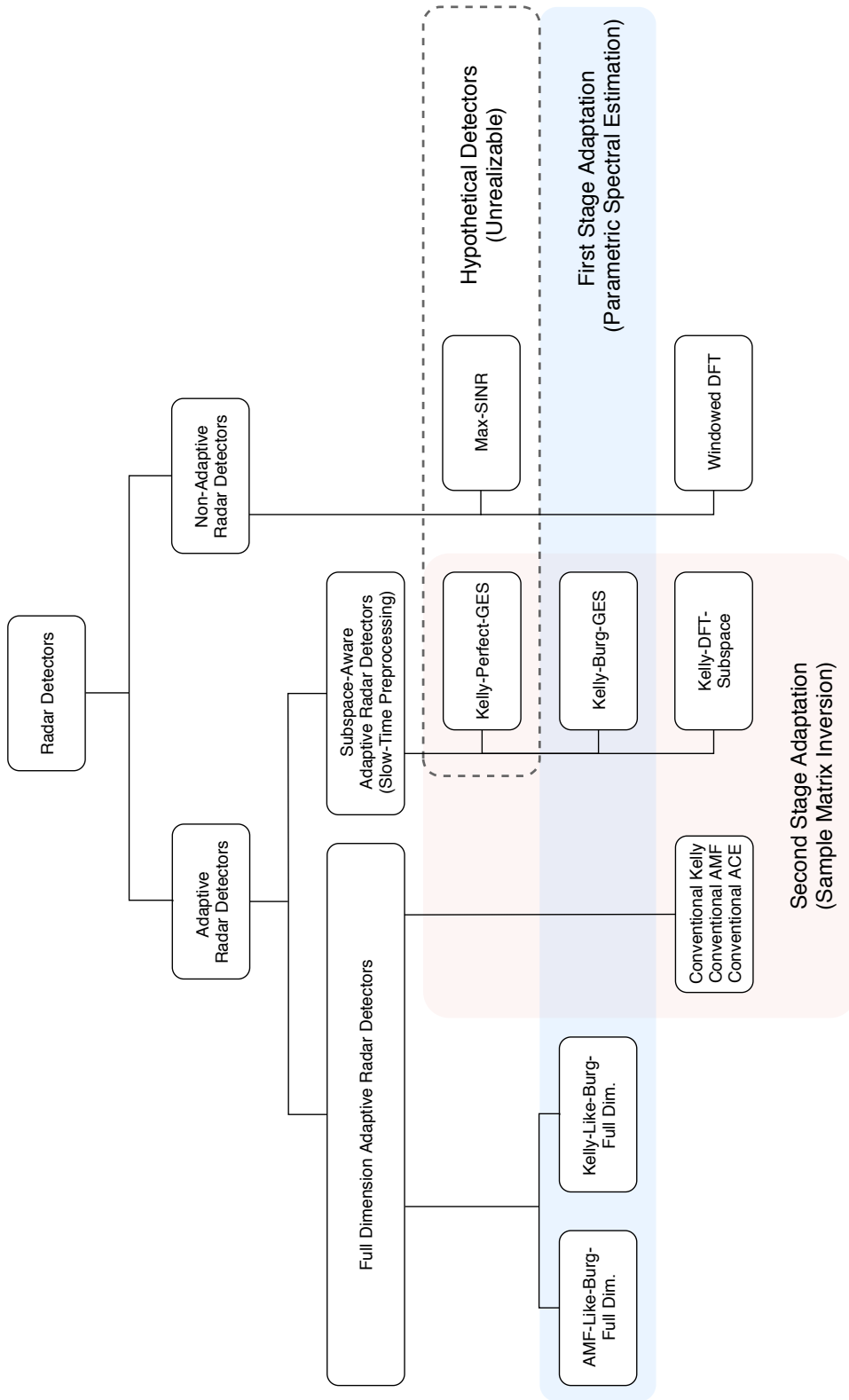


Figure 4.1: The tree of detectors described in this thesis

4.1 Non-Adaptive Detectors

In radar detection, the main goal is to determine whether a range cell contains a target or not. To distinguish between the clutter and the targets, the difference between the slow-time characteristics of them can be used. The adaptive detectors can use an estimate of the slow-time characteristics of the clutter (and noise) in order to eliminate it in the received observations. However, it is also possible to detect targets under clutter without using the clutter characteristics. The detectors which do not use the interference characteristics in detection are called as non-adaptive detectors.

In this section, two non-adaptive detectors are going to be explained. First one is an upper bound on all detectors, namely the max-SINR detector, which is not realizable. Wiener filtering is briefly discussed in the explanation of this detector. Second one is a conventional and significantly easy-to-implement non-adaptive detector, which is called windowed DFT.

4.1.1 Genie-Aided Max-SINR Detector

In this section, an upper bound to the performance of the detectors examined in this thesis is provided. This upper bound is in terms of the knowledge of the ICM. In other words, this detector is provided with the exact full-dimension ($N \times N$) covariance matrix of the interference signal in the CUT. The estimate of ICM is then:

$$\hat{\mathbf{R}}_{\psi} = \mathbf{R}_{\psi,0} \quad (4.1)$$

With the knowledge of the true covariance matrix of the interference, the detector can escape the interference by applying a Wiener filter approach. The fast-time pre-processed observation vector from CUT, $\bar{\mathbf{y}}_0$, is the data to which the detection test is applied and it can be written as:

$$\bar{\mathbf{y}}_0 = \mathbf{s}_0 + \bar{\boldsymbol{\psi}}_0 = \rho \mathbf{d}_\phi + \bar{\boldsymbol{\psi}}_0 \quad (4.2)$$

where \mathbf{s}_0 is the target steering vector in the CUT. It should be noted that the fast-time preprocessing is not explicitly explained under this section because this section is more related to the detector itself. However, in order to integrate energy and truly

detect the range of the target, a fast-time processing is almost always done in the very first parts of the radar receivers. In the scope of this thesis, whether it is the fast-time matched filter or the fast-time unitary transformation, the first column of the fast-time preprocessing matrix \mathbf{Q} is matched to the pulse code \mathbf{b} . Since the pulse code is selected to be unit-norm, the target steering vector in the CUT can be written as $\rho\mathbf{d}_\phi$. The effect of fast-time preprocessing on the interference vector is implicitly considered in $\mathbf{R}_{\psi,0}$.

The observation vector is filtered with an N -tap discrete-time filter \mathbf{w} to give the detection test:

$$t_{\text{Genie}} = \left| \mathbf{w}^H \bar{\mathbf{y}}_0 \right|^2 \underset{H_0}{\overset{H_1}{\gtrless}} \gamma \quad (4.3)$$

The aim of using the discrete-time filter \mathbf{w} is to reduce the effects of interference in the observation signal $\bar{\mathbf{y}}_0$ while keeping the useful target signal untouched, namely, to increase the Signal-to-Interference-plus-Noise-Ratio (SINR) in the data which is to be tested. The error vector in the filtering operation is defined as:

$$\mathbf{e} \triangleq \mathbf{w}^H \bar{\mathbf{y}}_0 - s_0 \quad (4.4)$$

The discrete-time filter which minimizes the mean-square of \mathbf{e} (optimum filter in the MMSE sense) is then [25]:

$$\mathbf{w} = \frac{(\mathbf{R}_{\psi,0})^{-1} \mathbf{d}_\phi}{\sqrt{\mathbf{d}_\phi^H (\mathbf{R}_{\psi,0})^{-1} \mathbf{d}_\phi}} \quad (4.5)$$

The denominator of Eq. (4.5) is a scalar value which has no effect to the detection performance of the genie-aided full-dimension detector. It is a scaling to the discrete-time filter \mathbf{w} whose purpose is to make the residue interference power at the output of the filter equal to unity. In order to show this, the filtered data vector is called as \mathbf{z} and it is examined in two parts:

$$\mathbf{z} = \mathbf{w}^H \bar{\mathbf{y}}_0 = \mathbf{w}^H \mathbf{s}_0 + \mathbf{w}^H \bar{\boldsymbol{\psi}}_0 = \rho \mathbf{w}^H \mathbf{d}_\phi + \mathbf{w}^H \bar{\boldsymbol{\psi}}_0 \quad (4.6)$$

The first term in Eq. (4.6) corresponds to the target signal and the second term corresponds to the interference. The average power of the interference after the filtering

is:

$$\begin{aligned}
\mathbb{E} \left\{ |\mathbf{w}^H \bar{\boldsymbol{\psi}}_0|^2 \right\} &= \mathbb{E} \left\{ \mathbf{w}^H \bar{\boldsymbol{\psi}}_0 \bar{\boldsymbol{\psi}}_0^H \mathbf{w} \right\} \\
&= \mathbf{w}^H \mathbb{E} \left\{ \bar{\boldsymbol{\psi}}_0 \bar{\boldsymbol{\psi}}_0^H \right\} \mathbf{w} \\
&= \frac{\mathbf{d}_\phi^H (\mathbf{R}_{\psi,0})^{-1} \mathbf{R}_{\psi,0} (\mathbf{R}_{\psi,0})^{-1} \mathbf{d}_\phi}{\mathbf{d}_\phi^H (\mathbf{R}_{\psi,0})^{-1} \mathbf{d}_\phi} = 1
\end{aligned} \tag{4.7}$$

Making the residue clutter power constant is desired when the false alarm rate is wanted to be kept independent from the input interference power. Detectors that achieve this property, like the genie-aided max-SINR detector, are called as Constant False-Alarm Rate (CFAR) detectors. Detailed information about CFAR detectors can be found in [3].

After the substitution of max-SINR filter \mathbf{w} in Eq. (4.5) into the test in Eq. (4.3), the hypothesis test for this detector can be rewritten as:

$$t_{\text{Genie}} = \frac{|\bar{\mathbf{y}}_0^H \mathbf{R}_\psi^{-1} \mathbf{d}_\phi|^2}{\mathbf{d}_\phi^H \mathbf{R}_\psi^{-1} \mathbf{d}_\phi} \underset{H_0}{\overset{H_1}{\gtrless}} \gamma \tag{4.8}$$

The genie-aided max-SINR detector is optimal in the sense that it knows the interference characteristics perfectly and uses the MMSE estimate of the target signal in order to make the decision. However, it does not know the exact target velocity, instead it uses a Doppler filter bank. This means that the discrete-time filters are created for a finite number of \mathbf{d}_ϕ steering vectors. The actual target Doppler frequency, however, can be any real number, so an amount of target Doppler mismatch and consequently a straddle loss is unpreventable for the genie-aided detectors as well as all other detectors used in this thesis.

4.1.2 Windowed DFT

This detector is a DFT filter bank, multiplied with an appropriate time (or frequency) window. Each filter in the DFT filter bank is actually a steering vector for a specific Doppler frequency, which is one of the DFT bins described in Section 3.2.2. Therefore, there are N Doppler filters located at the N DFT bins in this detector.

The observation in the CUT could be directly filtered with the steering vectors corresponding to each DFT bin. Then, the metric with largest magnitude could be com-

pared with the threshold to make the detection test. This way, the detector would be called as DFT detector. However, this detector would suffer from the effects of DFT leakage so that the performance of the filters would be low. In order to eliminate the effects of DFT leakage, a low-pass window can be applied to the filters. This filter decreases the frequency sidelobes of the clutter process, meanwhile increases the width of its main lobe. This way, the performance of the filters can be significantly improved in the clutter-free or near-clutter regions; however, the minimum detectable velocity also increases after windowing. Such detectors are called as windowed DFT detectors, and there are lots of different windows in the literature [26].

If the length- N time-domain window is denoted as ζ , then the filter for n^{th} DFT bin is:

$$\mathbf{w} = \zeta \odot \mathbf{d}_{(n-1)/NT} \quad (4.9)$$

where $\mathbf{d}_{(n-1)/NT}$ is the steering vector corresponding to the n^{th} DFT bin following the notation of Section 3.2.2; and \odot sign represents Hadamard product, which is the operation of element by element multiplication of vectors or matrices. Then, the hypothesis test for this detector is:

$$t_{\text{Windowed-DFT}} = \left| \mathbf{w}^H \bar{\mathbf{y}}_0 \right|^2 \underset{H_0}{\overset{H_1}{\geq}} \gamma \quad (4.10)$$

In this thesis, ζ is chosen to be N -length Chebyshev window with 70 dB sidelobe attenuation [27].

4.2 Full-Dimension Adaptive Detectors

In this thesis, the observation vector \mathbf{y} consists of N slow-time samples, meaning that it represents a point in an N -dimensional space. In this section, four detectors which works in N -dimensional space for slow-time operations are going to be explained. These detectors are called as full-dimensional detectors because they perform interference elimination in whole observation space rather than a reduced-dimension subspace of it. On the other hand, each detector introduced in this section is dependent on the interference characteristics. In other words, the detectors in this section adapt themselves to the interference signals they receive, namely they are adaptive detectors.

4.2.1 Full Dimension Adaptive Matched Filter Using Burg Method

In this section, a full-dimension detector which uses Burg's parametric spectral estimation method to estimate the interference characteristics is explained in detail. This detector is similar to the genie-aided full-dimension detector in the sense that both apply a magnitude-square operation to the filtered observation vector before conducting thresholding. The filter applied to the observation vector \mathbf{y}_0 is also similar and its form is rewritten as:

$$\mathbf{w} = \frac{\left(\widehat{\mathbf{R}}_{\psi}\right)^{-1} \mathbf{d}_{\phi}}{\sqrt{\mathbf{d}_{\phi}^H \left(\widehat{\mathbf{R}}_{\psi}\right)^{-1} \mathbf{d}_{\phi}}} \quad (4.11)$$

where $\widehat{\mathbf{R}}_{\psi}$ is the estimation of the ICM. The only distinction between this detector and the genie-aided full-dimension detector is that this detector uses the estimated ICM while the genie-aided detector uses the correct one.

The first step in the calculation of $\widehat{\mathbf{R}}_{\psi}$ is estimating the p^{th} order AR coefficients from the N slow-time samples for each secondary range cell using Burg's method. The details of this step is explained in Appendix A. The second step is the creation of the p -length autocorrelation sequences using the AR coefficients and constructing the $N \times N$ autocorrelation matrices via the extrapolation algorithm explained in Algorithm 3.1. The last step is taking the mean of the L different autocorrelation matrices created by using L secondary range cells. This whole process is also described in Section 3.2.3.2 as well.

The filter \mathbf{w} is applied to the fast-time preprocessed observation vector \mathbf{y}_0 to give the detection test:

$$t_{\text{AMF-Burg-Full}} = \left| \mathbf{w}^H \bar{\mathbf{y}}_0 \right|^2 = \frac{|\bar{\mathbf{y}}_0^H \widehat{\mathbf{R}}_{\psi}^{-1} \mathbf{d}_{\phi}|^2}{\mathbf{d}_{\phi}^H \widehat{\mathbf{R}}_{\psi}^{-1} \mathbf{d}_{\phi}} \underset{H_0}{\overset{H_1}{\gtrless}} \gamma \quad (4.12)$$

This kind of adaptive filtering is first proposed in [6] and called *Adaptive Matched Filter (AMF)*. The only difference of AMF-Burg-Full from the original AMF is that AMF-Burg-Full uses Burg's method to estimate the ICM while the original AMF uses sample matrix inversion (SMI).

4.2.2 Full Dimension Kelly-Like Detector Using Burg's Method

In this section, a full-dimension alternative to the proposed detector in this thesis is described. The detector has two adaptation stages. First step is the construction of the estimate of ICM, $\widehat{\mathbf{R}}_{\psi}$. This step uses L observation vectors from the secondary cells, therefore it is considered as the first adaptation stage. The second step of adaptation is conducted in the detector itself. The detector also uses L observation vectors taken from secondary range cells, so it is the second adaptation stage. The observation vectors used in this detector is in full-dimension, that is, they have N elements.

The first adaptation stage is the process of constructing $\widehat{\mathbf{R}}_{\psi}$ from the L range cells. This process is explained in detail in Section 3.2.3.2. As a brief explanation of this step, for each secondary range cell, the p^{th} order AR coefficients of the interference process is found by Burg's method. Then the AR coefficients are used to construct the $N \times N$ autocorrelation matrix estimates of interference. Finally, the different estimates from different secondary range cells are averaged to find the final estimate $\widehat{\mathbf{R}}_{\psi}$.

The hypothesis test for this detector is given as:

$$t_{\text{Kelly-Like-Burg-Full}} = \frac{|\bar{\mathbf{y}}_0^H \widehat{\mathbf{R}}_{\psi}^{-1} \mathbf{d}_{\phi}|^2}{\mathbf{d}_{\phi}^H \widehat{\mathbf{R}}_{\psi}^{-1} \mathbf{d}_{\phi} (1 + (1/L) \bar{\mathbf{y}}_0^H \widehat{\mathbf{R}}_{\psi}^{-1} \bar{\mathbf{y}}_0)} \underset{H_0}{\overset{H_1}{\gtrless}} \gamma \quad (4.13)$$

for positive L values. For convenience, the case where no secondary cells are used ($L = 0$) is also defined. For that case, the hypothesis test of this detector becomes:

$$t_{\text{Kelly-Like-Burg-Full}} = \frac{|\bar{\mathbf{y}}_0^H \widehat{\mathbf{R}}_{\psi}^{-1} \mathbf{d}_{\phi}|^2}{\mathbf{d}_{\phi}^H \widehat{\mathbf{R}}_{\psi}^{-1} \mathbf{d}_{\phi} (\bar{\mathbf{y}}_0^H \widehat{\mathbf{R}}_{\psi}^{-1} \bar{\mathbf{y}}_0)} \underset{H_0}{\overset{H_1}{\gtrless}} \gamma \quad (4.14)$$

This detector is the same as the full-dimension AMF detector described in Section 4.2.1 except for the $(1 + \bar{\mathbf{y}}_0^H \widehat{\mathbf{R}}_{\psi}^{-1} \bar{\mathbf{y}}_0 / L)$ term in the denominator. This term, in a sense, normalizes the detector with the power of the filtered observation vector in CUT. Without using this term, as in the AMF in Eq. (4.12), the detection metric can become indefinitely large when the clutter power in any secondary range cell becomes near to zero. In such cases, even if there is no target in the CUT (hypothesis H_0), the metric becomes so large that the threshold must be set to a higher value in order to keep the false-alarm rate constant. This undesired increase in the threshold effectively

reduces the detection performance. Adding the normalization term, however, compensates for the effects of abruptly low clutter powers in the secondary cells. This scenario is more likely to occur in heterogeneous clutter environments. Therefore, the detectors which include the $(\bar{\mathbf{y}}_0^H \hat{\mathbf{R}}_{\psi}^{-1} \bar{\mathbf{y}}_0)$ term in their denominators are expected to be more robust to clutter heterogeneity than the ones which do not.

4.3 Subspace-Aware Adaptive Detectors

In this section, detectors working on a D -dimensional subspace of N -dimensional observation space are going to be introduced. As discussed in Section 3.2, the reduction of dimension helps improving the performance of adaptation to the interference environment when a small amount of training data is available. In a heterogeneous clutter environment like in the scenario of this thesis, the source of training data can be limited to only a few secondary range cells and therefore, the reduced dimension techniques may manifest themselves in such environments.

Subspace-aware detectors apply both fast-time and slow-time operations on the observation matrix \mathbf{Y} . The preprocessed observation matrix with which the detectors are fed is:

$$\mathbf{Z}_{D \times (L+1)} \triangleq (\mathbf{U}_{N \times D})^H \mathbf{Y}_{N \times K} \mathbf{Q}_{K \times (L+1)} \quad (4.15)$$

where \mathbf{Q} and \mathbf{U} are the fast and slow-time preprocessing matrices described in Section 3.1 and Section 3.2, respectively. The number of columns of \mathbf{U} , D , is the dimension in which the detection occurs and the number of columns of \mathbf{Q} , $L + 1$, is the number of secondary cells used in the detection, L , plus one for the range cell under test. It should be noted that the \mathbf{Q} matrix was defined to be $K \times K$ in Section 3.1; however, the detectors use only the first $L + 1$ columns of this matrix so it is convenient to write \mathbf{Q} as a $K \times L + 1$ matrix in this section where the detectors are being explained.

Although both fast and slow-time preprocessing can be expressed as matrix operations, in some detectors, they are not nonsequential. This is caused by the dependence of \mathbf{U} matrix on the $\mathbf{Y}\mathbf{Q} = \bar{\mathbf{Y}}$ matrix. When the slow-time operations use secondary cells in order to estimate the characteristics of interference, the target con-

tamination on the secondary cells becomes a problem. Contaminated secondary cells reduces the robustness of adaptive detectors to target Doppler mismatch. The same effect is seen in the beamforming literature as the target contamination deteriorates the angular mismatch robustness of the beamformers. In order to mitigate this effect, Robust Capon Beamformer is proposed in the beamforming literature [28]. Exactly the same phenomenon occurs in the adaptive target detection, and the solution is eliminating the effects of targets in the secondary cells. The fast-time preprocessing method explained in Section 3.1.2 achieves this goal and provides the slow-time preprocessing operation with an uncontaminated observation matrix. Some detectors use these target-free secondary cells to create the slow-time preprocessing matrix, so the fast-time operation must be done prior to the slow-time operation in such detectors. The details of such detectors are going to be explained in the related subsections.

4.3.1 Subspace-Aware Kelly Detector Using GES with Burg's Method

The adaptive detector proposed in this thesis is explained in this section. This detector is an approximate Kelly's GLRT detector [5], which assumes uncorrelated secondary cells. However in the scenario of this thesis, the secondary cells are correlated as explained in Section 2.3.2, that's why the detector is called an approximate to Kelly's GLRT detector.

The proposed detector uses the unitary transformation based fast-time preprocessing matrix described in Section 3.1.2 in order to decontaminate the secondary cells from the effects of range sidelobes of target signals. Using the purified secondary range cells, Subspace-aware Kelly Detector applies GES operation described in Section 3.2.1 in order to reduce the dimension in which detection occurs. In the process of applying GES operation, the detector finds the ICM estimate by using the algorithm involving Burg's method, which is explained in Section 3.2.3.2. After reducing the dimension of the observations, Kelly's GLRT detector again uses the target-free secondary data in order to escape the interference and detect the existence of a target in the CUT.

A two-stage adaptation is present in the working method of the proposed detector. First adaptation is done during the reduction of the dimension of observations, in the

process of determination of the generalized eigenspace. In this stage, the ICM is estimated adaptively in order to select a good subspace for dimension reduction. The second adaptation is done in the detection stage in order to escape the interference in the subspace which is already cleansed from interference as much as possible in the adaptive dimension reduction process. This method of two-stage adaptation in a reduced dimension significantly increases the detection performance when there is a strong constraint on the number of available training data.

For convenience, the hypothesis test given in Section 2.3.1 is recalled:

$$\begin{aligned} H_0 : \mathbf{Y} &= \mathbf{\Psi} \\ H_1 : \mathbf{Y} &= \rho \mathbf{d}_\phi \mathbf{b}^T + \mathbf{\Psi} \end{aligned} \quad (4.16)$$

where $\mathbf{\Psi}$ is the total interference received at the receiver whose autocorrelation matrix is \mathbf{R}_ψ . Kelly's GLRT detector assumes that both ρ and \mathbf{R}_ψ are unknown nonrandom parameters and uses the estimate of \mathbf{R}_ψ , $\hat{\mathbf{R}}_\psi$, to make the estimation of ρ . After estimating ρ , or any other sufficient statistic, the detector can compare the estimated value with a threshold and decide whether there is a target signal in the observations or not.

The preprocessed observation matrix is called as \mathbf{Z} as it is explained in Section 4.3. The columns of \mathbf{Z} are called as \mathbf{z}_l for $l = \{0, 1, \dots, L\}$, \mathbf{z}_0 being the data from CUT and other vectors being related to the secondary cells. In this notation, the Kelly's GLRT test is:

$$t_{\text{Kelly-GES-Burg}} = \frac{|\mathbf{z}_0^H \mathbf{S}^{-1} \tilde{\mathbf{d}}_\phi|^2}{\tilde{\mathbf{d}}_\phi^H \mathbf{S}^{-1} \tilde{\mathbf{d}}_\phi (1 + \mathbf{z}_0^H \mathbf{S}^{-1} \mathbf{z}_0)} \underset{H_0}{\overset{H_1}{\gtrless}} \gamma \quad (4.17)$$

where

$$\mathbf{S} = \sum_{l=1}^L (\mathbf{z}_l \mathbf{z}_l^H + \lambda_d \mathbf{I}_{D \times D}) \quad (4.18)$$

and

$$\tilde{\mathbf{d}}_\phi = \mathbf{U}^H \mathbf{d}_\phi \quad (4.19)$$

$\tilde{\mathbf{d}}_\phi$ in Eq. (4.17) is the reduced dimension steering vector, and it is found by applying the dimension reduction operation to the target steering vector. λ_d in Eq. (4.18) is called as the diagonal loading factor. \mathbf{S} matrix in Eq. (4.18) is an estimate to the autocorrelation matrix for \mathbf{z}_0 . This estimation, followed by the inversion of \mathbf{S} matrix, is called as Sample Matrix Inversion (SMI) in reduced dimension and it is based on averaging the simplest autocorrelation matrix estimates of the secondary data cells. The

conventional Kelly detector assumes a homogeneous clutter environment in making this autocorrelation estimate [5] and this is another difference of the proposed detector from the Kelly's GLRT detector. Full information on the derivation of Kelly's test is available at [29]. The second term in \mathbf{S} matrix, which is a scaled identity matrix, is called *diagonal loading*. Diagonal loading is a widely used technique to increase the robustness of the detectors to the target Doppler mismatch. A clear explanation of this technique can be found in [28], investigating the well-known Robust Capon Beamformer which is also based on diagonal loading. Finding the optimum amount of loading is an issue which is not discussed in this thesis. In contrast to this, the diagonal loading factor is selected as a constant λ_d , and $\lambda_d \mathbf{I}$ is added to each autocorrelation estimate.

The algorithm that the proposed subspace aware Kelly detector uses can be summarized as:

Algorithm 4.1 Calculation of the detection metric in Kelly-Burg-GES

- 1: **Initialize with the observation matrix \mathbf{Y}**
 - 2: Fast-time preprocess \mathbf{Y} to get $\bar{\mathbf{Y}} = \mathbf{Y}\mathbf{Q}$
 - 3: Find the ICM estimate $\hat{\mathbf{R}}_{\psi}$ from the L secondary cells in $\bar{\mathbf{Y}}$ using Burg's spectral estimation method described in Algorithm 3.1 (first adaptation stage)
 - 4: Find the signal subspace estimate $\hat{\mathbf{R}}_{\mathbf{s}}$ for the target Doppler frequency which is of interest, as explained in Section 3.2.3.1
 - 5: Apply GES operation with $\hat{\mathbf{R}}_{\psi}$ and $\hat{\mathbf{R}}_{\mathbf{s}}$ to find the dimension reducing matrix \mathbf{U} , as explained in Section 3.2.1
 - 6: Reduce the dimensions of all observation and steering vectors: $\mathbf{Z} = \mathbf{U}^H \bar{\mathbf{Y}}$ and $\tilde{\mathbf{d}}_{\phi} = \mathbf{U}^H \mathbf{d}_{\phi}$
 - 7: Find the autocorrelation matrix estimate of the interference in the CUT (\mathbf{S} matrix) by the SMI technique and diagonal loading, using the secondary cells in reduced dimension as explained in Section 4.3.1 (second adaptation stage)
 - 8: Apply Kelly's GLRT detector using \mathbf{Z} , \mathbf{S} and $\tilde{\mathbf{d}}_{\phi}$ to find the metric which is used in thresholding operation (Eq. (4.17))
 - 9: **Use the metric in thresholding.**
-

4.3.2 Subspace-Aware Kelly Detector Using GES with Perfect Interference Knowledge

The detector which is going to be explained in this section is not a realizable one but it is considered as a benchmark. The detector assumes that the covariance matrix of the interference in the CUT is perfectly known, just like the case in the Genie-Aided Max-SINR detector explained in Section 4.1.1. However, this detector does not apply the max-SINR detector, but it uses the knowledge of ICM only in the dimension reduction operation. After reducing the dimension, this detector applies Kelly's GLRT detector to find the metric to be compared with the threshold. In other words, this detector is the limit of the proposed detector of this thesis when the subspace being worked on is perfectly constructed.

The hypothesis test of this detector is:

$$t_{\text{Kelly-Perfect-GES}} = \frac{|\mathbf{z}_0^H \mathbf{S}^{-1} \tilde{\mathbf{d}}_\phi|^2}{\tilde{\mathbf{d}}_\phi^H \mathbf{S}^{-1} \tilde{\mathbf{d}}_\phi (1 + \mathbf{z}_0^H \mathbf{S}^{-1} \mathbf{z}_0)} \underset{H_0}{\overset{H_1}{\gtrless}} \gamma \quad (4.20)$$

where

$$\mathbf{S} = \sum_{l=1}^L (\mathbf{z}_l \mathbf{z}_l^H + \lambda_d \mathbf{I}_{D \times D}) \quad (4.21)$$

In Eq. (4.20), it can be seen that this detector is the same as the proposed Kelly detector. However the \mathbf{z} vectors, which are the columns of the matrix \mathbf{Z} , and the $\tilde{\mathbf{d}}_\phi$ vector are in a different subspace. It should be recalled that $\mathbf{Z} = \mathbf{U}^H \bar{\mathbf{Y}}$ and $\tilde{\mathbf{d}}_\phi = \mathbf{U}^H \mathbf{d}_\phi$. The \mathbf{U} matrix in this detector is composed of the D generalized eigenvectors corresponding to the D largest generalized eigenvalues satisfying the generalized eigenvalue problem:

$$\widehat{\mathbf{R}}_s \mathbf{e}_n = \lambda_n \mathbf{R}_\psi \mathbf{e}_n \quad (4.22)$$

The equation Eq. (4.22) is similar to the Eq. (3.12) in Chapter 3. The only difference between these equations is that the ICM is not an estimate but perfectly known in equation Eq. (4.22). In the literature, the GES operation with perfect ICM is shown to be the operation which gives the optimal dimension reduction matrix in several senses [19].

The detector explained in this section can be compared with the proposed detector of this thesis in the sense that the proposed detector's failure relative to the detector of

this section stems from the failure of Burg's method relative to a hypothetical perfect spectral estimation method. In other words, the difference between the performances of these two detectors may be diminished by using better spectral estimation methods than Burg's one. However, it should be noted that no spectral estimation method can make perfect estimations when only a few secondary data are available; and Burg's method is considered as a high performance detector in such cases.

4.3.3 Subspace-Aware Kelly Detector Using Conventional DFT Subspace

The detector of this section is a Kelly detector working in a reduced dimension subspace, like the detectors explained in Section 4.3.1 and Section 4.3.2. However in this detector, the subspace on which the detection occurs is not selected via a GES operation. Instead of estimating the interference and signal subspaces and using GES operation to find the dimension reducing matrix \mathbf{U} , which is costly in computational sense, this detector uses the D dimensional DFT subspace as the \mathbf{U} matrix. The most significant difference between this detector and the detectors in Section 4.3.1 and Section 4.3.2 is that this detector does not use the knowledge of ICM in order to determine the dimension reducing matrix. In other words, this detector has only one adaptation stage which is on the Kelly detection part, whilst the other detectors have one more adaptation stage which is on the part of selecting the dimension reducing matrix.

The slow-time preprocessing method used in this detector is called as Post-Doppler processing, which is explained in Section 3.2.2. In that section, the process of finding the dimension reducing matrix \mathbf{U} is clearly described, therefore it will not be restated in this section. With the \mathbf{U} matrix found via Post-Doppler processing, the fast-time preprocessed observation matrix $\bar{\mathbf{Y}}$ and steering vectors \mathbf{d}_ϕ are projected onto the reduced dimension DFT subspace to give \mathbf{Z} and $\tilde{\mathbf{d}}_\phi$. Then, the hypothesis test is:

$$t_{\text{Kelly-DFT-Subspace}} = \frac{|\mathbf{z}_0^H \mathbf{S}^{-1} \tilde{\mathbf{d}}_\phi|^2}{\tilde{\mathbf{d}}_\phi^H \mathbf{S}^{-1} \tilde{\mathbf{d}}_\phi (1 + \mathbf{z}_0^H \mathbf{S}^{-1} \mathbf{z}_0)} \underset{H_0}{\overset{H_1}{\gtrless}} \gamma \quad (4.23)$$

where

$$\mathbf{S} = \sum_{l=1}^L (\mathbf{z}_l \mathbf{z}_l^H + \lambda_d \mathbf{I}_{D \times D}) \quad (4.24)$$

By comparing this detector with the proposed detector explained in Section 4.3.1, the importance of selecting the reduced dimension subspace can be investigated. In fact, examining the performance of this detector is inevitable if the significance of applying the first adaptation stage and GES operation is wanted to be understood.

In the next chapter, the MATLAB simulation results about these detectors are going to be provided along with some comments on them.

CHAPTER 5

NUMERICAL RESULTS

This chapter is dedicated to the simulation results related to the radar detectors which are described in the previous chapter. At the time this thesis is composed, the detectors have not yet been realized within a radar system. Therefore, the detector performances are compared with Monte Carlo simulations which are done in MATLAB. In the first section of this chapter, the necessary parameters and methods related to the simulations are going to be provided. After the simulation environment is described, various figures for comparing different aspects of the detectors are presented in the second section of this chapter. Together with the figures, some explanations and comments are also going to be provided in order to make clear the significance of the thesis.

5.1 Scenario

This thesis is about improving the detection performance of a radar system in a specific scenario. In this section, the parameters about the scenario which are used in the simulations are going to be described. In Table 5.1, these parameters are given in a tabular form, including their notations used throughout the thesis.

Table 5.1: Parameters used in the simulations

Name	Notation	Value	Unit
Sea Clutter			
Average Power	τ_{sea}	50	dB
Mean Velocity	v_{sea}	3.156	m/s
Velocity Spread	σ_{sea}	1	m/s
Rain Clutter			
Average Power	τ_{rain}	40	dB
Mean Velocity	v_{rain}	10.853	m/s
Velocity Spread	σ_{rain}	2	m/s
Target			
Average Power (SNR)	ρ	Variable	—
Mean Velocity	v_t	Variable	—
Doppler Frequency	f_d	Variable	—
RCS Type		Swerling-1	
Clutter Texture Parameter	ω_k	Variable	—
Clutter Shape Parameter	m_k	Variable	—
Radar RF Frequency	f_{RF}	10	GHz
Radar Wavelength	λ_{RF}	30	mm
PRF	PRF	10	kHz
PRI	T	100	μ s
# of Pulses in a CPI	N	16	—
# of Filters in a Filter Bank	—	16	—
AR Estimation Order	p	4	—
Dimension of the Subspaces	D	Variable	—
# of Secondary Cells Used	L	Variable	—
Length of the Pulse Code	K	16	—
Pulse Code Used	—	P4 Code	—
# of Monte Carlo Trials	—	10000	—
False Alarm Rate	P_{fa}	10^{-3}	—
Diagonal Loading Factor	λ_d	3	—
# of steering vectors averaged	N_f	10	—

5.2 Results

In this section, the simulation results are provided along with the comments about the detector performances. There are four subsections which stand for four different value of clutter heterogeneity. As discussed in Section 2.2.2, the clutter shape parameter m_k determines how the clutter power is distributed among range cells. A lower shape parameter means a higher possibility to see spiky clutter powers and a higher shape parameter means a more homogeneous clutter environment.

Each subsection of this section starts with the probability of detection (P_d) versus Target Doppler Frequency (f_d) curves. These figures help comparing the robustness of the detectors to Doppler mismatch as well as the minimum detectable velocities of them. The SNR loss of some of the detectors in the clutter-free region of Doppler spectrum can also be seen in these figures. The Doppler frequency axis of each figure is normalized to the PRF of the system, in order for it to be independent of the PRF.

After the P_d vs. Doppler curves, P_d vs SNR curves are provided. These curves are the ones where the SNR gains (or losses) of the detectors with respect to each other can be determined. These figures also represents the maximum range a radar system can be operated because target SNR is strongly dependent on the distance of the target to the radar system. The P_d vs SNR curves are plotted for different target Doppler frequency values in order to compare the robustness of detectors to Doppler mismatch.

Following the P_d vs SNR curves are the P_d vs number of secondary cells used (L) curves. These figures indicates how many secondary cells the detectors need in order to properly estimate and eliminate the interference. The non-adaptive detectors do not use secondary cells, therefore they perform the same for all L values. The other detectors usually perform better as L increases because they use at least one adaptation stage in which they estimate the ICM. However, the rate of increase in the performances of the detectors can be compared through these figures. The less amount of secondary cells a detector needs to reach its maximum P_d , the faster it converges when the clutter environment is changed abruptly. Therefore, P_d vs L curves can actually be used to infer a robustness to fast-changing clutter environments.

The subsections end with the P_d vs subspace dimension (D) curves. These figures

indicate the importance of reducing the dimension in which the adaptation occurs when the secondary information is limited. The detectors which do not use dimension reduction at all performs the same for all D values in these figures. When D reaches the maximum possible value, which is the number of pulses in a CPI (N), it can be examined that how the reduced dimension detectors would perform if they worked in full dimension. P_d vs D curves are plotted for different L values, which are the number of secondary cells used, in order to examine the relation between these two parameters.

In all of the figures given in this chapter, the proposed detector of this thesis is the red curve with the legend name of "Kelly-Burg-GES". The dark blue curve with dashed line represents the max-SINR filter and it provides an upper bound for the other detectors. The yellow curve with dotted line, whose legend name is "Kelly-Perfect-GES", is another upper bound, which is the same as proposed detector but with the perfect knowledge of ICM in the dimension reducing operation. The green curve with dashed and dotted line is the Windowed DFT, it represents a benchmark radar detector. The gray curve with star-shaped marker is another detector put forward in this thesis, its legend name is "Kelly-Like-Burg-Full Dim.". It is similar to the Kelly's GLRT detector but it does not use SMI, instead it uses a parametric ICM estimate in full dimension. The purple curve with dotted line and plus-shaped marker is the detector which tries the Wiener filtering as the max-SINR detector, but with a parametric estimate of ICM instead of the actual ICM. It is called "AMF-Like-Burg-Full Dim." in the legend. Finally, the cyan curve with cross-shaped marker is the so called "Kelly-DFT-Subspace", which is the reduced dimension Kelly's detector using DFT subspace instead of using the subspace found with GES operation.

5.2.1 Homogeneous Clutter

In this subsection, the figures are created in a homogeneous clutter environment. In such cases, using higher number of secondary cells increases detection performance, therefore the proposed detector which uses a small number of secondary cells may seem to be ineffective. However, using reduced amount of secondary data can help track the abrupt changes in the clutter power and it also helps resolving targets which

are near to each other in range dimension. Because of this, the simulations are done with a small number of secondary cells and a reduced dimension subspace parallel to this.

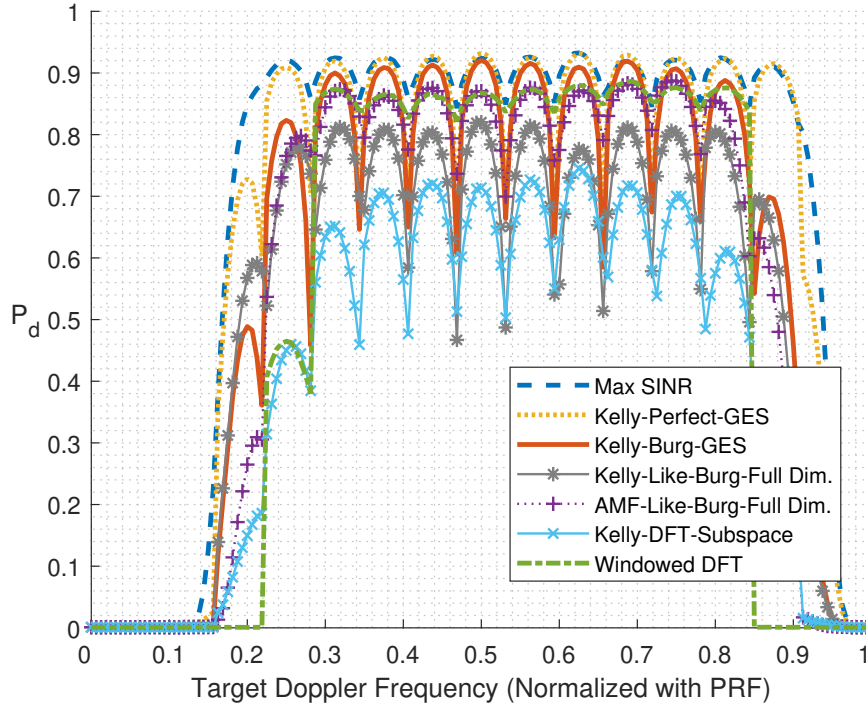


Figure 5.1: P_d vs Doppler Curves, SNR = 20 dB, $D = 3$, $L = 3$, Homogeneous Clutter

In Fig. 5.1, P_d vs target Doppler frequency curves for all seven detectors examined in this thesis are provided. It can be seen that at 20 dB SNR, no detection is possible for targets whose Doppler frequency is up to nearly 0.14 PRF. For the targets with 0.18-0.2 PRF Doppler frequency, Kelly-like full dimension detector has the best detection probability; however, this probability is still near 0.6, which can be considered a low P_d . If the P_d value for which a target can be considered as "detectable" is chosen as 0.8, then Fig. 5.1 shows that the best detector is the proposed one in terms of minimum detectable velocity when SNR is 20 dB. However, the Kelly-like-Burg-Ful Dimension detector has a lower minimum detectable velocity at high SNR values. In the clutter-free region (CFR), which is between nearly 0.3 and 0.8 PRF, the proposed detector is the best one in terms of peak detection probability. This can be considered as the SNR-loss of the proposed detector is the smallest among all. In highly mismatched Doppler frequencies, some detectors perform better than the proposed one; however, this performance loss is only due to straddle loss and it can be compensated

by increasing the number of filters used in the filter bank. This comment is going to be proved with the P_d vs SNR curves.

By looking at Figs. 5.2 to 5.5, the proposed detector can be compared to other detectors at different Doppler mismatch values. For example, when $f_d = 0.225$ PRF and looking at $P_d = 0.8$, Kelly-Burg-GES performed 7-8 dB better than the Kelly-DFT-Subspace and 3 dB worse than Kelly-Perfect-GES. This comparison shows that selecting a good subspace is significantly important for the detectors which reduce the dimension and perform Kelly detection. On the other hand, Kelly-Burg-GES performed 2.5 db better than AMF-Like-Burg and 3 dB better than Kelly-Like-Burg which both work in full dimension. This observation indicates that estimating the ICM with Burg’s method is not enough for a good detection performance, but reducing the dimension in a clever manner helps the adaptive detectors (etiher KELLY or AMF) identify and eliminate the interference better. It can also be seen that the P_d vs SNR characteristics are similar for different Doppler mismatches except only for $f_d = 0.2$ PRF. As a final comment, Windowed DFT, which is significantly easy to implement, is still a considerable option in clutter-free region, but it fails in near-clutter region.

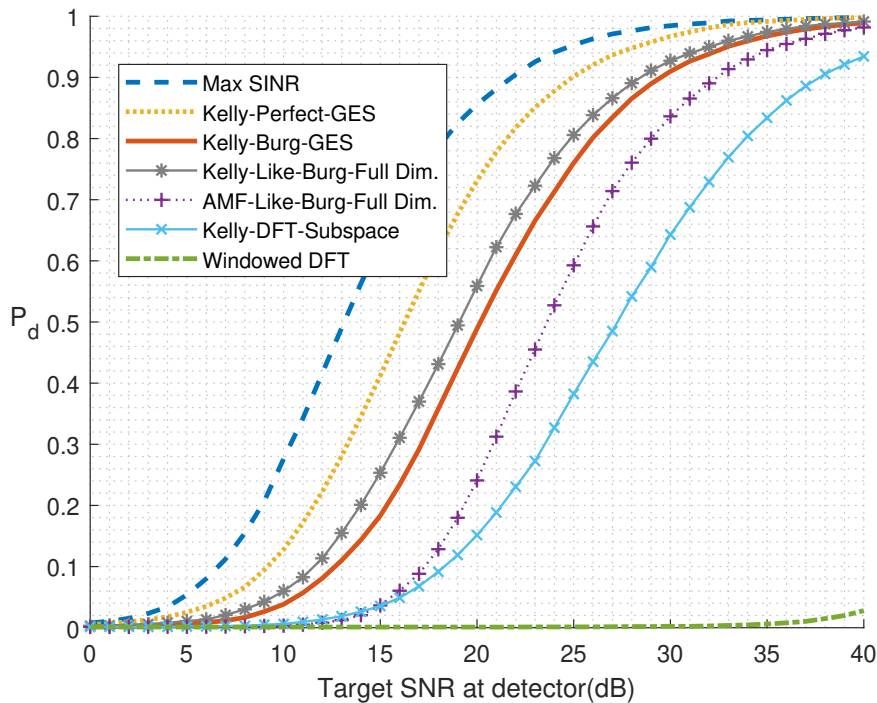


Figure 5.2: P_d vs SNR Curves, $f_d = 0.2$ PRF, $D = 3$, $L = 3$, Homogeneous Clutter

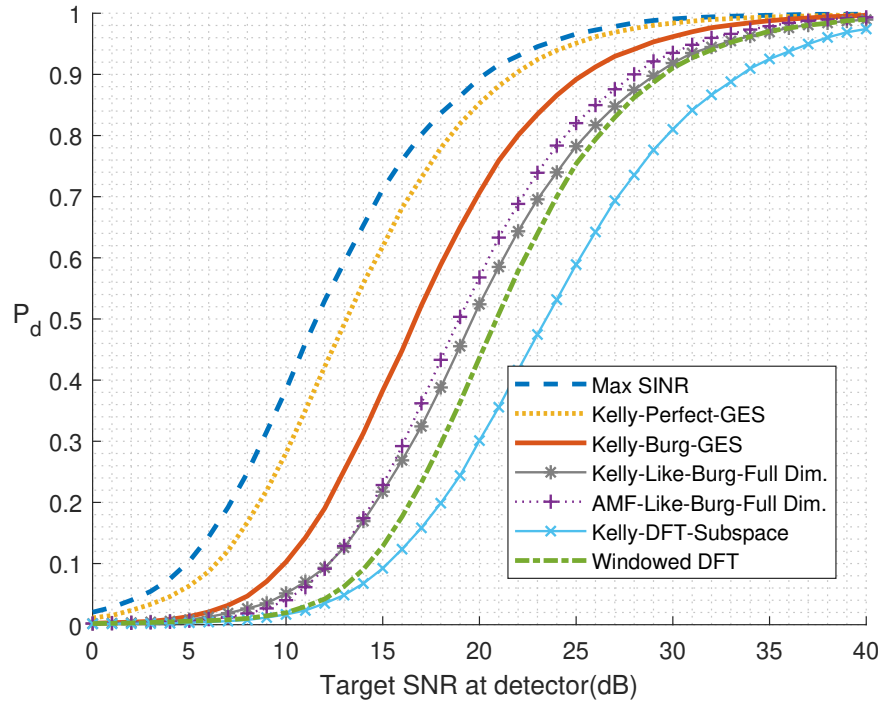


Figure 5.3: P_d vs SNR Curves, $f_d = 0.225$ PRF, $D = 3$, $L = 3$, Homogeneous Clutter

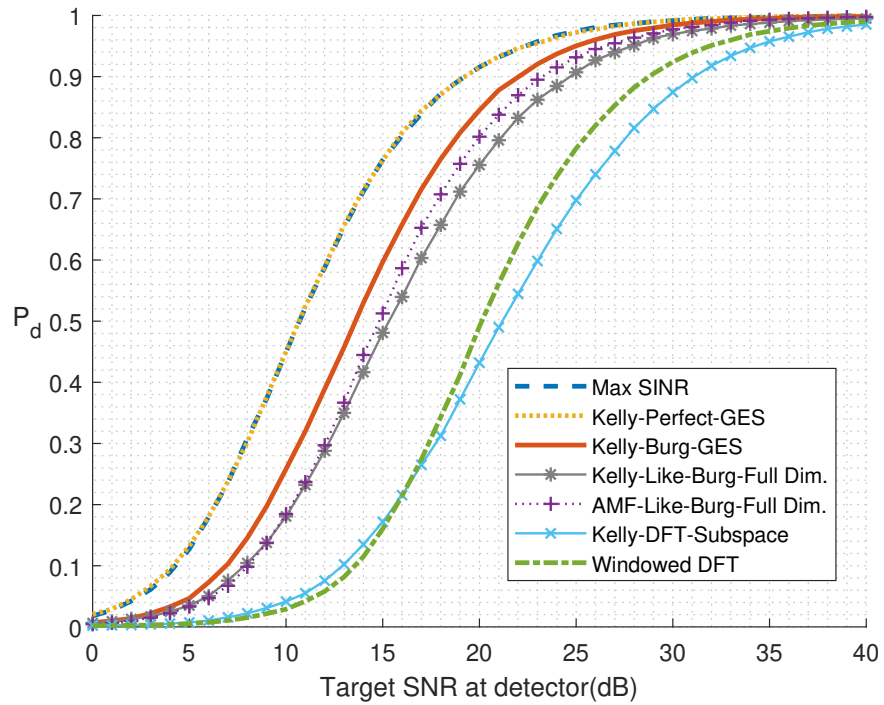


Figure 5.4: P_d vs SNR Curves, $f_d = 0.25$ PRF, $D = 3$, $L = 3$, Homogeneous Clutter

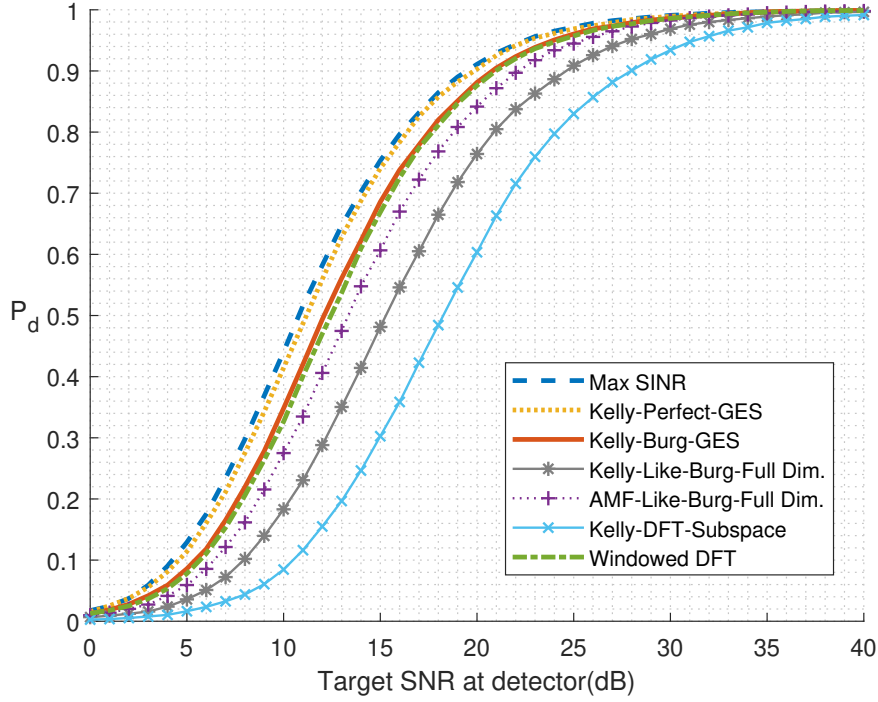


Figure 5.5: P_d vs SNR Curves, $f_d = 0.3$ PRF, $D = 3$, $L = 3$, Homogeneous Clutter

In Figs. 5.6 and 5.7, Kelly-Burg-GES shows its ability to converge much faster than the other detectors. It can be seen that all adaptive detectors increase their performances with increasing number of secondary cells, which is expected in homogeneous clutter environments. However, Kelly-Burg-GES reaches nearly 0.9 P_d with 6 secondary cells when there is mismatch and only 2 secondary cells when there is no mismatch. On the contrary, other detectors reach the same P_d value with 3-6 secondary cells when there is no mismatch and they cannot even reach it with 16 secondary cells when there is mismatch. This shows that the proposed detector can work with a significantly smaller amount of secondary data comparing to the other ones, which make it adapt faster to the changing clutter schemes. Nevertheless, the robustness to clutter heterogeneity in fast-time can only be seen by comparing these detectors in a heterogeneous clutter environment.

In Figs. 5.8 to 5.10, it can be seen that dimension reduction is beneficial for increasing the detection performance of the detectors which applies SMI. When the subspace dimension is increased, the detectors behave as if they are more like full-dimension. However, this deprecates their performances significantly. This is because the space in which the detection occurs include too much interference and GES operation can-

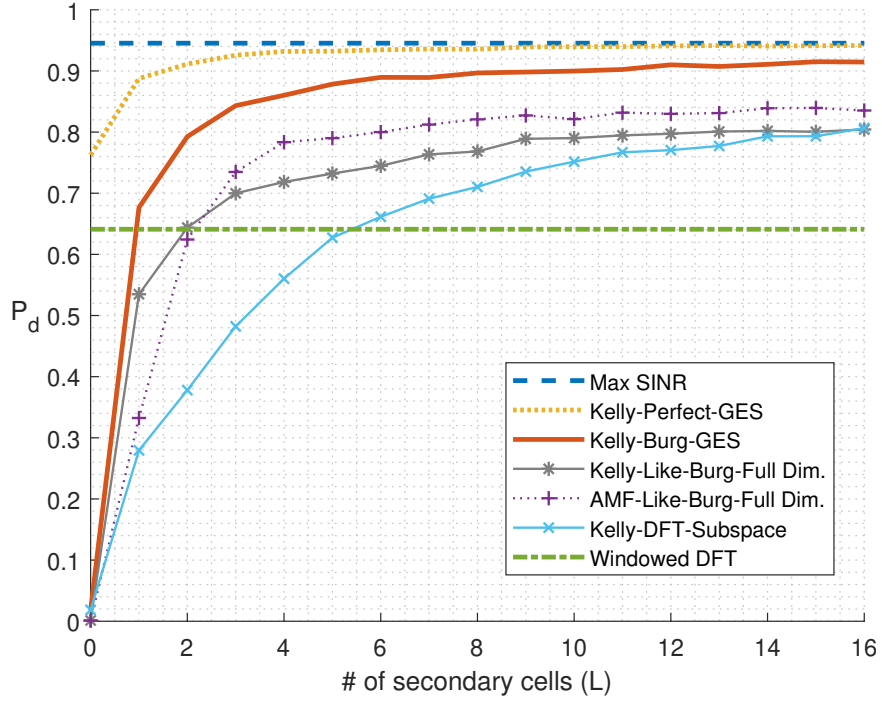


Figure 5.6: P_d vs L Curves, $f_d = 0.225$ PRF, SNR = 23 dB, $D = 3$, Homogeneous Clutter

not find any place to avoid the interference space. Decreasing the dimension too much, on the other hand, causes an efficient interference suppression in first place but it is also not preferable because the second adaptation stage also needs some space to distinguish between the interference and the target. In the extreme case, when the dimension is one, the estimated ICM after the dimension reduction becomes a scalar value, meaning that no interference suppression is available at the second stage. This discussion shows that there is an optimum dimension to reduce, which is consistent with the figures.

In the next section, the case when clutter environment is heterogeneous with shape parameter $SP = 1$ is going to be investigated.

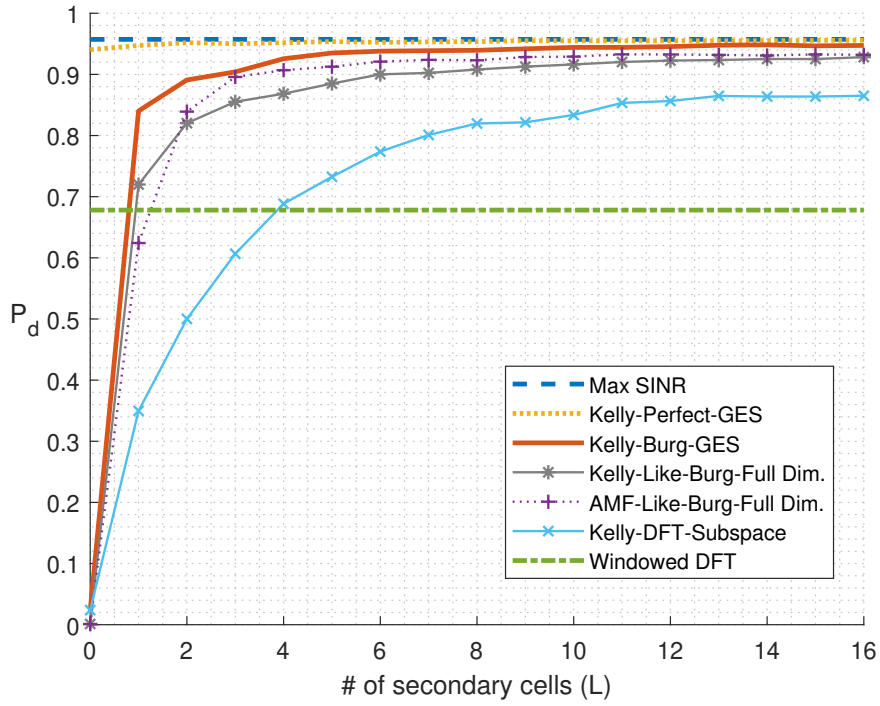


Figure 5.7: P_d vs L Curves, $f_d = 0.25$ PRF, SNR = 23 dB, $D = 3$, Homogeneous Clutter

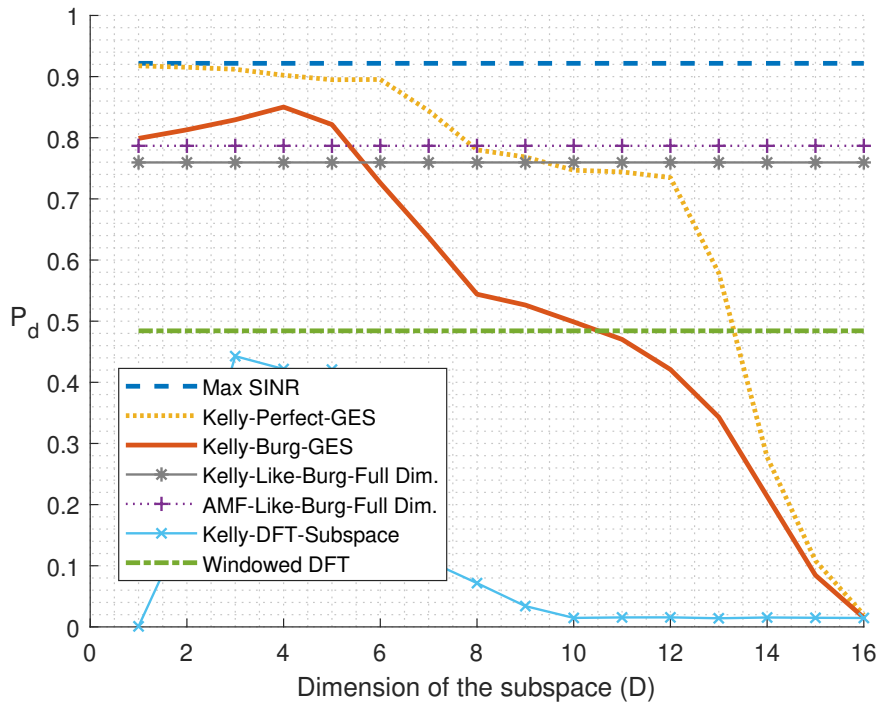


Figure 5.8: P_d vs D Curves, $f_d = 0.25$ PRF, SNR = 20 dB, $L = 3$, Homogeneous Clutter

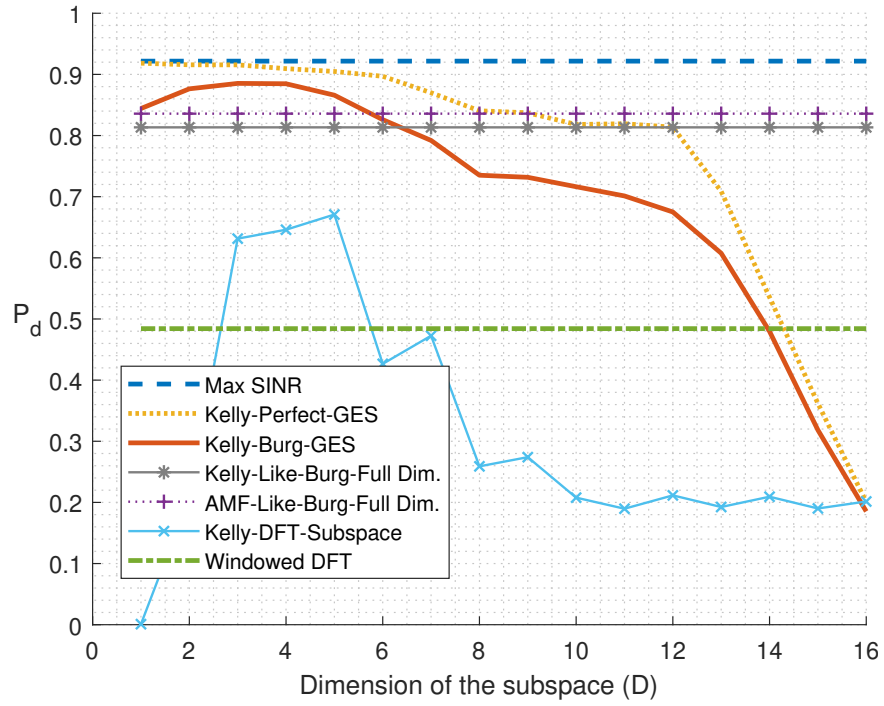


Figure 5.9: P_d vs D Curves, $f_d = 0.25$ PRF, SNR = 20 dB, $L = 6$, Homogeneous Clutter

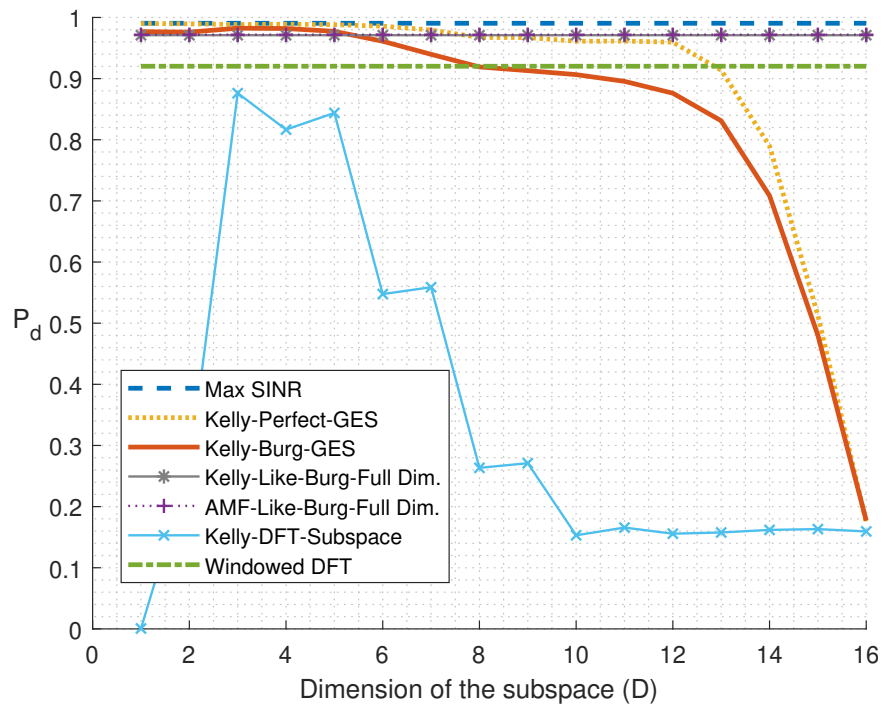


Figure 5.10: P_d vs D Curves, $f_d = 0.25$ PRF, SNR = 30 dB, $L = 3$, Homogeneous Clutter

5.2.2 Heterogeneous Clutter with Shape Parameter = 1

In this subsection, the figures are created in a heterogeneous clutter environment whose texture parameter ω_k is Weibull-distributed with mean 1 and shape parameter 1. This distribution is the same as the exponential distribution with mean 1. In this case, the mean clutter power in the CUT may be different than the secondary cells. Therefore, the detectors may underestimate the interference and do not suppress it enough or overestimate it and suppress the target signal more than needed. On the other hand, the detectors may also use the powerful clutter in the secondary cells in estimating the ICM and suppress the interference better.

In Fig. 5.11, it can be seen that the P_d vs Doppler frequency curves do not differ significantly from homogeneous clutter case when the clutter is heterogeneous with $SP = 1$. Kelly-Burg-GES is still seen to be the best detector in clutter-free region and there is no target Doppler mismatch. However, the performance drop of Kelly-Like-Burg-Full Dim. in the case of target Doppler frequency mismatch is obvious from the graph. This shows that the proposed detector seems more robust to clutter heterogeneity when there is Doppler mismatch.

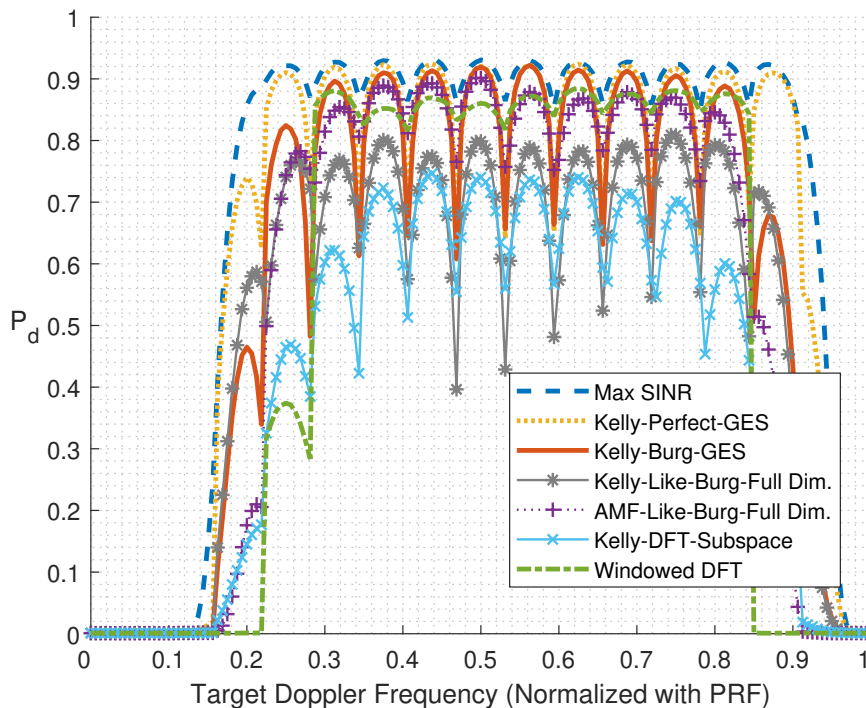


Figure 5.11: P_d vs Doppler Curves, SNR = 20 dB, $D = 3$, $L = 3$, $SP = 1$

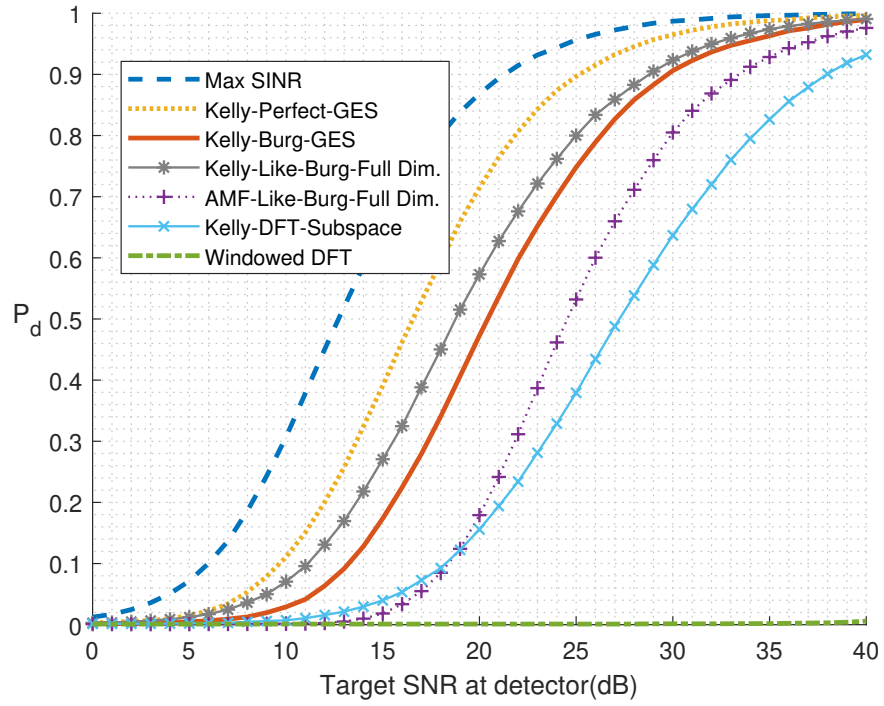


Figure 5.12: P_d vs SNR Curves, $f_d = 0.2$ PRF, $D = 3$, $L = 3$, $SP = 1$

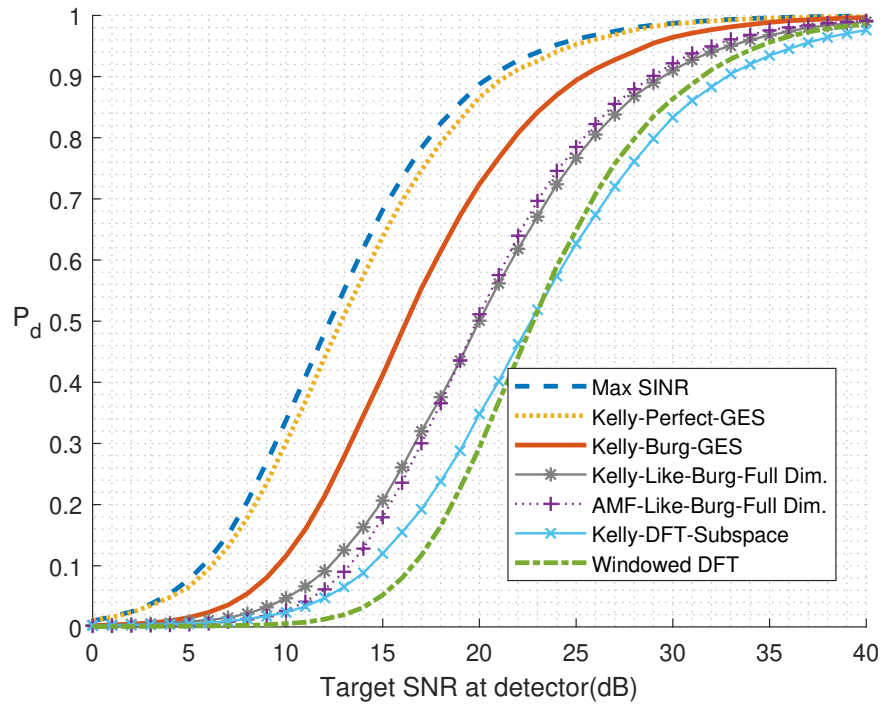


Figure 5.13: P_d vs SNR Curves, $f_d = 0.225$ PRF, $D = 3$, $L = 3$, $SP = 1$

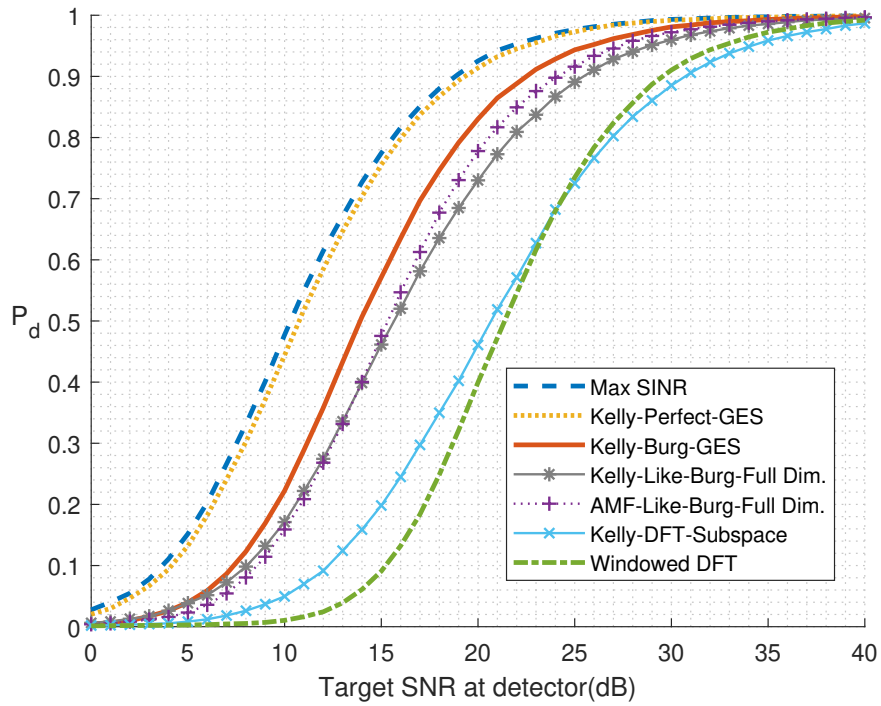


Figure 5.14: P_d vs SNR Curves, $f_d = 0.25$ PRF, $D = 3$, $L = 3$, $SP = 1$

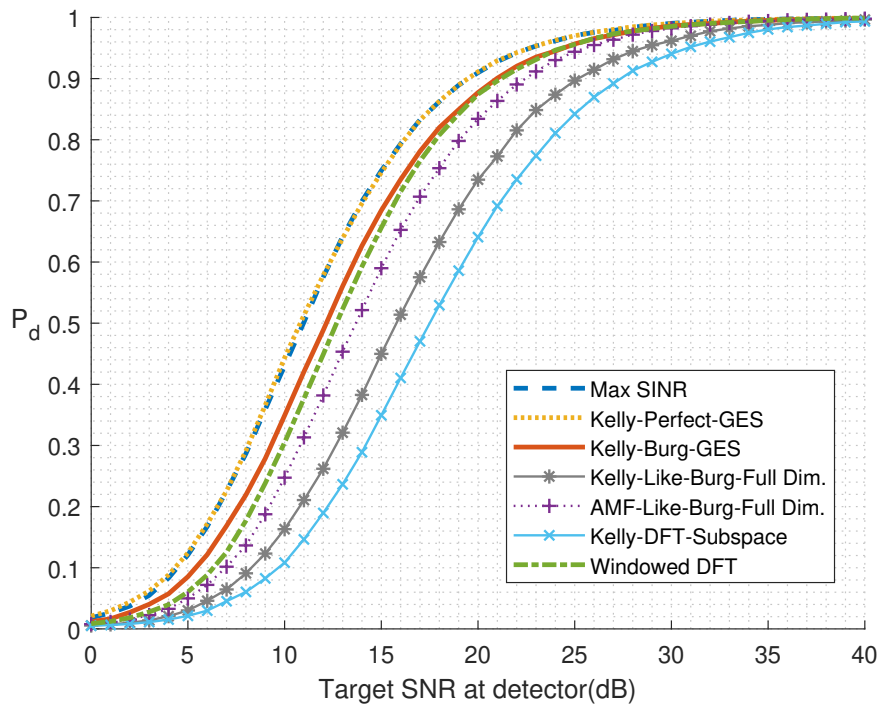


Figure 5.15: P_d vs SNR Curves, $f_d = 0.3$ PRF, $D = 3$, $L = 3$, $SP = 1$

In Figs. 5.13 to 5.15, the dominating performance of the Kelly-Burg-GES can be seen. In Fig. 5.12, the Kelly-Like-Burg-Full Dim. again outperforms the proposed detector but this case is true only for a specific target Doppler frequency region. Comparing these figures with the homogeneous clutter case reveals that heterogeneous clutter with $SP = 1$ is not significantly different from homogeneous clutter.

In Figs. 5.16 and 5.17, it can be seen that the proposed detector still converges faster than the other ones in heterogeneous clutter case with $SP = 1$.

In Figs. 5.18 to 5.20, it is proved again for the heterogeneous clutter case with $SP = 1$ that there is an optimum dimension to reduce for the best performance.

In summary, heterogeneous clutter with $SP = 1$ is not significantly different from homogeneous clutter. In the next section, the shape parameter is reduced to 0.25 and the results are provided in the same order.

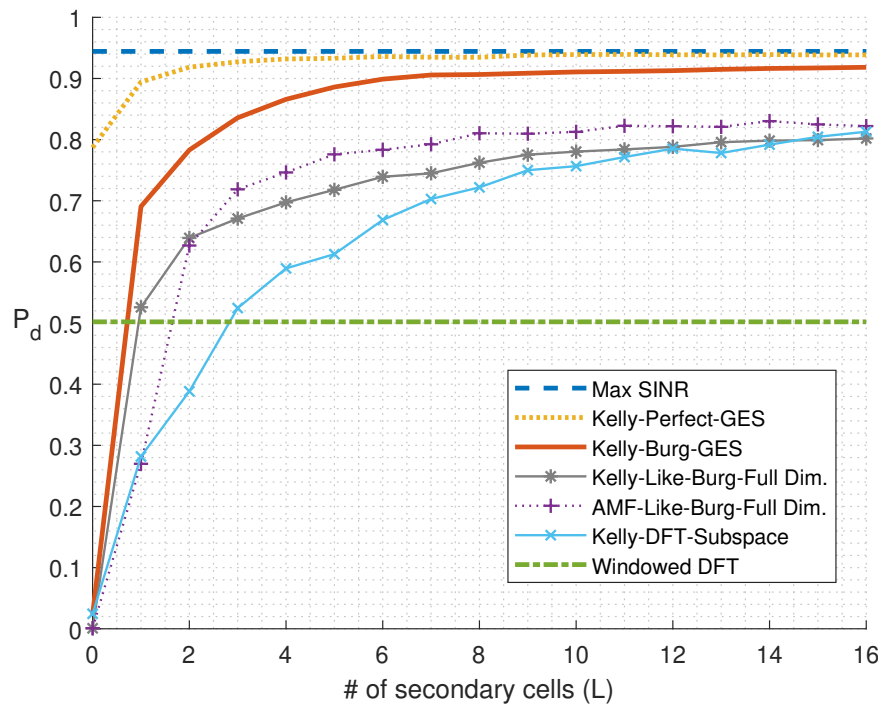


Figure 5.16: P_d vs L Curves, $f_d = 0.225$ PRF, SNR = 23 dB, $D = 3$, $SP = 1$

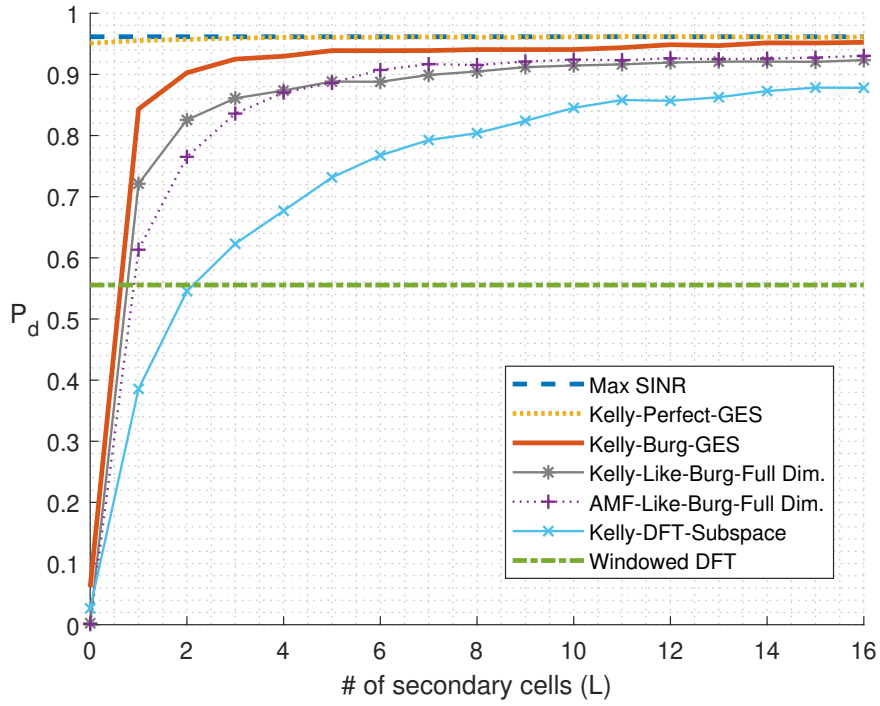


Figure 5.17: P_d vs L Curves, $f_d = 0.25$ PRF, SNR = 23 dB, $D = 3$, SP = 1

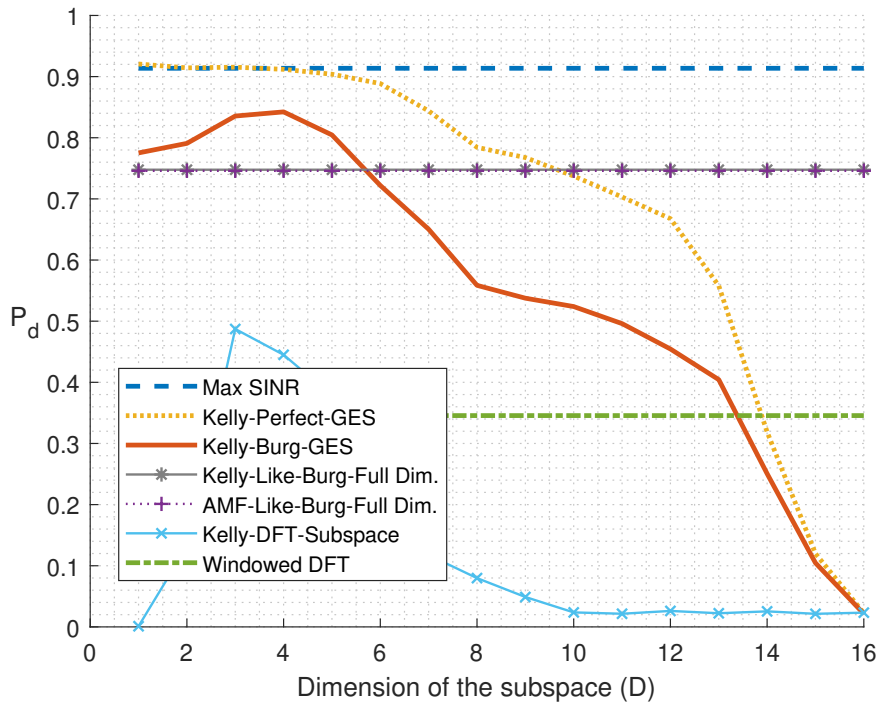


Figure 5.18: P_d vs D Curves, $f_d = 0.25$ PRF, SNR = 20 dB, $L = 3$, SP = 1

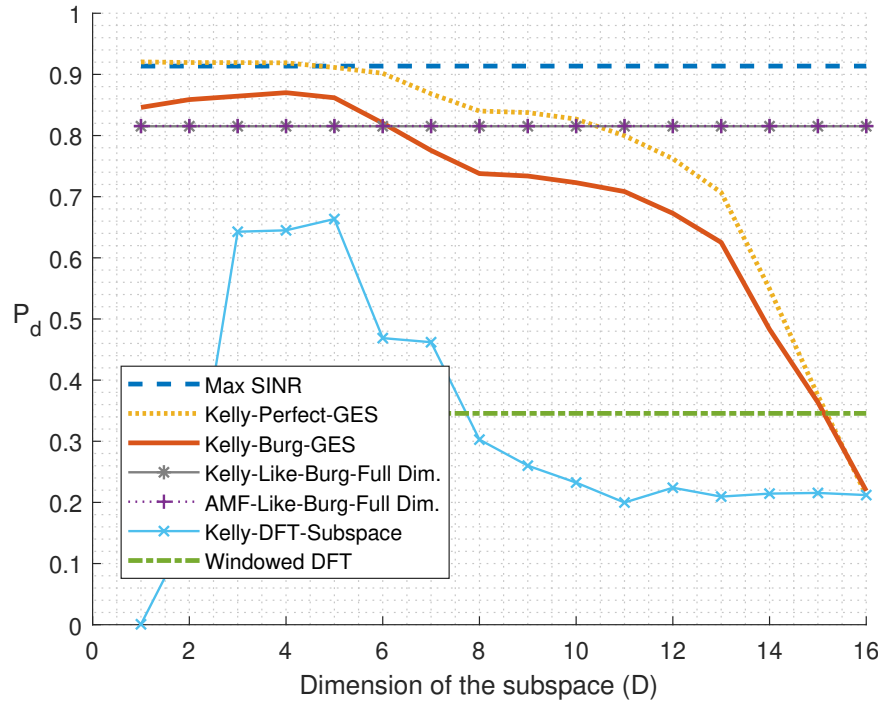


Figure 5.19: P_d vs D Curves, $f_d = 0.25$ PRF, SNR = 20 dB, $L = 6$, SP = 1

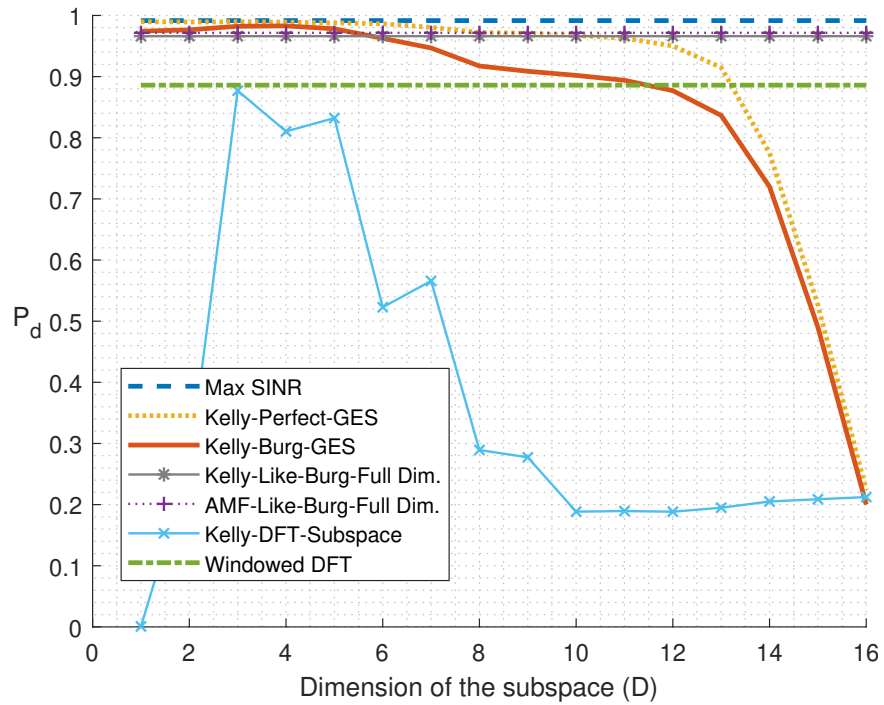


Figure 5.20: P_d vs D Curves, $f_d = 0.25$ PRF, SNR = 30 dB, $L = 3$, SP = 1

5.2.3 Heterogeneous Clutter with Shape Parameter = 0.25

In this subsection, the figures are created in a heterogeneous clutter environment whose texture parameter ω_k is Weibull-distributed with mean 1 and shape parameter 0.25. This shape parameter is low enough to see the significant changes in the clutter environment.

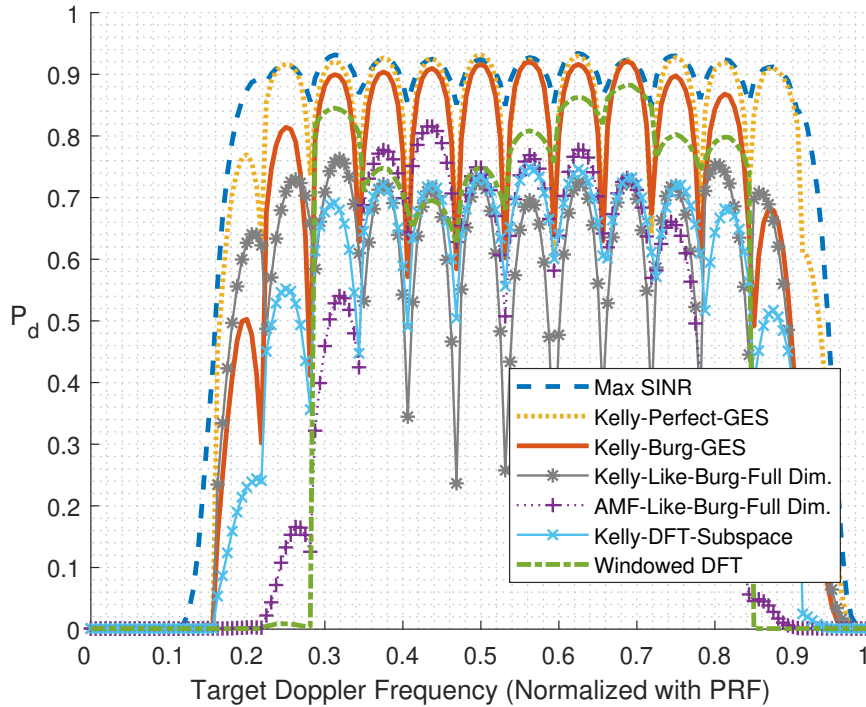


Figure 5.21: P_d vs Doppler Curves, SNR = 20 dB, $D = 3$, $L = 3$, SP = 0.25

When 5.21 is examined, the robustness of Kelly-Burg-GES is revealed. While the other detectors' performances start to fall of, the proposed detector still reaches its theoretical limits in clutter-free region. On the other hand, the robustness of the proposed detector to target Doppler mismatch is reduced with increasing heterogeneity; however, the other detectors seem to lose more of their robustness to Doppler mismatch in highly heterogeneous environments.

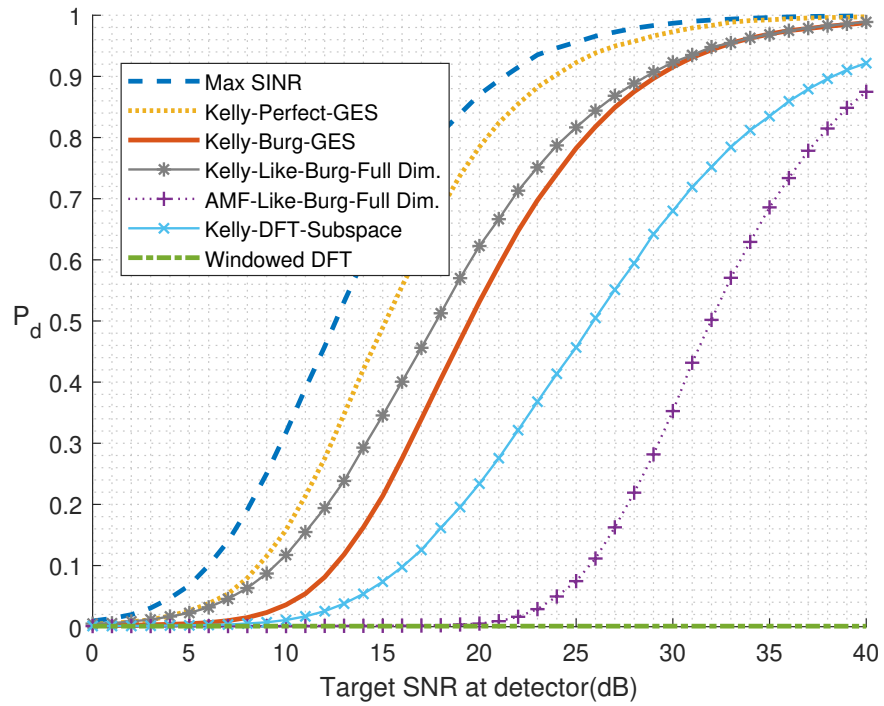


Figure 5.22: P_d vs SNR Curves, $f_d = 0.2$ PRF, $D = 3$, $L = 3$, $SP = 0.25$

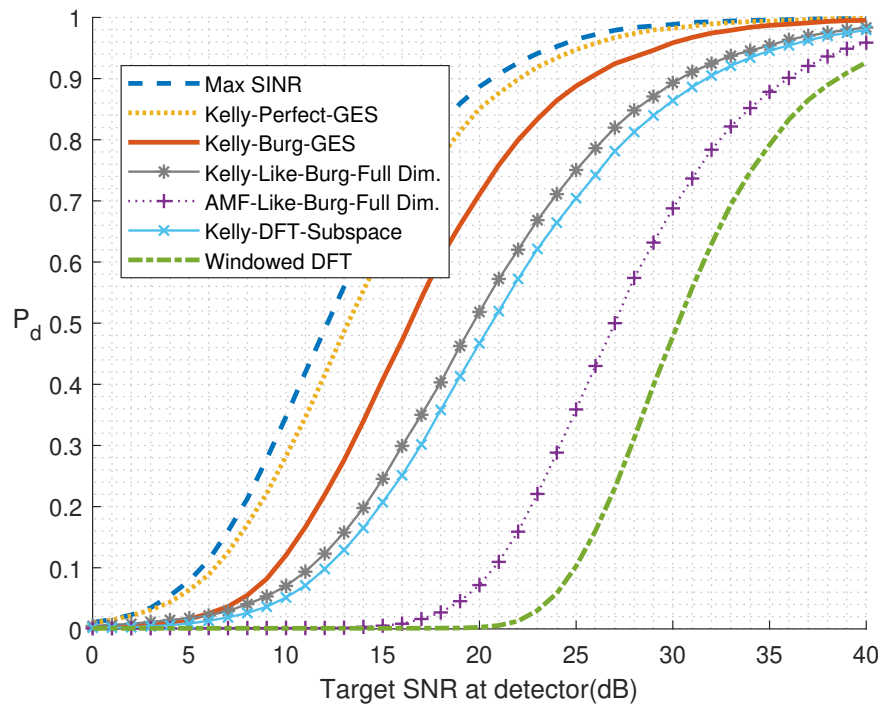


Figure 5.23: P_d vs SNR Curves, $f_d = 0.225$ PRF, $D = 3$, $L = 3$, $SP = 0.25$

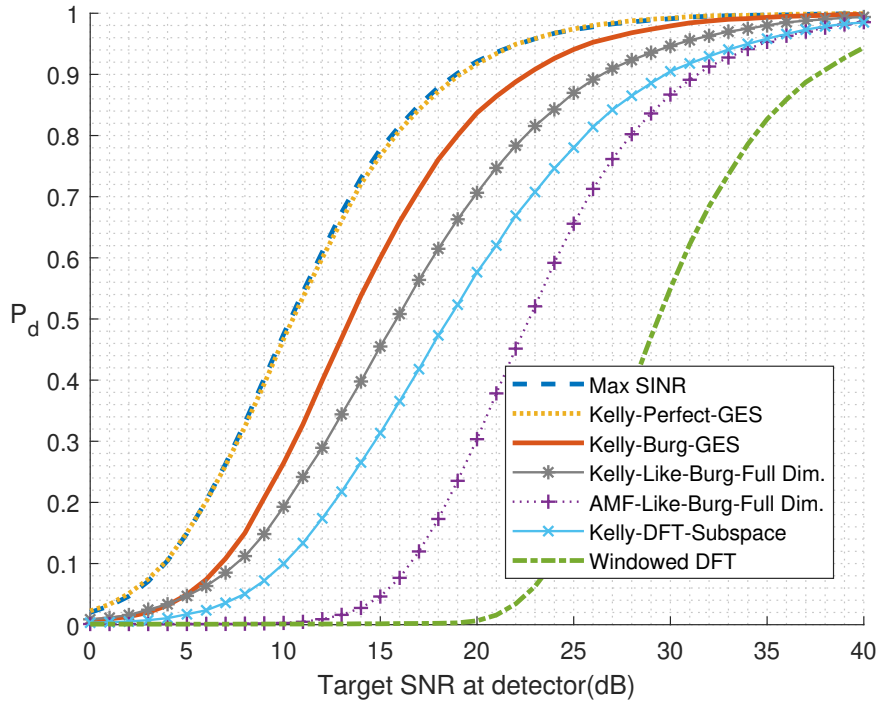


Figure 5.24: P_d vs SNR Curves, $f_d = 0.25$ PRF, $D = 3$, $L = 3$, $SP = 0.25$

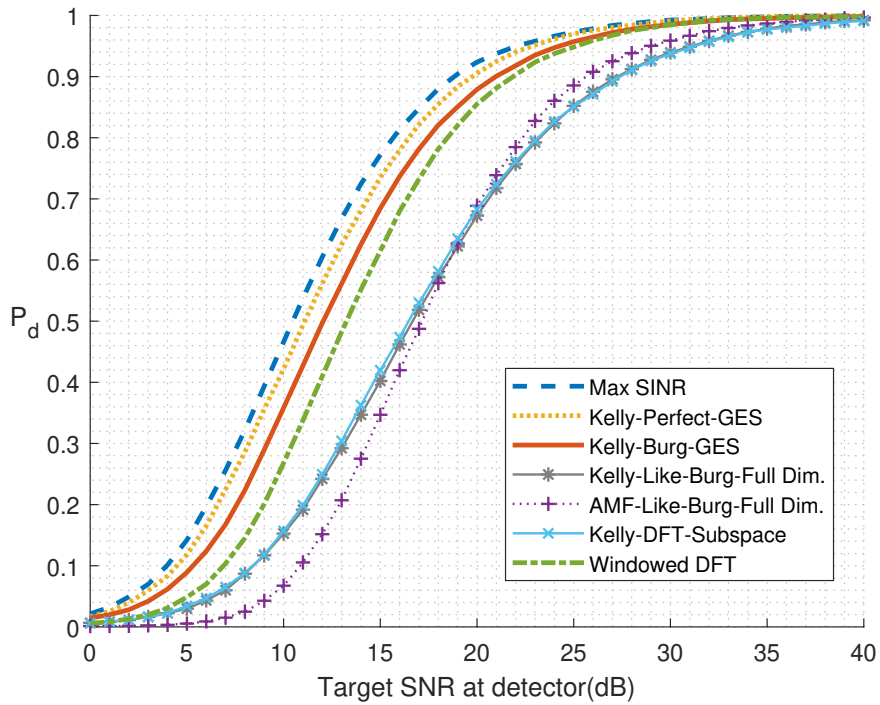


Figure 5.25: P_d vs SNR Curves, $f_d = 0.3$ PRF, $D = 3$, $L = 3$, $SP = 0.25$

In Figs. 5.22 to 5.25, it can be seen that the proposed detector keeps its leading characteristics in highly heterogeneous environments. The most significant performance drop among the adaptive detectors is seen in AMF-Like-Burg-Full Dim. because it lacks the power-normalizing term in its denominator. That term, as explained in ??, helps the Kelly (and Kelly-like) detectors adjust the detection metric according to the power of CUT, eliminating the effects of abruptly changing clutter power in secondary cells. The importance of this term is thus supported with simulation results.

In Figs. 5.26 and 5.27, it can be seen that the proposed detector still converges to its maximum performance faster than the other ones, but this time, the maximum P_d value it can have is decreased. Nevertheless, Kelly-Burg-GES reaches $P_d = 0.8$ with only two secondary cells even if there is a target Doppler mismatch.

In Figs. 5.28 to 5.30, it can be seen that the importance of selecting a good D value increases as heterogeneity increases. On the other hand, the proposed detector outperforms the others if the correct subspace dimension is selected.

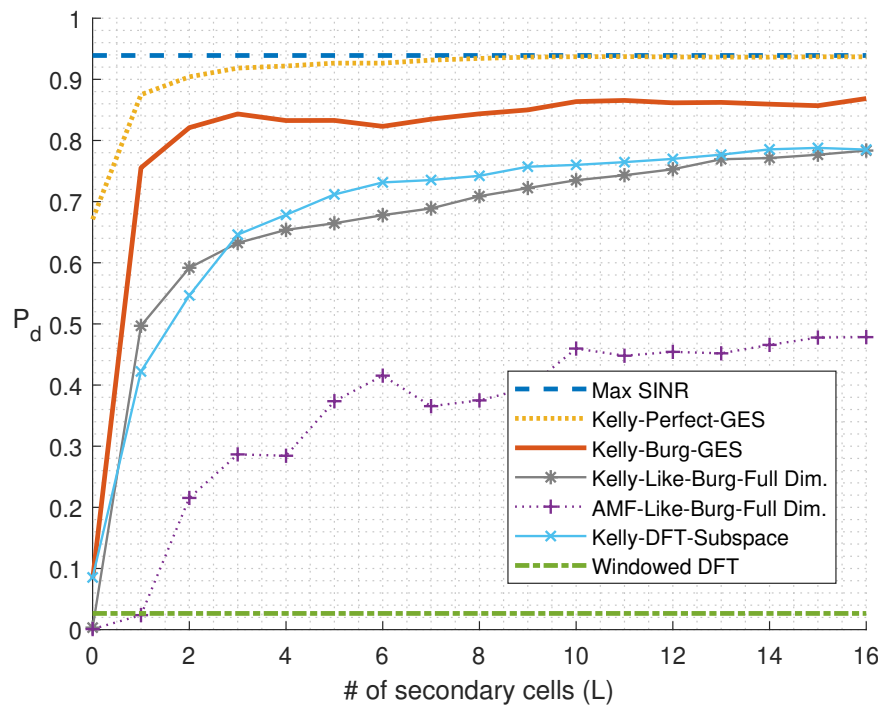


Figure 5.26: P_d vs L Curves, $f_d = 0.225$ PRF, SNR = 23 dB, $D = 3$, SP = 0.25

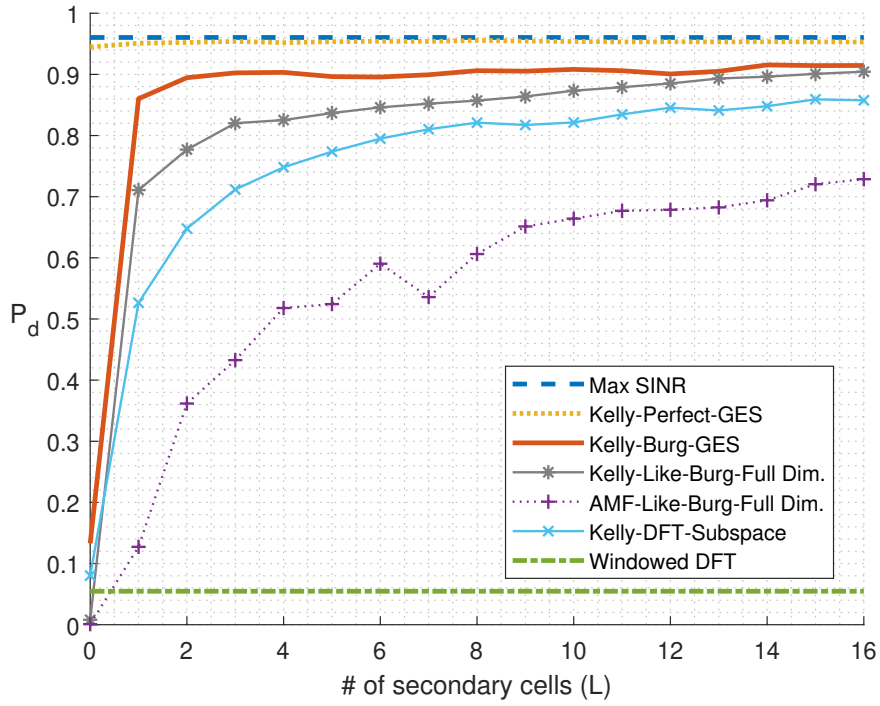


Figure 5.27: P_d vs L Curves, $f_d = 0.25$ PRF, SNR = 23 dB, $D = 3$, SP = 0.25

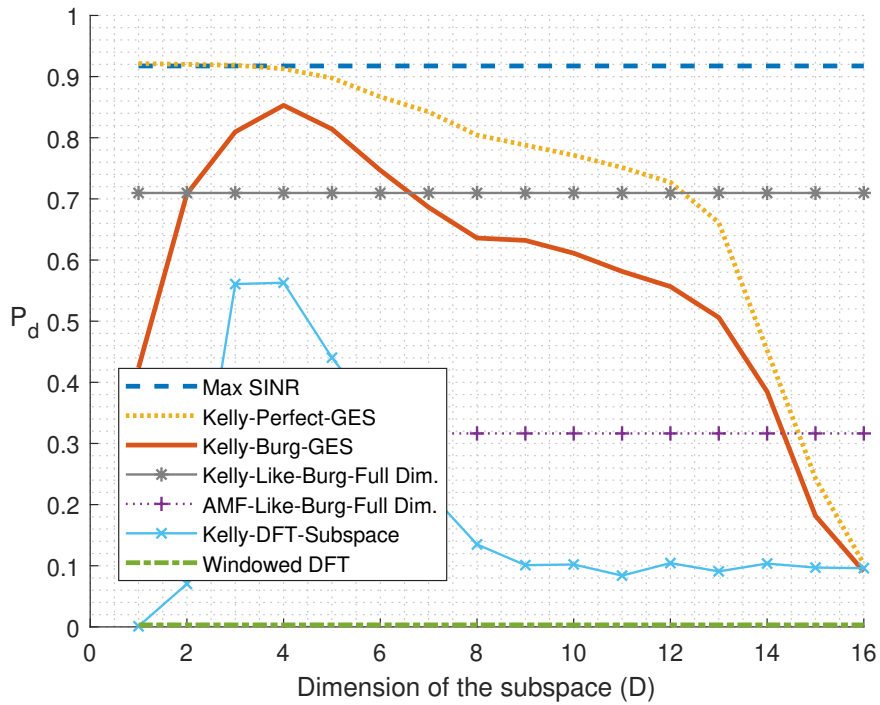


Figure 5.28: P_d vs D Curves, $f_d = 0.25$ PRF, SNR = 20 dB, $L = 3$, SP = 0.25

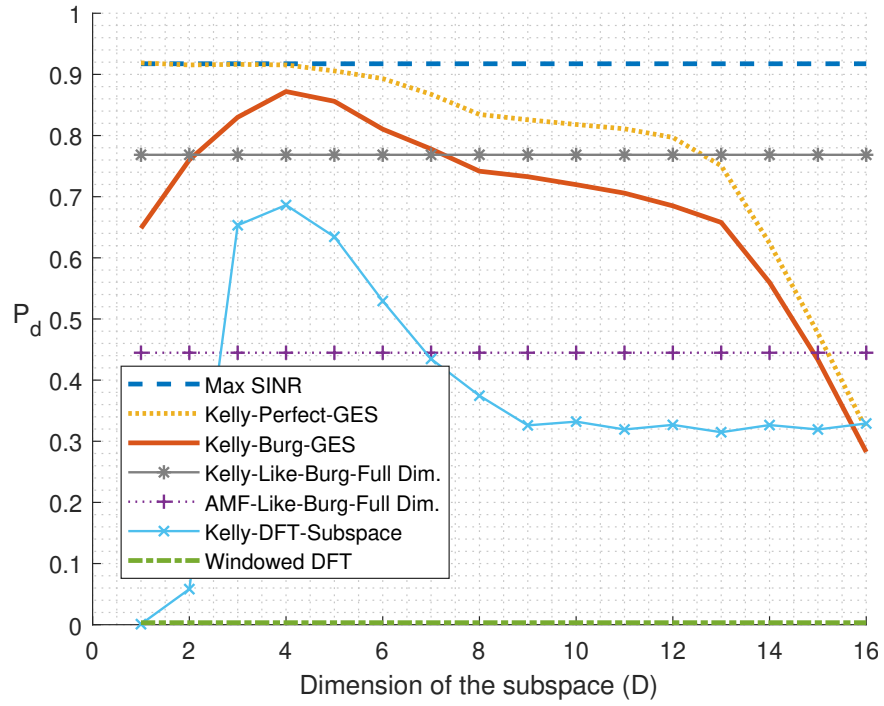


Figure 5.29: P_d vs D Curves, $f_d = 0.25$ PRF, SNR = 20 dB, $L = 6$, SP = 0.25

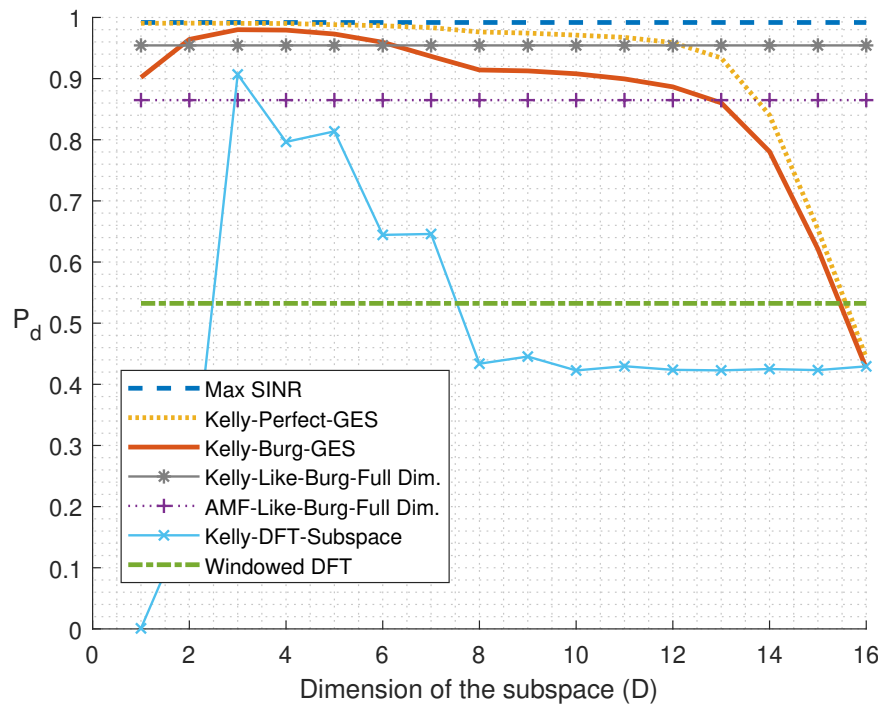


Figure 5.30: P_d vs D Curves, $f_d = 0.25$ PRF, SNR = 30 dB, $L = 3$, SP = 0.25

5.2.4 Heterogeneous Clutter with Shape Parameter = 0.1

In this subsection, the figures are created in a heterogeneous clutter environment whose texture parameter ω_k is Weibull-distributed with mean 1 and shape parameter 0.1. This is an extremely heterogeneous clutter environment, therefore the effects of heterogeneity are most obvious for this case. It should be remembered that the mean of the texture parameter among fast-time is one, so the average clutter power is kept the same among the range cells. Therefore, having large spikes in the distributed clutter power requires having smaller clutter powers in most range cells. This may increase the performances of the detectors in some trials but fortunately, the Monte-Carlo simulation helps observing the average behaviors.

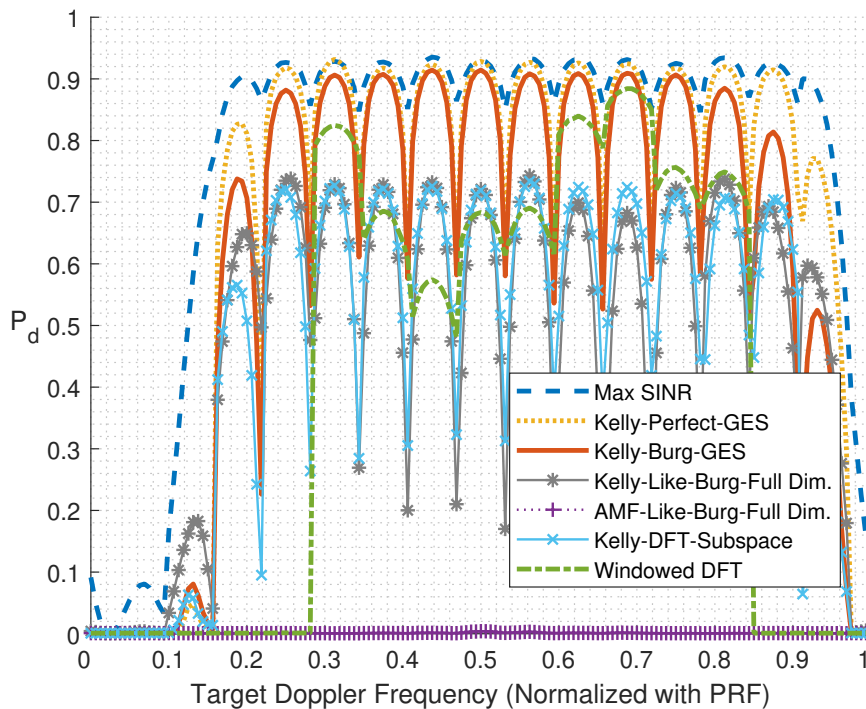


Figure 5.31: P_d vs Doppler Curves, SNR = 20 dB, $D = 3$, $L = 3$, SP = 0.1

In 5.31, it can be seen that in clutter free region at 20 dB SNR, the proposed Kelly-Burg-GES dominates the other detectors by far. An important fact to notice is that AMF-Like-Burg-Full Dim. detector completely vanishes at this SNR when heterogeneity is too high. This observation proves that the power normalizing term in Kelly's detector increases the robustness for heterogeneous clutter environments. The proposed detector also outperforms the other ones in terms of the robustness to target

Doppler mismatch.

In Figs. 5.32 to 5.35, it can be seen that Kelly-Burg-GES completely dominates all other detectors. When there is no target Doppler mismatch, at 0.9 P_d , Kelly-Burg-GES is 6 dB better than the Kelly-Like-Burg-Full Dim. and Kelly-DFT-Subspace, and only 2 dB below the Kelly-Perfect-GES. This indicates a substantial increase in the detector performance with respect to conventional post-Doppler processing under highly heterogeneous clutter environments.

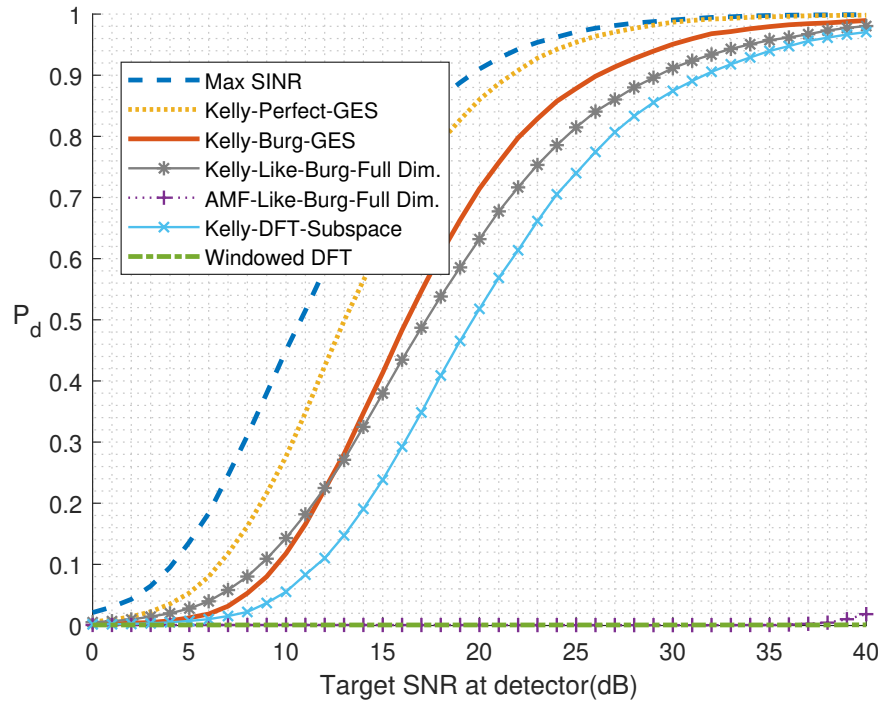


Figure 5.32: P_d vs SNR Curves, $f_d = 0.2$ PRF, $D = 3$, $L = 3$, $SP = 0.1$

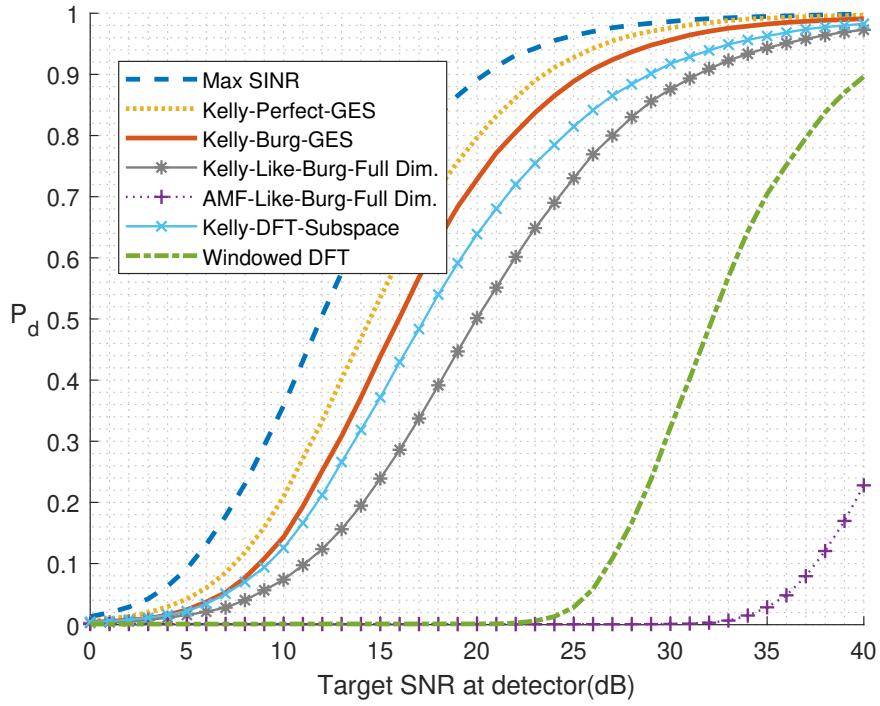


Figure 5.33: P_d vs SNR Curves, $f_d = 0.225$ PRF, $D = 3$, $L = 3$, $SP = 0.1$

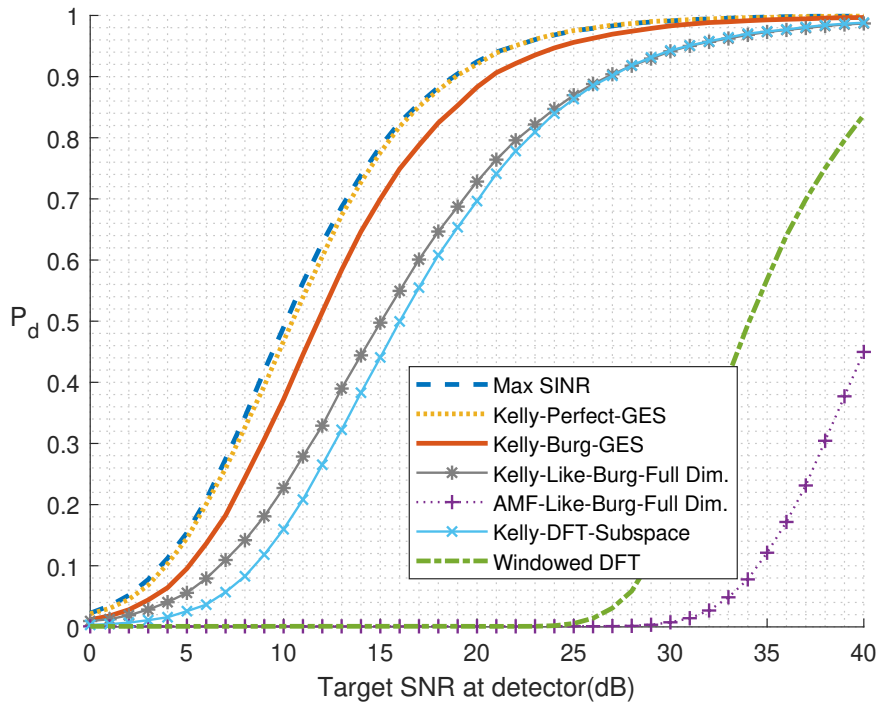


Figure 5.34: P_d vs SNR Curves, $f_d = 0.25$ PRF, $D = 3$, $L = 3$, $SP = 0.1$

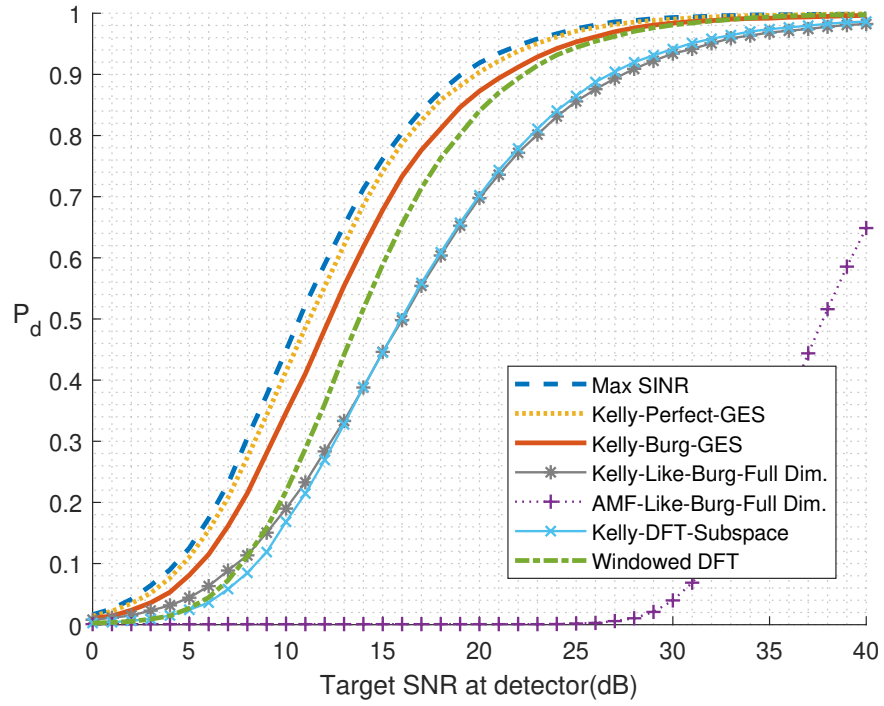


Figure 5.35: P_d vs SNR Curves, $f_d = 0.3$ PRF, $D = 3$, $L = 3$, $SP = 0.1$

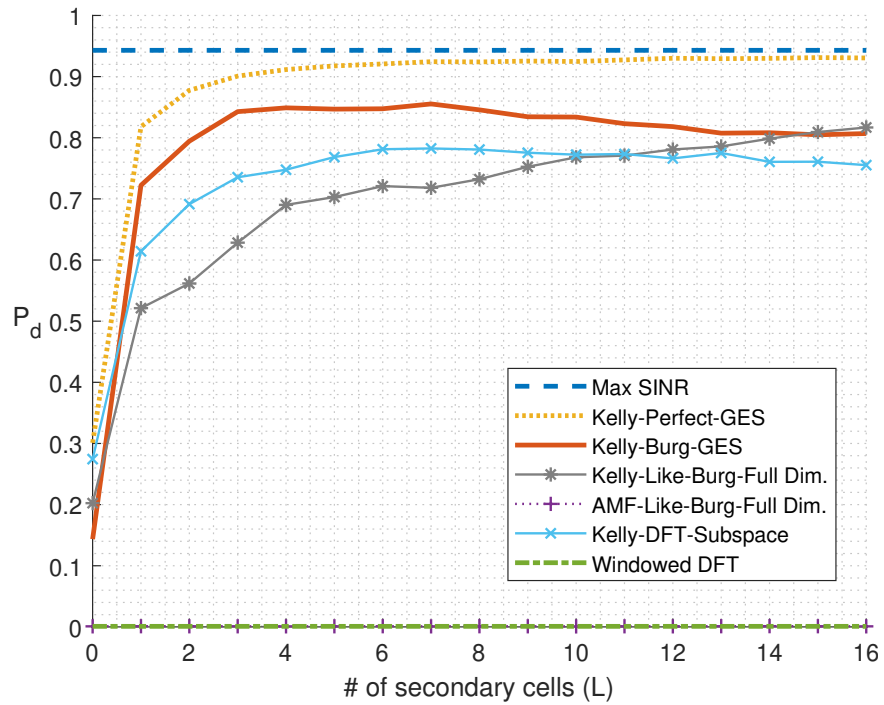


Figure 5.36: P_d vs L Curves, $f_d = 0.225$ PRF, SNR = 23 dB, $D = 3$, $SP = 0.1$

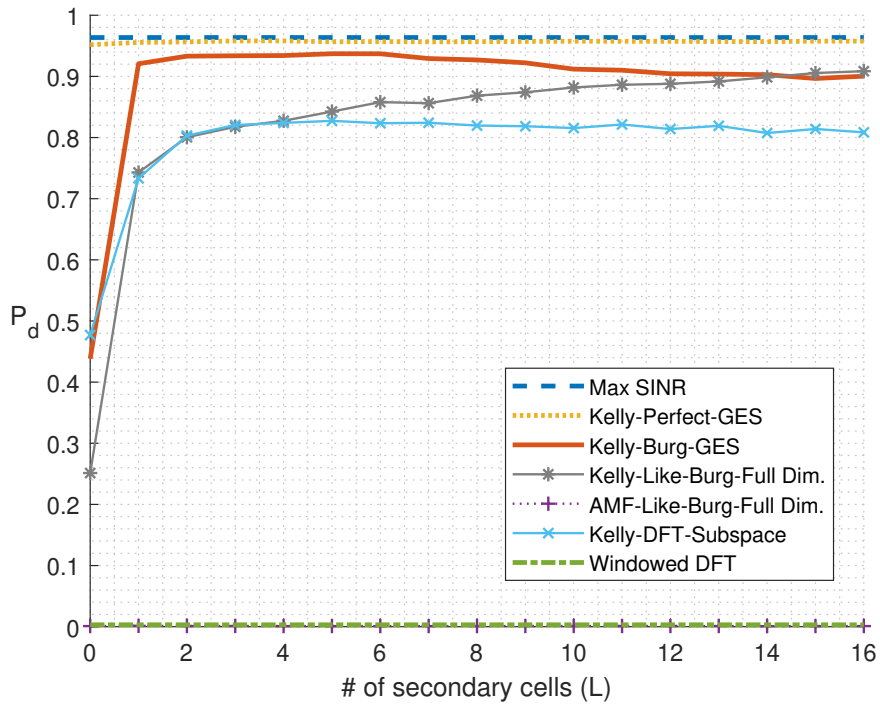


Figure 5.37: P_d vs L Curves, $f_d = 0.25$ PRF, SNR = 23 dB, $D = 3$, SP = 0.1

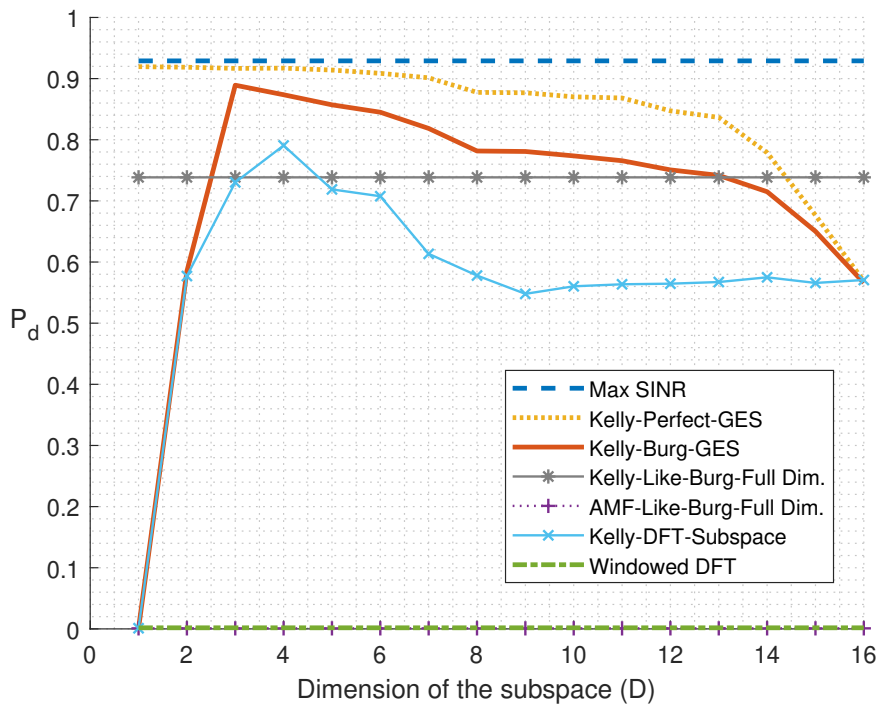


Figure 5.38: P_d vs D Curves, $f_d = 0.25$ PRF, SNR = 20 dB, $L = 3$, SP = 0.1

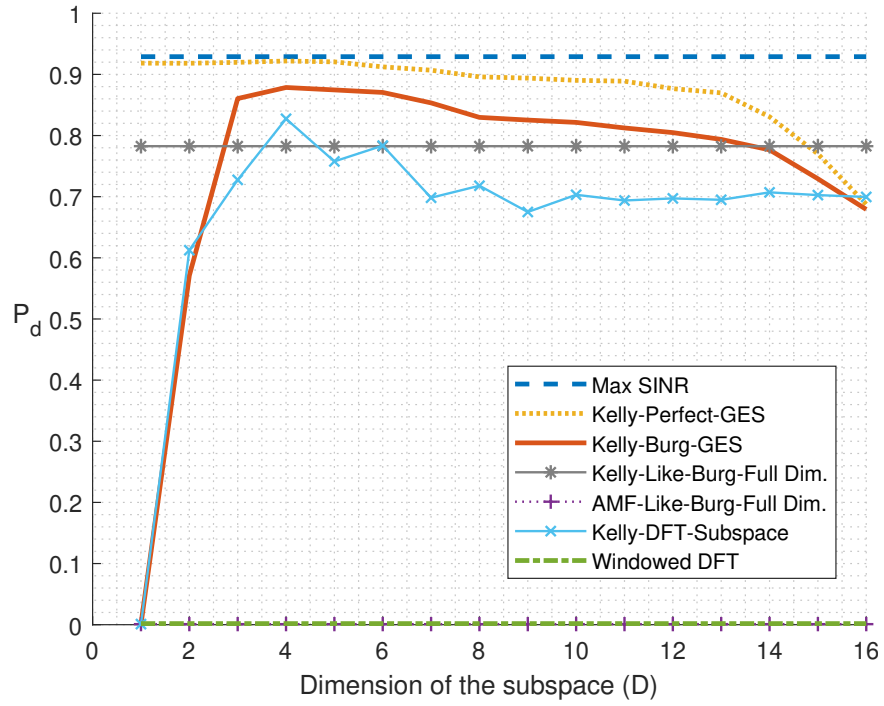


Figure 5.39: P_d vs D Curves, $f_d = 0.25$ PRF, SNR = 20 dB, $L = 6$, SP = 0.1

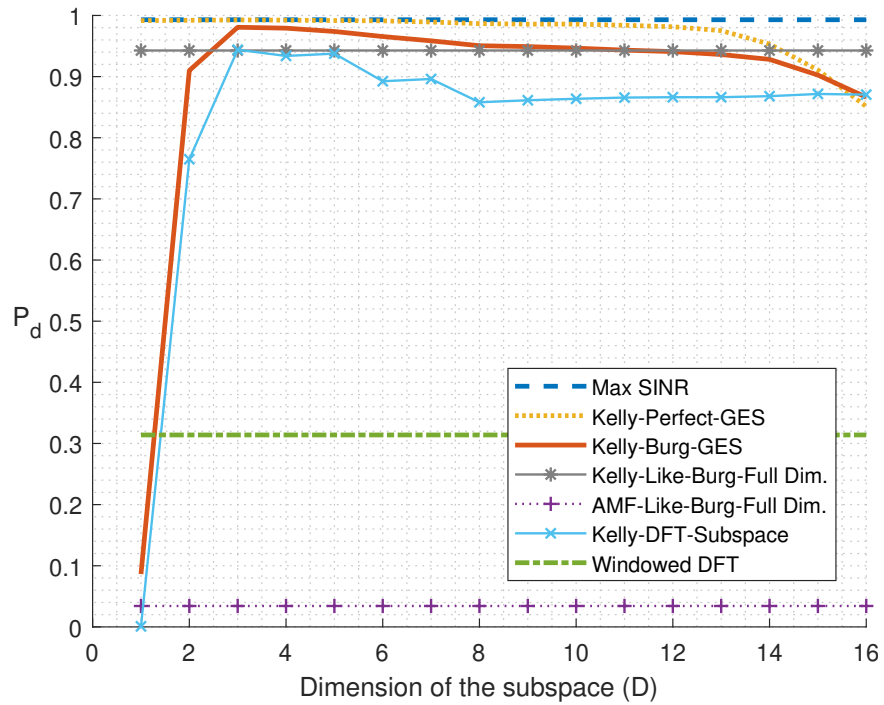


Figure 5.40: P_d vs D Curves, $f_d = 0.25$ PRF, SNR = 30 dB, $L = 3$, SP = 0.1

In Figs. 5.36 and 5.37, it can be seen that the fast convergence rate of the proposed detector still exists in this extremely heterogeneous clutter case. However, increasing the number of secondary cells now starts to decrease the detector performances at some point. This makes sense as increased heterogeneity disables the detectors to correctly take information from distant range cells.

In Figs. 5.38 to 5.40, it can be seen that the optimum dimension to reduce still exists at this highly heterogeneous environments. It can be deduced that whether the clutter is homogeneous or heterogeneous, the subspace dimension must be determined in order to efficiently design a detector.

This chapter included the simulation results created in MATLAB. The proposed Kelly detector using GES operation with Burg's method is shown to be ahead of other conventional detectors. In the next and last chapter, concluding remarks are going to be provided.

CHAPTER 6

CONCLUSION

This thesis is about a robust adaptive radar detector based on fast-and-slow-time preprocessing. By examining the positive and negative features of the existing adaptive radar detectors, this thesis combines different methods and approaches to propose a solution to the problem of radar detection under heterogeneous compound Gaussian clutter.

The main motivation of this thesis is doing radar detection under heterogeneous clutter environments, which sea clutter usually is. This heterogeneity results in the fact that the interference characteristics change rapidly in fast-time. This is why only a small number of secondary cells can be used to estimate the ICM of the CUT. Without any preprocessing, it is shown in the literature that lots of secondary cells are needed to estimate this matrix with reasonable error. In the literature, there also exist studies on subspace techniques to overcome the issue of restricted secondary cells. The proposed detector of this thesis also uses subspace processing, but it exhibits a novel method to find a good subspace.

In subspace radar detection, a good subspace can be considered as the one which involves the target signal and avoids including unnecessary amounts of interference at the same time. It should be noted that some amount of interference must be included in the subspace if an adaptive detection is going to be conducted in that subspace because adaptive detectors need to estimate the ICM using the interference signals. In the literature, the optimum subspace in several senses is found with generalized eigenspace operation when the target and interference covariance matrices are exactly known. In real cases this is not possible, therefore the estimates of these matrices must be used to find a subspace which is near to the optimum one. In this thesis, both

signal and interference subspace estimations are made and these estimates are used in the generalized eigenspace operation. By comparing this subspace with conventional DFT subspace (which is used in post-Doppler processing), this thesis proves that cleverly selecting the subspace significantly increases the detection performance.

As the subspace selection requires ICM estimation, how to estimate ICM before dimension reduction gains importance in subspace radar detection. In the works of this thesis, it is shown that a perfect ICM estimation used in subspace adaptive radar detection reaches performances that are nearly the same as the performance of max-SINR filter. Since the scenario of this thesis restricts the amount of secondary cells, the ICM estimation before dimension reduction must also be done with only a few secondary data. In this stage, a novel method which finds ICM estimates from each secondary cell and takes the average of them is proposed. In heterogeneous environments where one secondary cell can include a powerful clutter while the next one having a near-zero clutter, averaging different ICM estimates can help avoiding extreme power estimates for the interference and finding a good threshold. Other than the averaging operation it conducts, the ICM estimation is novel also in the spectral estimation method it exploits. The detector assumes that the interference is an AR process and finds its AR coefficient estimates using Burg's method. However, in order to avoid the noise effects in the AR coefficient estimation, the AR prediction order is kept much smaller than the dimension of the interference. After the coefficients are estimated, they are extrapolated to the dimension of interference via well-defined Yull-Walker equations.

This thesis also addresses another challenge in adaptive radar detection, the target contamination on secondary cells. The explained methods for cleverly selecting a subspace and adapting to the interference environment require that observations used in adaptation include only unwanted interference signals. However without any fast-time operation, the impulse response of the target to the pulse code creates nonzero echoes of the target in the secondary cells. In conventional radar systems a guard interval around the CUT may help reducing this sidelobe level; however, in a scenario in which the clutter is heterogeneous, there are already a few secondary cells so that eliminating them with a guard interval is not beneficial. Reducing the sidelobes to zero requires infinite pulse length and using an uncoded pulse makes time synchro-

nization significantly hard. Therefore, a fast-time preprocessing method is used to eliminate the target contamination effect on secondary cells. This method filters the CUT with a matched filter but applies such filters to secondary cells that the observations in the secondary cells are projected into a fast-time subspace orthonormal to the target space in the fast-time. This method eliminates the target contamination completely in the expense of adding a correlation to the interference process in fast-time. Nevertheless, the slow-time preprocessing method proposed in this thesis does not use fast-time correlation characteristics of interference at all, and it is shown explicitly in this thesis that fast-time preprocessing does not affect the slow-time correlation characteristics of interference.

The scenario in which the target is longer than a range cell, namely the extended target case, is not examined in this thesis and the preprocessing methods can be developed accordingly in the future works. Other than this, the optimum AR prediction order is also not discussed in this thesis, and it can be a good starting point in the future studies. Spectral estimation methods other than Burg's one can also be investigated in future works. On the other hand, assuming a Gaussian ICM and estimating the mean and spread parameters for the two clutter sources may be a different adaptive detection method and may increase the performance due to the match of the ICM models. However, that method would probably fail under ICM model mismatches while the proposed method of this thesis is more robust to model mismatches because it uses an AR model. Nonetheless, mean and spread estimation can be integrated into AR coefficient estimation in future studies in order to increase the robustness to model mismatches. In addition to these, the scenario in which two clutter sources have two independent texture parameters may be a challenge to the proposed detector of this thesis. Such a scenario suggests different range cells have different ICM models; therefore, adaptive radar detectors may fail in this kind of scenarios. Investigating such cases may be a further study of this thesis.

The proposed detector in this thesis is not yet tested with real data. This test may be a good opportunity to find the capabilities and weaknesses of the detector and a good source for the future works. On the other hand, testing this detector with real data requires a good threshold determining algorithm, which is absent in this thesis. Nevertheless, using training data to find good thresholds is always an option when

interference characteristics cannot change very fast. In addition to these, the exact probabilities of detection and false alarm for this detector may be found analytically in the future. These studies may help this detector become a benchmark for the future studies on adaptive radar detection.

REFERENCES

- [1] C. Wolff. Radar basics. [Online]. Available: <http://www.radartutorial.eu/07.waves/Waves%20and%20Frequency%20Ranges.en.html>
- [2] M. I. Skolnik. (2019, Mar.) Radar. [Online]. Available: <https://www.britannica.com/technology/radar>
- [3] M. A. Richards, *Fundamentals of Radar Signal Processing*, 2nd ed. McGraw-Hill Education, 2014.
- [4] *IEEE Standard Letter Designations for Radar-Frequency Bands*, IEEE Aerospace & Electronic Systems Society, 3 Park Avenue New York, NY 10016-5997, USA, Jan. 2003.
- [5] E. Kelly, “An adaptive detection algorithm,” *IEEE Trans. Aerospace and Electronic Systems*, vol. AES-22, no. 2, pp. 115–127, Mar. 1986.
- [6] F. C. Robey, D. R. Fuhrmann, E. J. Kelly, and R. Nitzberg, “A CFAR adaptive matched filter detector,” *IEEE Transactions on Aerospace and Electronic Systems*, vol. 28, no. 1, pp. 208–216, Jan 1992.
- [7] I. S. Reed, J. D. Mallett, and L. E. Brennan, “Rapid convergence rate in adaptive arrays,” *IEEE Transactions on Aerospace and Electronic Systems*, vol. AES-10, no. 6, pp. 853–863, Nov 1974.
- [8] S. Kraut and L. L. Scharf, “The CFAR adaptive subspace detector is a scale-invariant GLRT,” *IEEE Transactions on Signal Processing*, vol. 47, no. 9, pp. 2538–2541, Sep. 1999.
- [9] E. Conte, M. Lops, and G. Ricci, “Asymptotically optimum radar detection in compound-Gaussian clutter,” *IEEE Transactions on Aerospace and Electronic Systems*, vol. 31, no. 2, pp. 617–625, April 1995.

- [10] O. Besson and D. Orlando, “Adaptive detection in nonhomogeneous environments using the generalized eigenrelation,” *Signal Processing Letters, IEEE*, vol. 14, pp. 731 – 734, 11 2007.
- [11] C. D. Richmond, “Performance of a class of adaptive detection algorithms in nonhomogeneous environments,” *IEEE Transactions on Signal Processing*, vol. 48, no. 5, pp. 1248–1262, May 2000.
- [12] J. S. Goldstein and I. S. Reed, “Theory of partially adaptive radar,” *IEEE Transactions on Aerospace and Electronic Systems*, vol. 33, no. 4, pp. 1309–1325, Oct 1997.
- [13] ———, “Reduced-rank adaptive filtering,” *IEEE Transactions on Signal Processing*, vol. 45, no. 2, pp. 492–496, Feb 1997.
- [14] F. Gini, M. V. Greco, M. Diani, and L. Verrazzani, “Performance analysis of two adaptive radar detectors against non-Gaussian real sea clutter data,” *IEEE Transactions on Aerospace and Electronic Systems*, vol. 36, no. 4, pp. 1429–1439, Oct 2000.
- [15] A. De Maio, G. Foglia, E. Conte, and A. Farina, “CFAR behavior of adaptive detectors: an experimental analysis,” *IEEE Transactions on Aerospace and Electronic Systems*, vol. 41, no. 1, pp. 233–251, Jan 2005.
- [16] A. Younsi, M. Greco, F. Gini, and A. M. Zoubir, “Performance of the adaptive generalised matched subspace constant false alarm rate detector in non-Gaussian noise: an experimental analysis,” *IET Radar, Sonar Navigation*, vol. 3, no. 3, pp. 195–202, June 2009.
- [17] S. Watts, “Radar detection prediction in sea clutter using the compound K-distribution model,” in *IEE Proceedings F - Communications, Radar and Signal Processing*, vol. 132, no. 7, Dec. 1985, pp. 613–620.
- [18] K. B. Petersen and M. S. Pedersen, *The Matrix Cookbook*. Technical University of Denmark, Nov. 2012, version 20121115.
- [19] G. M. Güvensen, Ç. Candan, S. Koç, and U. Orguner, “On generalized eigenvector space for target detection in reduced dimensions,” in *IEEE Radar Conference (RadarConf)*, May 2015, pp. 1316–1321.

- [20] G. M. Güvenses and Ç. Candan, “On the impact of fast-time and slow-time pre-processing operations on adaptive target detectors,” in *IEEE Radar Conference (RadarConf)*, April 2018, pp. 1183–1188.
- [21] S. Haykin, B. W. Currie, and S. B. Kesler, “Maximum-entropy spectral analysis of radar clutter,” in *Proceedings of the IEEE*, vol. 70, no. 9, Sept. 1982, pp. 953–962.
- [22] A. V. Oppenheim and R. W. Schaffer, *Discrete-Time Signal Processing*, 3rd ed. Upper Saddle River, NJ, USA: Prentice Hall Press, 2009.
- [23] P. Stoica and R. Moses, *Introduction to Spectral Analysis*. Prentice Hall, 1997.
- [24] S. M. Kay, *Modern spectral estimation : theory and application*. Englewood Cliffs, N.J. : Prentice Hall, 1988.
- [25] T. Kailath, A. Sayed, and B. Hassibi, *Linear Estimation*, ser. Prentice Hall Information and system sciences series. Prentice Hall, 2000.
- [26] J. O. Smith. (accessed July 07, 2019) Spectral audio signal processing. [Online]. Available: <http://ccrma.stanford.edu/~jos/sasp/>
- [27] P. Lynch, “The Dolph–Chebyshev window: A simple optimal filter,” *Monthly Weather Review*, vol. 125, no. 4, pp. 655–660, 1997. [Online]. Available: [https://doi.org/10.1175/1520-0493\(1997\)125<0655:TDCWAS>2.0.CO;2](https://doi.org/10.1175/1520-0493(1997)125<0655:TDCWAS>2.0.CO;2)
- [28] Jian Li, P. Stoica, and Zhisong Wang, “On robust Capon beamforming and diagonal loading,” *IEEE Transactions on Signal Processing*, vol. 51, no. 7, pp. 1702–1715, July 2003.
- [29] F. Bandiera, D. Orlando, and G. Ricci, *Advanced Radar Detection Schemes Under Mismatched Signal Models*. Morgan & Claypool Publishers, 2009.
- [30] S. Haykin, B. W. Currie, and S. B. Kesler, “Maximum-entropy spectral analysis of radar clutter,” *Proceedings of the IEEE*, vol. 70, no. 9, pp. 953–962, Sep. 1982.

APPENDIX A

BURG'S PARAMETRIC SPECTRAL ESTIMATION METHOD

Throughout the thesis, the focus is on Burg's method because it is fast especially for the case when the number of pulses in a CPI is small.

Burg's formula for parametric spectral estimation [21] is used in estimation of the interference subspace, in slow-time preprocessing stage. This method takes as the input N equally spaced (in time, space or any other dimension) observations, assumes they are from a realization of an auto-regressive (AR) process and estimates the AR coefficients by using Levinson-Durbin recursion, up to a predefined AR order $p \leq N$.

The theoretical background of Burg's method can be found in the literature [30, 24]. The summary of this method is given in Algorithm A.1.

Algorithm A.1 Burg's Algorithm for Calculation of the AR Parameters

Initialize with:

$$\hat{\mathbf{r}}_{\bar{\mathbf{y}},0} = \frac{1}{N} \sum_{n=0}^{N-1} |\bar{\mathbf{y}}_n|^2$$

$$\hat{\tau}_0 = \hat{\mathbf{r}}_{\bar{\mathbf{y}},0}$$

$$\hat{e}_{0,n}^f = \bar{\mathbf{y}}_n \quad n = 1, 2, \dots, N-1$$

$$\hat{e}_{0,n}^b = \bar{\mathbf{y}}_n \quad n = 0, 1, \dots, N-2$$

for $i = 1$ to p **do**

Calculate the reflection coefficient:

$$\hat{\beta}_i = \frac{-2 \sum_{n=i}^{N-1} (\hat{e}_{i-1,n}^f)(\hat{e}_{i-1,n-1}^b)^*}{\sum_{n=i}^{N-1} (|\hat{e}_{i-1,n}^f|^2 + |\hat{e}_{i-1,n-1}^b|^2)}$$

Update the power estimate:

$$\hat{\tau}_i = (1 - |\hat{\beta}_i|^2) \hat{\tau}_{i-1}$$

Update the AR Coefficient estimates:

if $i = 1$ **then**

$$\hat{a}_{1,1} = \hat{\beta}_1$$

else

$$\hat{a}_{i,k} = \begin{cases} \hat{a}_{i-1,k} + \hat{\beta}_i \hat{a}_{i-1,i-k}^* & \text{for } k = 1, 2, \dots, i-1 \\ \hat{\beta}_i & \text{for } k = i \end{cases}$$

end if

Update \hat{e}_n^f **and** \hat{e}_n^b **:**

$$\hat{e}_{i,n}^f = \hat{e}_{i-1,n}^f + \hat{\beta}_i \hat{e}_{i-1,n-1}^b \quad n = i+1, i+2, \dots, N-1$$

$$\hat{e}_{i,n}^b = \hat{e}_{i-1,n-1}^b + \hat{\beta}_i^* \hat{e}_{i-1,n}^f \quad n = i, i+1, \dots, N-2$$

end for

p^{th} order AR coefficient estimates $\{\hat{a}_k\}_{k=1}^p = \{\hat{a}_{p,1}, \hat{a}_{p,2}, \dots, \hat{a}_{p,p}\}$

Find the power estimate at the range of interest $\hat{\tau} = \hat{\tau}_p$
